

# For Reference

---

NOT TO BE TAKEN FROM THIS ROOM

# For Reference

NOT TO BE TAKEN FROM THIS ROOM

EX LIBRIS  
UNIVERSITATIS  
ALBERTAENSIS



## Regulations Regarding Theses and Dissertations

[illegible]





Thesis  
1969(P)  
124

THE UNIVERSITY OF ALBERTA  
MASS TRANSFER AT BUBBLE FORMATION

by



HARISH KALRA, B.Sc.

A THESIS

SUBMITTED TO THE FACULTY OF GRADUATE STUDIES  
IN PARTIAL FULFILLMENT OF THE REQUIREMENTS FOR THE DEGREE  
OF MASTER OF SCIENCE IN CHEMICAL ENGINEERING

DEPARTMENT OF CHEMICAL AND PETROLEUM ENGINEERING

EDMONTON, ALBERTA

FALL, 1969



Digitized by the Internet Archive  
in 2019 with funding from  
University of Alberta Libraries

<https://archive.org/details/Kalra1969>

UNIVERSITY OF ALBERTA  
FACULTY OF GRADUATE STUDIES

The undersigned certify that they have read, and recommend to the Faculty of Graduate Studies for acceptance, a thesis entitled "Mass Transfer at Bubble Formation" submitted by Harish Kalra, B.Sc., in partial fulfilment of the requirements for the degree of Master of Science in Chemical Engineering.



## ABSTRACT

High speed cine photography was used to study mass transfer at bubble formation for the  $\text{CO}_2$ -water system. The amount of mass transfer was determined by the difference of the bubble volume at formation as determined from photographs and the bubble volume calculated from flow rate and frequency measurements.

Point data of the bubble periphery was taken from photographic films and was processed using computer programs to determine the bubble surface area and volume. Two programs were written for the purpose; one of them used a numerical approach and the other was based on an empirical equation used to describe the bubble shape. Variation of bubble surface and volume with time could be studied using the numerical program.

Bubble surface area was found to vary according to the equation  $A = k_1 t^{n_1}$  only up to the point where bubble necking and oscillations start.  $n_1$  was found to be of the order of 0.850. Sharp increases in area were observed during necking. The volume of the bubble was found to vary in a substantially linear manner with time.

Mass transfer coefficients for bubble formation were determined for the  $\text{CO}_2$ -water system in a column having a diameter of 20.2 cm., for a liquid velocity of 1.0 cms/sec., bubble frequencies of 0.5 to 10.0 bubbles/sec., an orifice



internal diameter of 0.408 cms., gas flow rates of 0 to 1.5 cc/sec, and at a liquid temperature of 25.0°C. The values obtained were in the range of 98 to 222 cms/hr for the frequencies studied. The order of magnitude agrees well with results of previous investigations for mass transfer during bubble rise [3,30,50,52,69,70,71,72], but the value of the mass transfer coefficient during bubble formation was found to be greater than that measured during bubble rise. This difference was thought to be due to a liquid velocity superimposed on bubble growth. The total amount of mass transfer was found to depend more closely on  $T_f^{0.685}$ , where  $T_f$  is the total bubble age, rather than  $T_f^{0.5}$  as suggested by some previous investigators during studies of mass transfer from drops in liquid-liquid systems [5,42 53,54,55,56,57].







## ACKNOWLEDGEMENTS

The author wishes to express his appreciation of the criticism and assistance given by Dr. F.D. Otto who supervised this investigation.

The many valuable suggestions and critical guidance rendered by Dr. K. Koide is gratefully acknowledged.

To Mr. S. Aggarwal a graduate student of the University of Alberta for his assistance in conducting the titration analysis, the author expresses his sincere thanks.

To Mr. D. Sands of Photographic services for his assistance with high speed photography, the author is obliged.

To the staff of the Chemical and Petroleum Engineering Department for their assistance in building the equipment, the author is truly grateful.

The author appreciates the financial aid of the National Research Council of Canada and the Department of Chemical and Petroleum Engineering of the University of Alberta received in the course of this work.



## TABLE OF CONTENTS

	Page
<u>LIST OF FIGURES</u>	1
<u>LIST OF TABLES</u>	4
1. <u>INTRODUCTION</u>	6
2. <u>LITERATURE REVIEW</u>	9
2.1 Bubble Behaviour	10
2.2 Mass Transfer during Bubble Rise and Bubble Formation	20
2.3 Effect of Surface Activity on Bubble Behaviour and Mass Transfer	35
3. <u>THEORY</u>	39
3.1 Evaluation of Mass Transfer Coefficient	39
3.2 Evaluation of Bubble Area and Volume	40
3.3 Evaluation of the Sample Size Required for Bubble Analysis	47
3.4 Liquid Velocity Profile	49
4. <u>EXPERIMENTAL</u>	54
4.1 General Approach	54
4.2 Experimental Equipment	55
4.3 Experimental Procedure	76
5. <u>RESULTS</u>	88
5.1 General	88
5.2 Liquid Velocity Profiles	88
5.3 Air-Water System	89
5.4 Mass Transfer During Bubble Formation: CO <sub>2</sub> -Water System	99



6.	<u>DISCUSSION</u>	Page 111
6.1	Air-Water System	111
6.2	CO <sub>2</sub> -Water System	111
7.	<u>CONCLUSIONS AND RECOMMENDATIONS</u>	127
	<u>NOMENCLATURE</u>	131
	<u>REFERENCES</u>	137
	<u>APPENDICES</u>	
A.	Evaluation of Bubble Surface and Volume for Programs I and II	A-1
B.	Documentation and Method for use of Programs I, II and III	B-1
C.	Equipment Calibration, Titration Analysis and Details of Liquid Velocity Profile Measurement	C-1
D.	Evaluation of the Mass Transfer Coefficient from CO <sub>2</sub> -Water Data	D-1



## LIST OF FIGURES

S.No.	Page
1. Coordinates For an Axisymmetric Body of Revolution	23
2. The Cardioid: $r=a(1+\cos\theta)$	42
3. Plot of Equations 3.7 and 3.8 in comparison to actual Bubble Periphery	45
4. Plot of Polarographic Current vs. Applied Voltage.	51
5. Experimental Layout	56
6. Details of the Experimental Column	58
7. Photograph of Titration Equipment	64
8. Photograph of Demineralizer	65
9. Circuit Diagram for Measurement of Liquid Velocity Profile	66
10. Details of the Platinum Probe	68
11. Photograph of the Calibration Tank	69
12. Circuit Diagram for Measurement of Bubble Frequency	71
13. Schematic Layout of the Photographic Equipment	72
14. Ray Line Diagram for The Correction Lens	74
15. Photograph of the Digitizer	75
16. Plot of Liquid Velocity Profiles at Different Diametric Orientations	90
17. Liquid Velocity Profiles at Different Bubble Frequencies for an average liquid velocity of 1.0 cms/sec	91







S.No.	Page
18. Liquid Velocity Profiles at different Bubble Frequencies for an average liquid velocity of 2.0 cms/sec	92
19. Plot of Bubble Diameter vs. Orifice Reynolds Number	94
20. Plot of Bubble Frequency vs. Orifice Reynolds Number	95
21. Comparison of Bubble volume from Gas flow rate and bubble frequency with Bubble volume from Photographs	97
22. Photographs of Bubble Behaviour	98
23. Plot of Bubble Surface Area vs. Time for Runs M-1, M-2 and M-3	101
24. Plot of Bubble Surface Area vs. Time for Runs M-4, M-5 and M-6	102
25. Plot of Bubble Surface Area vs. Time for Run M-7	103
26. Bubble Volume vs. Time for Runs M-1, M-2 and M-3	104
27. Bubble Volume vs. Time for Runs M-4, M-5 and M-6	105
28. Bubble Volume vs. Time for Run M-7	106
29. Log-Log Plot of Bubble Area vs. Time for Runs M-1, M-2 and M-3	113
30. Log-Log Plot of Bubble Area vs. Time for Runs M-4, M-5 and M-6	114
31. Log-Log Plot of Bubble Area vs. Time for Run M-7	115
32. Plot of Bubble Area vs. Time on transformed Time Coordinates	118



S.No.	Page
33. Plot of Total Mass Transfer vs. Total Bubble Age	121
34. Plot of Mass Transfer Coefficient vs. Bubble Frequency	122
35. Plot of Mass Transfer Coefficient vs. Equivalent Bubble Diameter	125
36. Sequence of Reading the Bubble Periphery	B-3
37. Calibration Curves for Rotameters	C-3
38. A Typical pH Titration Curve	C-5
39. Blank and CO <sub>2</sub> titration curves	C-13
40. Curves of Polarographic Current vs. Applied Voltage for Probe 1	C-16
41. Curves of Polarographic Current vs. Applied Voltage for Probe 2	C-17
42. Calibration Curve for Probe 1	C-20
43. Calibration Curve for Probe 2	C-21
44. Details of the position of the probe with respect to the column and details of the characteristic length	C-22



LIST OF TABLES

S.No.	Page
1. Range of Experimental Conditions for the Air-Water System	93
2. Experimental Conditions used for CO <sub>2</sub> -Water Runs	100
3. Data for Mass Transfer with CO <sub>2</sub> -Water System	108
4. Data for Mass Transfer with CO <sub>2</sub> -Water System	109
5. Mass Transfer Coefficients for the CO <sub>2</sub> -Water System	110
6. Percentage Neck Formation Time in relation to Bubble Frequency and Mass Transfer Coefficient	123
7. Data for Calibration of Rotameters	C-2
8. Standardization of Barium Hydroxide Solution	C-6
9. Standardization of Hydrochloric Acid Solution	C-7
10. Polarographic Current vs. Applied Voltage at different Liquid Velocities	C-15
11. Calibration Data for Probes 1 and 2	C-19
12. Radial Position vs. Characteristic Length for Probes 1 and 2	C-24



S.No.		Page
13.	Point Velocity measurements in different diametric directions	C-26
14.	Point Velocity measurements for average liquid velocity of 1.0 cms/sec	C-27
15.	Point Velocity measurements for average liquid velocity of 2.0 cms/sec	C-28

- 13. Point Velocity measurements in different diametric directions C-26
- 14. Point Velocity measurements for average liquid velocity of 1.0 cm/sec C-27
- 15. Point Velocity measurements for average liquid velocity of 2.0 cm/sec C-28



## CHAPTER 1

### INTRODUCTION

Gas liquid contactors are indispensable in industry and because of their extensive application it is desirable to be able to design such equipment reliably. To do this it is useful to have as much information as possible on the fundamental aspects of gas liquid contacting. This study, namely the study of mass transfer during bubble formation, was undertaken with this viewpoint in mind.

The dispersion of a gas phase in the form of bubbles in a liquid is one of the modes of gas-liquid contact. The study of the mechanisms of bubble formation and of mass transfer to or from such bubbles has been in progress for the last thirty years. Bubbling phenomena has been categorically subdivided into three distinct regions namely:

- (i) Bubble formation
- (ii) Bubble rise
- (iii) Bubble breakup at the free liquid surface.

Mass transfer will occur during each of the above mentioned regions.

Most of the work done to date in the study of mass transfer has been restricted to the bubble rise period. Mass transfer during bubble formation has been treated as an end effect and any quantitative information obtained for the amount of mass transfer occurring during these regions



has therefore been indirect. Calderbank [1], Haselden et. al. [2], Bowman et. al. [3], Licht et. al. [4,5] and Dixon et. al. [6,7] conducted studies of mass transfer during bubble rise. In order to separate the amount of mass transfer occurring during this period it was necessary that the amount of mass transfer occurring during bubble formation and during bubble breakup be either known or be eliminated by a modification of the experimental technique. The end effect due to bubble breakup or bubble coalescence could be eliminated through equipment modifications but an estimate of the amount of mass transfer during bubble formation was obtained by an extrapolation of a plot of total mass transfer versus liquid height to zero liquid height. Their conclusions indicated that a considerable amount, varying from 25 to 50%, of the total mass transfer occurred during bubble formation [1,2,4,5,6,7]. From this it was concluded that the rate of mass transfer during bubble formation is probably enhanced. No attempt was made to measure the actual rate of mass transfer during bubble formation, even though theoretical postulations for an enhanced rate of transfer during this region were put forward [1,2].

Subsequently, however, Calderbank et. al. [8] reported a direct study of mass transfer during bubble formation for Carbon dioxide, Sulphur dioxide and Acetylene bubbles formed in a stagnant water phase at low bubble



frequencies. High speed cine photography was used to determine the change of bubble surface area with time and the mass transfer coefficient was represented by a Higbie [9] type of equation. It was reported that no enhanced rate of mass transfer occurred during bubble formation but no quantitative data were given to support this conclusion.

The presence of a considerable amount of uncertainty as to the amount of mass transfer occurring in the region of bubble formation justified a further study of this phenomena so that concrete evidence may be obtained one way or the other. An experimental program similar in approach to Calderbank et. al. [8] was drawn up wherein the range of investigation was extended and the effect of liquid velocity was also imposed on the system. High speed cine photography was used to photograph the forming bubbles and computer programs were written to evaluate the bubble area and volume as a function of time.





## CHAPTER 2

### LITERATURE REVIEW

An extensive study of dispersions has been done with both gas-liquid and liquid-liquid systems. A dispersed liquid phase is referred to as drops whereas a gas is said to form bubbles. The general mechanisms of drop and bubble behaviour are very similar in a number of ways and thus an understanding of one throws considerable light on the behaviour of the other.

The formation of drops or bubbles has been found to be a function of the physical properties of the system involved, gas or liquid velocity, and the dimensions of the apparatus such as the orifice diameter.

Mass transfer during bubble rise has been studied in considerable detail and the effect, on mass transfer, of variables governing the formation of bubbles has been established. The study of mass transfer during bubble formation has been somewhat limited in comparison.

The literature review on this subject has been subdivided into the following categories:

- (1) Bubble behaviour
- (2) Mass transfer during bubble (or drop) rise and during bubble (or drop) formation.
- (3) Effect of Surface Activity on Bubble behaviour and Mass Transfer.





## 2.1 Bubble Behaviour.

### Effect of gas flow rate on bubble formation.

The phenomena of bubble formation may be categorized into the following regions based on increasing gas flow rate:

- (a) Constant Volume region
- (b) Transition region
- (c) Constant frequency region
- (d) Turbulent region.

As the gas flow rate is increased the bubble behaviour corresponds to one of the above mentioned regions in the order in which they have been mentioned. The change from one region to the other has been characterized in terms of the orifice Reynolds number which is defined by:

$$Re = \frac{\rho_d U_g \delta}{\mu_c} \text{-----} (2.1)$$

where  $\rho_d$  = density of the dispersed phase

$U_g$  = velocity of the gas at the orifice

$\delta$  = Orifice diameter

$\mu_c$  = Viscosity of the continuous phase.

This criteria is suitable for analysis of bubble behaviour in industrial size equipment only. Any values of Re mentioned in the subsequent discussion bear this restriction. In addition, some overlap of Reynolds numbers between



regions is often found.

(a) Constant Volume Region

At low gas flow rates corresponding to a value of  $Re$  upto 100 or 150, the gas bubble forms discretely and slowly at the given orifice and is substantially constant in volume. The volume of the bubble at detachment from the orifice may be evaluated by a force balance between the surface tension and the buoyant forces. The frequency of bubble formation is proportional to the gas flow rate. These observations have been supported by Van Krevelin et. al. [10], Quigley, Johnson and Harris [11], Hughes et. al [12], Coppock and Meiklejohn [13], Leibson et. al. [14] and Datta, Napier and Newitt [15].

Davidson et. al. [16], however, have reported that the bubble volume increased slightly with increase of gas flow rate in this region and thus that the bubble frequency is slightly less than proportional. Benzing and Myers [17] concluded from their investigations that the bubble volume had a tendency to increase with bubble frequency. In effect this substantiates the statement made by Davidson et. al. [16].

(b) Transition Region

The transition region is the changeover from the constant volume to the constant frequency region. A range of  $Re$  of 100 - 300 has been suggested for this region by



Valentin [18]. Neither the bubble volume nor the bubble frequency are constant in this region of bubble behavior. The bubble formation though discrete is characterized by a tendency of the bubbles to proceed up the column in pairs. A bubble forms at the orifice, breaks from it and appears to hover a few centimeters above the orifice till it is joined by the next bubble. Both of them then move up the column together. This phenomenon persists for short intervals of time. This implies that the bubble formation often reverts to the formation of single discrete bubbles as observed in the constant volume region. This observation has been supported by Davidson et. al. [16]. Benzing and Myers [17] and Davidson and Schöler [19] have reported an increasing predominance of the inertial effects during this region of bubble formation. Benzing and Myers [17] refer to it as a kinetic impingement. This effect, which is due to a higher velocity of gas flowing into the bubble, tends to dislodge the bubble at smaller volumes, but this effect is more than compensated by a large amount of gas flowing into the bubble at breakoff. As a result of this the bubble volume increases with increase of frequency.

(c) Constant Frequency Region

With a further increase in gas flow rate the bubble frequency becomes independent of gas flow rate and approaches a constant maximum value, which is a function of the orifice





diameter. The bubble volume, however, increases proportionally with gas flow rate. The orifice Reynolds numbers characterizing this region have been suggested as 1000 to 2100.

Due to a high gas flow rate, the gas bubbles tend to merge into one another resulting in coalescence after detachment from the orifice. The size of the bubbles at detachment, for a given gas flow rate in this region, is reproducible, indicating that the bubble formation is discrete. Though evidence to support the above statements has been provided by Davidson et. al. [16], Benzing and Myers [17], Eversole et. al. [20], and Calderbank [21], Leibson et. al. [14] have indicated that some small bubbles are formed in this region by the rupture and collapse of the elongated bubble neck. Thus some small bubbles accompany larger ones and their fraction gradually increases with increasing gas flow rate.

#### (d) Turbulent Region

As the gas flow rate is increased further from Re of about 2100 to 40,000, bubble coalescence begins to take place closer and closer to the orifice; it becomes difficult to see discretised bubbles forming at the orifice. A variety of sizes of bubbles is formed. Gas bubbles break up on formation into smaller bubbles and the size distribution of this break up differs in different regions of the fluid. There are larger bubbles near the orifice





and much smaller ones higher up the column. Bubbles during this region have been termed as being spherical capped or toroidal in shape [18].

A spherical bubble has a relatively stable configuration while a toroidal bubble breaks up on formation. At higher rates of gas flow the proportion of toroidal bubbles increases. Leibson et. al. [14], Seimes [22] and Calderbank [21] have reported agreement to the above mentioned facts. Leibson et. al. [14] have classified the bubble formation above a Reynolds number of 10,000 where turbulence is considered fully developed, as being similar to a disintegrating liquid jet in air. The gas ensuing from the orifice does so in the form of a jet and disintegrates into coarse and fine bubbles near the orifice. Rennie and Evans [23], however, indicate that even at Reynolds numbers as high as 40,000, there is still bubble formation followed by bubble breakup, the bubbles formed being all toroidal.

#### Effect of Chamber Volume

The chamber volume is defined as the volume upstream of the orifice to the nearest restriction in the gas line. Variation of the chamber volume serves as a very effective method to control bubble stability and results in a change of bubble volume. In order to study the effect of the chamber volume on bubble behaviour it is convenient to define a capacitance number  $N_c$  given as follows:



$$N_c = \frac{4g(\rho_c - \rho_d)V_c}{\pi \delta^2 \rho_d c^2} \text{-----}(2.2)$$

where

$\rho_c$  = density of continuous phase

$\rho_d$  = density of dispersed phase

$V_c$  = chamber volume

$\delta$  = orifice diameter

$c$  = acoustic velocity in the gas.

The formation of stable discrete bubbles occurs when  $N_c$  is below a certain critical value. For large chamber volumes where  $N_c$  is greater than critical the bubble formation becomes unstable and a phenomena referred to as chain bubbling occurs. During chain bubbling a large number of gas bubbles form in succession followed by a pause which is subsequently broken by another chain of bubbles. This process repeats itself. When the chamber volume is small the formation of one gas bubble is enough to decrease the gas pressure in the chamber upstream of the orifice sufficiently so as to prevent the next bubble from forming till such time that the gas flow restores the chamber pressure. The formation of a chain of bubbles at values of  $N_c$  greater than critical is due to the fact that one bubble does not decrease the chamber pressure sufficiently and as a result a chain of bubbles is formed till the chamber pressure drops. The pause





following a chain of bubbles is used to restore the chamber pressure to the pressure of the system. The formation of bubbles at very large chamber volumes is said to occur at constant pressure conditions.

When the chamber volume is very much smaller than the critical value, the volume of the bubbles formed is independent of the chamber volume. On increasing the chamber volume, the bubble volume increases till the value of  $N_c$  approaches the critical. At the critical value very sharp changes in bubble size take place. If the bubbling phenomena favours the formation of multiple bubbles the bubble volume drops sharply.

The critical chamber volume is itself a function of gas flow rate for a given orifice size. At high gas flow rates the critical value of  $N_c$  drops sharply. This implies that at high gas flow rates small changes of chamber volume could upset the stability of bubble formation. Hughes et. al. [12], Davidson et. al. [16], Bowman et. al. [3], Hayes et. al. [24], Leibson et. al. [14] and Mahoney et. al. [25] have conducted investigations of the effect of chamber volume on bubble behaviour and their conclusions are in agreement with the above given facts. Bowman et. al. [3] proposed a dimensionless correlation to predict the effect of this variable on bubble behaviour.





### Effect of Orifice Diameter

Most workers agree on the effect of orifice diameter on bubble formation. During the constant volume region the bubble size is proportional to the cube root of the orifice diameter. This is readily seen by making a force balance between the surface tension and the buoyancy forces at bubble breakoff. As the orifice size is increased the size of the constant volume bubble will eventually become smaller than the orifice diameter. The gas-liquid interface will then become horizontal at the orifice perimeter and this causes unstable bubble formation. Liquid weeping through the orifice is sometimes caused by the use of too large an orifice. Davidson et. al. [16] suggested that stable bubbles in the constant volume region cannot be formed at an orifice of radius 0.79 cms. but found that such bubbles could be formed at orifices of radius 0.64 cms. They then concluded for the systems they investigated, that orifices of radius larger than 0.7 cms. cannot produce stable bubbles in the constant volume region.

At high gas flow rates, that is during the constant frequency region, Van Krevelin et. al. [10] have reported that the bubble volume is independent of orifice diameter. The maximum frequency of bubble formation varies inversely with the orifice radius. Davidson et. al. [16] have proposed correlations relating the maximum bubble frequency



with the orifice radius. They suggested that the maximum frequency varies inversely as the cube root of the orifice radius. Other correlations relating bubble volume with gas flow rate and orifice diameter were also suggested by them and a data fit within 1% for high gas flow rates and within 5% for the transition region has been claimed.

### Effect of Liquid Seal Height

The effect of liquid seal height has been studied by several authors but common observations for all of them do not exist.

Quigley et. al. [11], Davidson et. al. [16], Coppock and Meiklejohn [13], Hayes et. al. [24] and Towell et. al. [26], have all reported a negligible effect of seal height on bubble formation. Bowman et. al. [3] have shown that this is not so. A range of seal heights from 2.54 to 30.5 cms. was investigated and their conclusions indicate that bubble frequency increases with increase of seal height, particularly for seal heights greater than 20 cms. ( $\text{CO}_2$  - water system). The bubble size therefore decreases with increase of seal height for the same gas flow conditions. They developed an exponential equation in an attempt to describe the submergence effect quantitatively. They suspected that the submergence effect may diminish with increasing orifice throat length. Leonard et. al. [27] also investigated this variable and their conclusions





reiterate the above facts.

#### Effect of Orifice Throat Length

Hughes et. al. [12], Leibson et. al. [14] and Hayes et. al. [24] have reported that there is no effect of varying orifice throat length on bubble behaviour. Benzing and Myers [17] disagreed with this and reported that for an orifice of size 0.438 cms. as the throat length was decreased from 4.6 cms. to 0.1 cms., no significant change in bubble volume occurred till the throat length reached a value of 0.33 cms. when the bubble volume dropped sharply. Bowman and Johnson [3] have reported that where chamber volume cannot be sufficiently reduced to get a discrete stable bubble, reduction of throat length helps to obtain stable bubble formation.

#### Effect of Column walls and wettability

The effect of the column wall on bubble formation becomes evident only when the column diameter becomes comparable with the bubble diameter. The gas bubble then gets elongated as in gas lifts. If the ratio of column to orifice diameter is 10 or greater, the wall effect is negligible.

Orifice surface wettability is important for preventing liquid leakages through the orifice. Stable bubble formation requires that the orifice surface be non-wettable



by the liquid. Teflon covers have been successfully used to enhance non-wettability where orifice diameters were too large and liquid leakages occurred [3].

## 2.2 Mass Transfer during Bubble Rise and Bubble Formation

### Bubble Rise

Mass transfer from or to bubbles or drops rising singly in a continuous phase is a function of the fluid properties, the bubble size and the flow conditions of the dispersed phase. The analysis of the rate of mass transfer in the continuous phase may be categorized as follows:

- 1) Mass transfer to or from immobile surfaces
- 2) Mass transfer to or from mobile surfaces

Each of the above mentioned categories may be further subdivided according to bubble size as follows:

- (a) Small spherical bubbles ( $d_e \leq 0.2$  cms.)
- (b) Fluid oblate spheroids ( $0.2 < d_e < 1.8$  cms.)
- (c) Fluid spherical caps ( $d_e \geq 1.8$  cms.)

Mass transfer from each of the above mentioned bubble sizes can be analysed according to the relative importance of viscous and inertial forces in a given fluid system. That is, the analysis differs with the magnitude of the Reynolds number.

The rates of mass transfer from small drops or bubbles in a continuous phase can be analysed rigorously because the bubbles are spherical in shape and rise or fall





in straight paths. Larger drops or bubbles are generally irregular both in shape and path. An exact theoretical treatment to determine the mass transfer rates from such bubbles is therefore very difficult. It is customary to assume the larger bubbles to have well defined shapes and to rise in straight lines. In addition bubble shapes are assumed to be axisymmetric, that is, symmetric about the axis in the direction of rise.

By assuming that the Peclet and Schmidt numbers are large Calderbank [28] has derived an equation in dimensionless coordinates relating the tangential velocity of the bubble surface with the concentration of the solute in the liquid phase. The restriction of large Peclet and Schmidt numbers is based on the fact that the concentration boundary layer is assumed to be far thinner than the velocity boundary layer. The equation derived is given as

$$(u_{10} + u'_{10}y_1) \frac{\partial C_1}{\partial x_1} - \frac{1}{r_1} \frac{\partial}{\partial x_1} [(u_{10}y_1 + u'_{10}y_1^2)r_1] \frac{\partial C_1}{\partial y_1} = \frac{2}{Pe} \frac{\partial^2 C_1}{\partial y_1^2} \quad \text{---(2.3)}$$

where  $u_{10} = u_1 \big|_{y_1=0}$

$$u'_{10} = \frac{\partial u_1}{\partial y_1} \big|_{y_1=0}$$

and

$$u_1 = \frac{u}{U}$$

$$v_1 = \frac{v}{U}$$



$$y_1 = \frac{y}{r_e}$$

$$r_1 = \frac{r}{r_e}$$

$$C_1 = \frac{C_A}{C_A^s}$$

$$x_1 = \frac{x}{r_e}$$

The significance of the coordinates  $u, v, x, y, r$  for an axisymmetric body of revolution is shown in Figure 1. The boundary conditions applicable to equation 2.3 are

$$C_1 = 1, \quad y_1 = 0 \quad \text{all } x_1$$

$$C_1 = 0, \quad y_1 = \infty \quad \text{all } x_1$$

Using these boundary conditions equation 2.3 can be solved for the mobile and immobile surfaces mentioned above.

#### Case 1: Immobile Interface

This implies that  $u_{10}=0$ . Using this fact equation 2.3 has been solved by Locheil [29] under the above given boundary conditions to give the following general mass transfer equation.

$$Sh = 0.641 \left( \frac{4\pi r_e^2}{A} \right) \left[ \int_0^{x_1} (u_{10}' r_1)^{1/2} r_1 dx_1 \right]^{2/3} Pe^{1/3} \text{ ----- (2.4)}$$

Where  $A$  is the total surface area of the body.



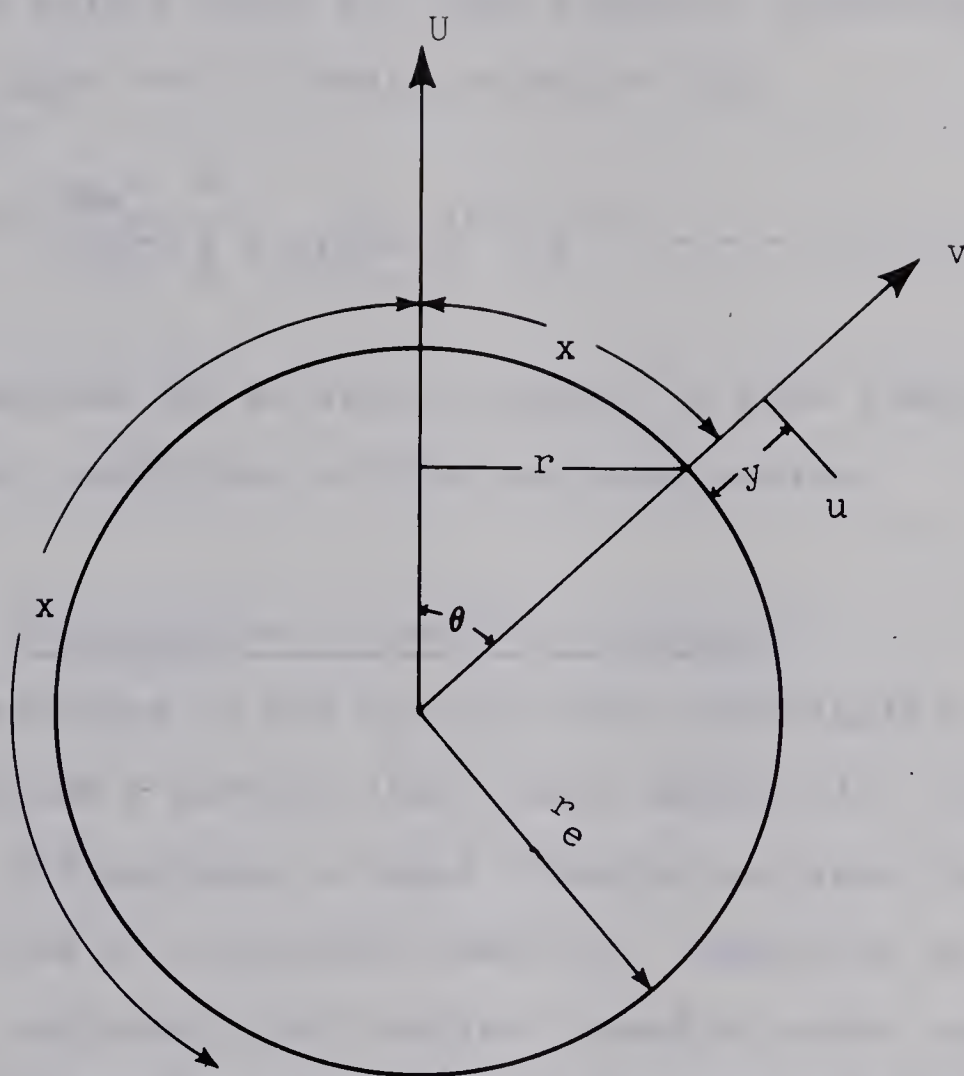


Figure 1: Coordinates For an Axisymmetric Body of Revolution





## Case 2: Mobile Interface

For a moving fluid boundary  $u_{10} \gg u'_{10} y_1$ , and equation 2.3 may be solved under the same boundary conditions as before to give the following equation [29].

$$Sh = \left(\frac{2}{\pi}\right)^{1/2} \left(\frac{4\pi r_e^2}{A}\right) \left[\int_0^{x_1} u_{10} r_1^2 dx_1\right]^{1/2} Pe^{1/2} \text{-----} (2.5)$$

These equations can be easily reduced to more familiar forms for special conditions of flow and bubble size.

### (a) Solid-Spheres (Immobile Interface)

Depending on the system under investigation, bubbles or drops below a certain size behave essentially like rigid spheres. For purposes of mass transfer analysis the interface may thus be considered immobile. Hammerton and Garner [30] have indicated that bubbles formed in water behave as rigid spheres below a size of 0.02 cms. and when formed in glycerol this limit goes up to 0.2 cms.

For a sphere  $r_1 = \sin \theta$ ,  $A = 4\pi r_e^2$  and  $dx_1 = d\theta$ . Substituting in equation 2.4, the equation for mass transfer becomes:

$$Sh = 0.641 \left[ \int_0^{\pi} (u'_{10} \sin \theta)^{1/2} \sin \theta d\theta \right]^{2/3} Pe^{1/3} \text{-----} (2.6)$$

This equation has been derived by Baird and Hamielec [31] also. For cases where the inertial terms are very small,



that is  $Re < 1$ , Friedlander [32] obtained the following simplification of equation 2.6.

$$Sh = 0.99 Pe^{1/3} \quad (Re < 1) \text{-----} (2.7)$$

Equation 2.7 has been verified for dissolution of small bubbles by Calderbank et. al. [33], for liquid drops by Ward et. al. [34] and for solid shperes by Aksel' Rud [35].

For cases where the inertial forces cannot be neglected, that is  $Re > 1$ , a boundary layer type of equation can be obtained from the Navier-Stokes equation and using a quartic profile for the velocity distribution in the boundary layer, assuming no separation at the sphere's surface, the following equation can be obtained.

$$Sh = 0.62 Re^{1/2} Sc^{1/3} \text{-----} (2.8)$$

Separation of the boundary layer, however, occurs at  $\theta \approx 108^\circ$  [36] and the equation for mass transfer occurring over the front surface of the sphere upto the point of separation is given as

$$Sh = 0.56 Re^{1/2} Sc^{1/3} \text{-----} (2.9)$$

This equation was also obtained by Froessling [37] and verified for dissolution of small drops by Calderbank et.al.



[33] and Hammerton and Garner [30].

(b) Fluid-Spheres (Mobile Interface)

If the values of  $r_1$ ,  $A$  and  $dx_1$  for a sphere be substituted in equation 2.5, the equation for a fluid sphere becomes

$$Sh = \left(\frac{2}{\pi}\right)^{1/2} \left[ \int_0^{\pi} u_{10} \sin^2 \theta \, d\theta \right]^{1/2} Pe^{1/2} \text{-----} (2.10)$$

Once again depending on whether  $Re < 1$  or  $> 1$ , specific substitutions for  $u_{10}$  may be made in equation 2.10 to obtain particular solutions for mass transfer from fluid spheres.

For  $Re < 1$  Hadamard [38] and Rybczynsky [39] developed velocity profile about a fluid sphere. Using their relations for the tangential surface velocity  $u_{10}$ , the equation for mass transfer becomes

$$Sh = 0.65 \left( \frac{\mu_c}{\mu_c + \mu_d} \right)^{1/2} Pe^{1/2} \text{-----} (2.11)$$

Where  $\mu_c$  and  $\mu_d$  are the viscosities of the continuous and dispersed phases respectively. Part of the work of Hammerton and Garner [30] and Ward et. al. [34] correlates to this equation reasonably well.

For cases where  $Re > 1$  Chao [40] has proposed equations for the velocity distribution both inside and outside the sphere as dimensionless perturbations from the potential





flow fields. Using his equations for the velocity profiles Locheil [29] has derived the following equation for mobile spheres.

$$Sh = 1.13 \left[ 1 - \frac{2 + (3\mu_d/\mu_c)}{1 + (\rho_d\mu_d/\rho_c\mu_c)^{1/2}} \frac{1.45}{Re^{1/2}} \right]^{1/2} Pe^{1/2} \text{-----} (2.12)$$

Griffith [41] and Herrtjes et. al. [42] have used this equation to correlate data for water drops in isobutanol and ethyl acetate drops in water.

For gas bubbles in a liquid phase, equation 2.12 can be reduced to

$$Sh = 1.13 \left[ 1 - \frac{2.90}{Re^{1/2}} \right]^{1/2} Pe^{1/2} \text{-----} (2.13)$$

This equation applies for Re in the range  $100 \leq Re \leq 400$ . For very high Re i.e. potential flow equation 2.13 reduces to the very familiar Higbie [9] equation.

$$Sh = 1.13 Pe^{1/2} \text{-----} (2.14)$$

This equation was first derived by Stefan [43] and later by Boussinesq [44] and Higbie [9]. The rates of dissolution of large bubbles has been satisfactorily correlated with this equation by Hammerton and Garner [30], Higbie [9], West [45] and Bowman and Johnson [3].

Ruckenstein [46] has also developed equations for



fluid spheres both in the range  $Re \gg 1$  and  $Re \ll 1$  by using an interpolation method. This allows an evaluation of mass transfer in the intermediate range also.

### Fluid Oblate Spheroids

When dealing with irregular but axisymmetric shapes such as oblate spheroids, it is difficult to specify precise relations for surface area. Use is made, therefore, of a shape factor called eccentricity which is defined as the ratio of the bubble width to bubble height. Oblate spheroids are in general ellipsoidal shapes and the eccentricity is given by the ratio of the major to minor axes.

The equivalent diameter of these bubbles lies in the range  $0.2 < d_e < 1.8$  cms. and the Reynolds numbers are very high. The flow is therefore, almost always assumed as potential. Zahm [47] has developed velocity profiles for flow around oblate spheroids and using his relations in combination with equation 2.5 the following equation for mass transfer can be obtained.

$$Sh = \left\{ \frac{2}{3}(1+K^*) \right\}^{1/2} \left\{ \frac{2.26 e_c^{1/3} (e_c^2 - 1)^{1/2}}{e_c (e_c^2 - 1)^{1/2} + \ln[e_c + (e_c^2 - 1)^{1/2}]} \right\} Pe^{1/2} \text{----} (2.15)$$

Where  $K^*$  is a complex function of the eccentricity  $e_c$ . This equation has been successfully used to interpret the data of Hammerton and Garner [30], Higbie [9] and West [45].



### Fluid Spherical Caps

When the bubble diameter exceeds about 1.8 cms. the bubbles assume mushroom like shapes that are termed as spherical caps. Potential flow is assumed to describe the velocity profiles of the fluid around such bubbles. The interfacial velocity is given by the potential flow value for a sphere namely

$$u_{10} = \frac{3}{2} \sin \theta \text{ ----- (2.16)}$$

Using equation 2.16 and neglecting mass transfer from the rear of the bubble, Locheil [29] obtained an equation given as

$$Sh = 1.79 \left[ \frac{(3e_c^2 + 4)^{2/3}}{e_c^2 + 4} \right] Pe^{1/2} \text{ ----- (2.17)}$$

Rosenberg [48] and Takadi and Maeda [49] have suggested a value for  $e_c = 3.5$  for all spherical capped bubbles. Using this value equation 2.17 reduces to

$$Sh = 1.28 Pe^{1/2} \text{ ----- (2.18)}$$

which is very nearly the same as the Higbie equation 2.14.

Most mass transfer studies from bubbles involve an analysis of the variation of the mass transfer coefficient with equivalent bubble diameter. This is generally presented in the form of a plot. If the range of bubble







diameters covered is wide, the mass transfer coefficient conforms to the Froessling [37] type of equation for rigid spheres i.e. small bubble diameters and then increases as the bubble diameter increases. For larger bubbles the Higbie type of equation is more closely followed. The curve for mass transfer coefficient vs. equivalent bubble diameter as determined by experiment thus lies in between the values predicted by the equations of Froessling [37] and Higbie [9]. The experimental curve passes through a maximum at a diameter which is a function of the properties of the system under study. These type of curves have been obtained by Hammerton and Garner [30], Leonard and Houghton [27], Zieminski et. al. [50] and Siddique [51].

The mass transfer studies so far reviewed have all been done in stagnant liquid systems. Himmelblau et. al. [52] have reported that the mass transfer coefficient from gas bubbles in a moving liquid is higher than that in the stagnant system. During a study of multiple dispersions, however, Calderbank [28] has stated that no such effect of liquid velocity is observed.

### Bubble Formation

In contrast to the bubble rise period, the study of mass transfer during bubble formation has been rather limited. As mentioned earlier, indications of a significant amount of mass transfer occurring during bubble formation, were



obtained by extrapolating the bubble rise data to zero liquid height. This was done after the coalescence end effect had been eliminated. To investigate these findings in greater detail, direct studies of mass transfer during drop or bubble formation have been undertaken by Licht and Pansing [5], Heertjes et. al. [42], Groothuis and Kramer [53], Ilkovic [54, 55], Michels [56], Popovich et. al. [57] and Calderbank and Patra [8].

Five different models for mass transfer during drop or bubble formation have been reported in the literature [5,42,53,(54,55),56]. All of them have been based on the unsteady-state diffusion of the solute in the continuous phase. Different assumptions describing the hydrodynamics of the system were superimposed to obtain explicit equations for the mass transfer occurring up to a time 't'. Popovich et. al. [57] assumed that the variation of drop surface area with time could be suitably described by the equation

$$A = k_1 t^{n_1} \text{-----} (2.19)$$

and reduced all the final equations developed in the five models mentioned above to two common equations of the form

$$N'_A = \text{const}(k_1)(C_A^s - C_A^b) \sqrt{\frac{D}{\pi}} t^{[(2n_1-1)/2]} \text{-----} (2.20)$$



Where  $N'_A$  is the mass transfer rate at time 't'. The equation for total mass transfer in time 't' is given by integration of equation 2.20 and is of the form

$$N'_A = \text{const}(k_1)(C_A^s - C_A^b) \sqrt{\frac{D}{\pi}} t^{[(2n_1+1)/2]} \text{-----} (2.21)$$

The constant in equations 2.20 and 2.21 is a function of the exponent  $n_1$  and assumes a different value for each model proposed. In all cases the value of  $n_1$  has been assumed to be close to 2/3 which is the value for a dispersed spherical particle growing uniformly with time. For a spherical drop or bubble  $k_1 = \pi d_f^2 T_f^{-2/3}$  and equations 2.20 and 2.21 take the form

$$N'_A = \text{const} (k_1)(C_A^s - C_A^b) \sqrt{D\pi} d_f^2 T_f^{-2/3} t^{1/6} \text{-----} (2.22)$$

and

$$N_A = \text{const} (C_A^s - C_A^b) \sqrt{D\pi} d_f^2 T_f^{-2/3} t^{7/6} \text{-----} (2.23)$$

To obtain the mass transfer during drop formation to the point of release, substitution of  $t = T_f$  reduces the above equations to

$$N'_A = \text{const} (C_A^s - C_A^b) \sqrt{D\pi} d_f^2 T_f^{-1/2} \text{-----} (2.24)$$







and

$$N_A = \text{const } (C_A^s - C_A^b) \sqrt{D\pi} d_f^2 T_f^{1/2} \text{-----} (2.25)$$

Popovich et. al. [57] found that their data corresponded most closely to the model proposed by Ilkovic [54, 55], wherein the value of the constants for equations 2.20 and 2.21 were predicted to be 1.53 and 1.31 respectively.

The study of Popovich et. al. [57] was confined to liquid drops of approximately 0.2 to 0.4 mm. in diameter. The assumption of spherical drop growth under these conditions is reasonable. However, bubbles forming at an orifice are generally less nearly spherical than liquid drops, especially if the bubble size is of the order of 0.5 to 1.0 cms. Under these circumstances the analogy of liquid drop behaviour to gas bubbles and the applicability of the above given theory is uncertain.

Calderbank and Patra [8] studied the mass transfer during bubble formation for carbon dioxide, acetylene and sulphur dioxide bubbles in water. They proposed an empirical relation for the variation of bubble surface area with time which is given as

$$\frac{A}{A_m} = 1 - \left( \frac{T_f - t}{T_f} \right)^{n_2} \text{-----} (2.26)$$

where  $(T_f - t)$  is the life expectancy of the element of surface generated at time  $t$ . For low bubble frequencies



ranging from 0.2 to 2.0  $\text{sec}^{-1}$ . the value of the exponent  $n_2$  was reported as  $1.86 \pm 0.06$ . Assuming that each fresh element of surface formed does not mix with the older ones, and using the theory of diffusion into a semi-infinite body, a Higbie type of equation was proposed [9]. This equation is valid for short exposure times only and is given as

$$\frac{d^2 N_A}{dt dA} = (C_A^s - C_A^b) \sqrt{\frac{D}{\pi(T_f - t)}} \text{-----} (2.27)$$

Substituting for  $dA$  from equation 2.26 and integrating between time limits 0 and  $T_f$  the following equation may be obtained.

$$N_A = \frac{4n_2}{2n_2 + 1} (C_A^s - C_A^b) \sqrt{\frac{D}{\pi}} A_m T_f^{1/2} \text{-----} (2.28)$$

With the value of  $n_2 = 1.86$  the above expression becomes

$$N_A = 1.56 (C_A^s - C_A^b) \sqrt{\frac{D}{\pi}} A_m T_f^{1/2} \text{-----} (2.28a)$$

Assuming that the quantity of material transferred as given by equation 2.28a is the same as would be dissolved if the bubble were formed instantaneously and remained at its maximum size for a time  $T_f$ , Calderbank et. al. [8] suggested the following equation for the mass transfer coefficient.



$$k_{Lav} = 1.56 \sqrt{\frac{D}{\pi T_f}} \text{-----} (2.29)$$

They have reported that a good agreement was obtained with equation 2.28 for the carbon-dioxide-water and acetylene-water systems. No data to this effect has been reported. As mentioned earlier, mass transfer during bubble rise may be given by equation 2.14 another form of which is given as

$$k_{Lav}^1 = 2 \sqrt{\frac{D}{\pi t_e}} \text{-----} (2.30)$$

Where  $t_e$  is the time taken by the bubble to rise a distance equal to its diameter at its vertical rise velocity. Based on this fact, Calderbank and Patra [8] have suggested that the mass transfer rate during bubble formation is not enhanced but is lower than that during bubble rise.

### 2.3 Effect of Surface Activity on Bubble Behaviour and Mass Transfer

A substance whose addition, even in extremely small quantities, changes the surface properties of the system under study, is termed as being surface active. The effect of surface active agents on bubble behaviour and on mass transfer from bubbles has been and still is a subject of extensive controversy, even though work on this variable has been in progress for some time.







There is more agreement amongst authors on the effect of surface active agents on bubble behaviour than there is on its effect on mass transfer.

Addition of surface active agents to the system being investigated reduces the surface tension. As a result of this, gas bubbles formed at a given orifice for identical conditions of gas flow rate are smaller in size than a system where no surface active agents have been added. Reduced surface tension and reduced bubble sizes have been observed by Kintner et. al. [58], Leibson et. al. [14], Towell et. al. [26], Coppock and Meiklejohn [13], Benzing and Myers [17], Eversole et. al. [20], Calderbank et. al. [33] and Zieminski et. al. [59]. However, reduction of bubble size is not indefinite but is a function of concentration of the surfactant in the system. Coppock and Meiklejohn [13] and Benzing and Myers [17], have reported that at low concentrations of the surfactant, the bubble size drops sharply, but as the concentration of the surface active agent is continuously increased beyond a certain limit, the bubble size remains unaffected. Benzing and Myers [17] attributed this to the fact that at higher concentrations the bubble surface is rapidly oriented to its new state, that is to say that the static surface tension value is reached in a very short period of time. Zieminski et. al. [59] have also reported a similar observation, but in addition they state that the structural



character of the surfactant is also a function in deciding how much a bubble size may be reduced. The long carbon chain compounds produce smaller bubbles, and hence a larger interfacial area for a given gas holdup.

The rate of coalescence of gas bubbles, after formation at the orifice, is also significantly reduced by the addition of surfactants. The use of surfactants is, therefore, sometimes advised for systems where coalescence becomes a serious problem. Experimental data on coalescence reduction has been presented by Zieminski et. al. [59] and Towell et. al. [26].

The mass transfer coefficient in a gas-liquid system is a function of bubble size and is reported to increase with increase of bubble size [27,33]. Since surface active agents reduce bubble size Calderbank et.al. [33] concluded that the mass transfer coefficient drops with addition of surface active agents. This phenomena has been supported by Hammerton and Garner [30], Baird and Davidson [60] and Leonard and Houghton [27]. On formation, a gas bubble has some surface disturbances referred to as rippling; this is considerably reduced by the action of surfactants in the system and the surface stagnation thus created reduces the mass transfer coefficient [60].

In contradiction to the above observations Quigley et. al. [11] have reported that no effect on mass transfer was observed by the addition of the surfactant





Alkanox to the system but their data indicates that the surfactant was added in fairly large concentrations, which may have been the reason for their conclusions. However, Houghton et. al. [61] have reported an increase in mass transfer coefficient in a system containing 0.05% byweight of Lubrol W.

The above facts indicate that both the concentration of the surfactant and its chemical nature govern the effect that its addition would have on the mass transfer coefficient. This was indeed found to be so. Zieminski et.al. [59] have reported that for a given surfactant, the mass transfer coefficient increases with concentration of the surfactant in the low concentration range and then drops at higher concentration finally levelling off at a fairly constant value at very high concentrations. The maxima of the mass transfer coefficient was found to occur at lower concentrations of the surfactant for higher carbon chain compounds.

Further work in this field is necessary to really establish the role played by surface active agents in dispersed systems.





## Chapter 3

### THEORY

#### 3.1 Evaluation of Mass Transfer Coefficient

The liquid phase mass transfer coefficient can be defined by the following equation.

$$\frac{dN_A}{dt} = k_L A(t) (C_A^s - C_A^b) \text{-----} (3.1)$$

Where  $N_A$  is the number of moles of solute transferred,  $C_A^s$  and  $C_A^b$  are the concentrations of the solute in the liquid phase at the interface and in the bulk respectively. The area available for mass transfer is given by  $A$  which is a function of the bubble age  $t$ .

The equation may be rearranged to give

$$dN_A = k_L (C_A^s - C_A^b) A(t) dt \text{-----} (3.2)$$

and integrating between the appropriate limits

$$N_A = k_{L_{av}} (C_A^s - C_A^b) \int_0^{T_f} A(t) dt \text{-----} (3.3)$$

Where  $k_{L_{av}}$  is the averaged mass transfer coefficient during the time of formation  $T_f$  of one bubble. The derivation of equation 3-3 assumes that the solute concentrations at the



interface and in the bulk are constant over the time  $T_f$ . If the resistance to mass transfer at the interface is negligible then  $C_A^S$  represents the solubility of the solute in the liquid phase.

Integration of equation 3.3 requires the value of the interfacial area  $A$  as a function of time. To determine  $C_A^b$  it is necessary that a suitable analytical procedure be available. Then if  $N_A$  is known,  $k_{Lav}$  can be evaluated.

### 3.2 Evaluation of Bubble Area and Volume

A record of bubble growth can be obtained by taking motion pictures of the bubble during formation. The evaluation of bubble area and volume from photographs requires that the bubble periphery be described either by a continuous function or by discrete data points. Then if the bubbles are assumed symmetrical about the axial direction, the surface and volume can be determined by the following integrals:

$$S = 2\pi \int_{a_1}^{b_1} f(v) \sqrt{1+f'(v)^2} dv \text{ -----(3.4)}$$

and

$$V = \pi \int_{a_1}^{b_1} f^2(v) dv \text{ -----(3.5)}$$

where  $f(v)$  is the function describing the periphery and



$f'(v)$  is the derivative of  $f(v)$  with respect to  $v$ . Thus, two approaches may be used to describe the bubble periphery.

### Continuous Function Approach - Computer Program I

Figure 2 represents a cardioid whose equation in the parametric form is

$$r = a(1 + \cos \theta) \text{ -----(3.6)}$$

If the portion of the curve below AB is sliced off the remaining part of the curve takes the shape of a gas bubble in its early stages of formation and immediately after detachment from the orifice. A continuous function which will describe the periphery of such a flat bottomed bubble can therefore be obtained by modifying the equation for a cardioid. Three modifications were attempted:

$$(i) \quad r = a(k + \cos \theta) \text{ -----(3.7)}$$

$$(ii) \quad r = a(k + \cos^n \theta) \text{ -----(3.8)}$$

$$(iii) \quad r^n = a(k + \cos \theta) \text{ -----(3.9)}$$

Equation 3.9 was found not to converge to a definite value of 'n' and was therefore discarded. The method used for testing whether or not equations 3.7 or 3.8 could be used to describe the bubble periphery was as follows:

Considering equation 3.7

$$r = a(k + \cos \theta) |_{\theta=0} = a(k+1) \text{ -----(3.10)}$$





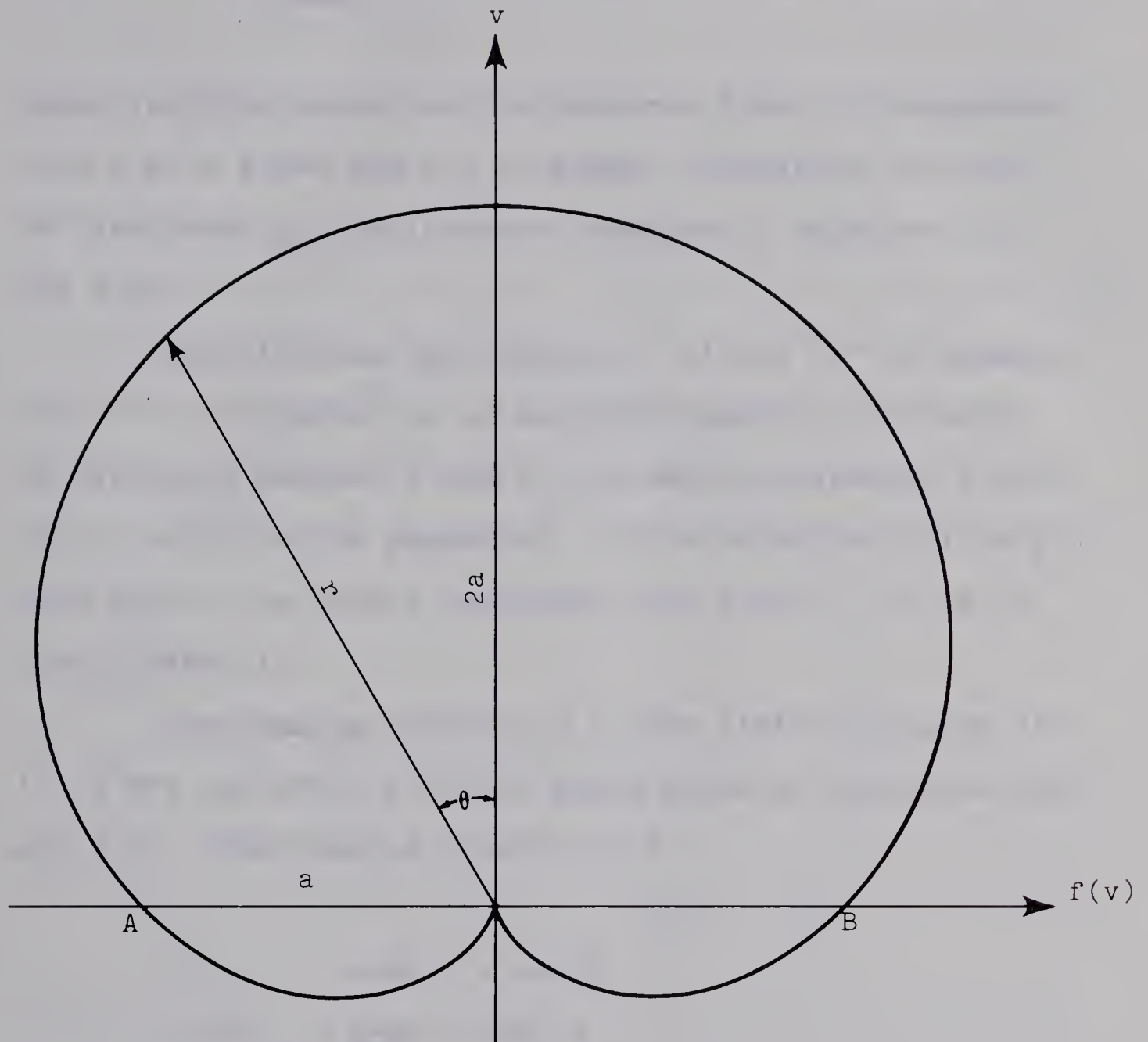


Figure 2: The Cardioid:  $r = a(1 + \cos \theta)$



$$r = a(k + \cos \theta) \big|_{\theta=\pi/2} = ak \text{ ----- (3.11)}$$

These limiting values can be measured from a photographic film i.e.  $r$  @  $\theta=0$  and  $\pi/2$  is known. Therefore 'a' and 'k' are known by simultaneous solution of equation 3.10 and 3.11.

Substituting the values of 'a' and 'k' in equation 3.7, 'r' is obtained as an explicit function of  $\theta$  only. By varying  $\theta$  between 0 and  $\pi/2$  at small intervals, a plot of 'r' vs.  $\theta$  can be generated. If the equation 3.7 is a good fit of the bubble periphery, the plot of 'r' vs.  $\theta$  should match it.

Considering equation 3.8, the limiting values of 'r' @  $\theta=0$  and  $\theta=\pi/2$  are once again given by equations 3.10 and 3.11. Rearranging equation 3.8

$$r - ak = a \cos^n \theta$$

$$\text{or} \quad \frac{r - ak}{a} = \cos^n \theta$$

taking logs of both sides

$$\log \left( \frac{r - ak}{a} \right) = n \log \cos \theta$$

$$\text{or} \quad \log \left( \frac{r}{a} - k \right) = n \log \cos \theta \text{ ----- (3.12)}$$

'a' and 'k' are known through equations 3.10 and 3.11. A data table of  $\log \left( \frac{r}{a} - k \right)$  vs.  $\log(\cos \theta)$  at values of  $0 \leq \theta \leq \pi/2$



can therefore be constructed using a photographic film.

The value of the exponent 'n' can be determined by a least square fit through the linear plot of  $\log(\frac{r}{a}-k)$  and  $\log(\cos \theta)$ .

'r' is then known explicitly as a function of  $\theta$  only. The generated data of 'r' vs  $\theta$  may be plotted to see if the fit obtained is satisfactory. Figure 3 shows both equations 3.7 and 3.8 plotted in comparison to the actual bubble periphery obtained from a film. The match shows clearly that equation 3.8 gives a satisfactory fit and can be used to develop the surface area and volume of flat-bottomed bubbles.

From Figure 2

$$v = r \cos \theta \text{ -----(3.13)}$$

$$\text{and } f(v) = r \sin \theta \text{ -----(3.14)}$$

$$f'(v) = \frac{d f(v)}{dv} = \frac{d f(v)}{d\theta} \cdot \frac{d\theta}{dv} \text{ -----(3.15)}$$

Using equations 3.13, 3.14 and 3.15 with equation 3.8 and substituting in equations 3.4 and 3.5, the following equations may be obtained.

$$S = 2\pi \int_{\pi/2}^0 -a^2 \sin \theta (k + \cos^n \theta) [\sin^2 \theta \{k + (n+1) \cos^n \theta\}^2 + \{n \sin^2 \theta \cos^{n-1} \theta - k \cos \theta - \cos^{n+1} \theta\}^2]^{1/2} d\theta \text{ -----(3.16)}$$





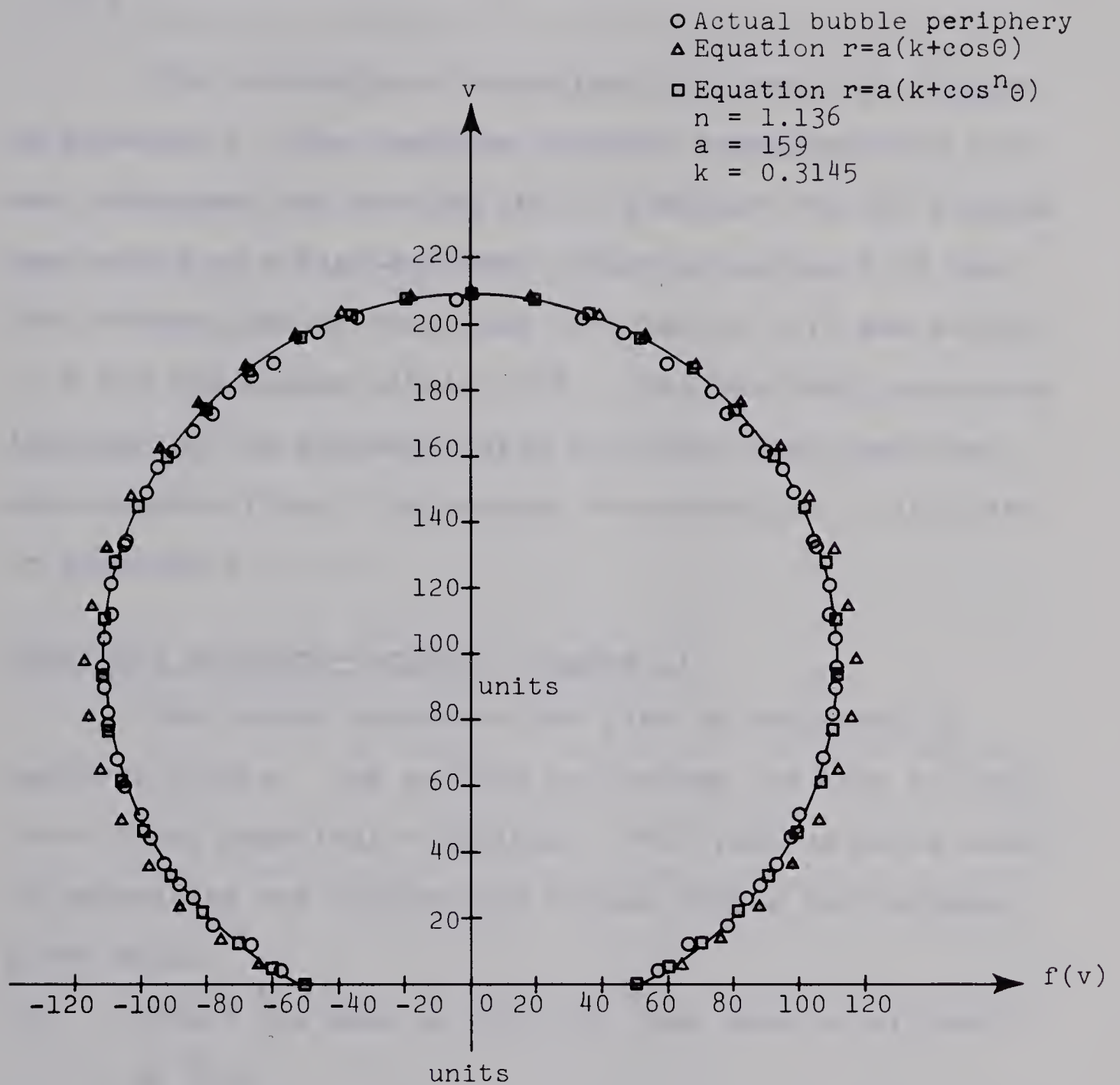


Figure 3: Plot of Equations 3.7 and 3.8 in comparison to actual Bubble Periphery



and

$$V = \pi \int_{\pi/2}^0 a^3 \sin^3 \theta (k + \cos^n \theta)^2 \{k + (n+1) \cos^n \theta\} d\theta \text{ ----- (3.17)}$$

The derivation of equations 3.16 and 3.17 is given in Appendix A. The complete analysis using equation 3.8 was programmed for the IBM 360/67 computer and the program was tested on a flat-bottomed sphere of radius 3.03 cms. The surface area as evaluated by equation 3.16 was within 0.5% and the volume within 1.0%. This includes the errors inherent in the procedure used to obtain data from the photographic film. The program documentation is included in Appendix B.

#### Numerical Approach-Computer Program II

The bubble periphery can also be described by discrete points. The surface and volume can then be evaluated using numerical techniques. The various steps used in generating the surface and volume follow the sequence given below:

- (i) Obtain raw data of  $(f(v), v)$  from bubble periphery on film.
- (ii) Smooth the raw data using Forsythe Orthogonal Polynomials [62].
- (iii) Find the derivative  $f'(v)$  at the smoothed points using Lagrangian Interpolation [63].
- (iv) Obtain  $g(v) = f(v) \sqrt{1 + f'(v)^2}$



- (v) Use Lagrangian Interpolation to generate equispaced data for  $g(v)$  [64].
- (vi) Integrate using Newton Cotes fourth order formula with  $m$  subintervals to obtain surface area [65].
- (vii) Use Lagrangian Interpolation to generate equispaced data for  $f(v)$  [64].
- (viii) Integrate using method (vi) above to obtain bubble volume.

The equations used for the Forsythe Polynomials, Lagrangian Interpolation and Newton Cotes Integration have been included in Appendix A.

This approach can be used to evaluate the surface and volume for any symmetrical shape and thus can be used for bubbles during the entire period of formation and during bubble rise provided the symmetry is not destroyed.

Program II was used for the analysis of data obtained during this investigation. The program was tested with the same test data as for program I and the errors are within 0.1% for surface and 1.0% for volume. The reliance on the surface area and volume is however limited to 1 to 2% because the errors involved in obtaining data from the film are of this magnitude.

### 3.3 Evaluation of the Sample Size Required For Bubble Analysis - Computer Program III

The procedure described here can be used to determine





the sample size of bubbles that is representative of a given normally distributed population. Such an analysis is necessary so as to determine the number of bubbles that must be analyzed in order to obtain reliable values for bubble volume and surface area.

If the size of the given population is  $N_p$  and it consists of individual readings  $x_i$ ;

Then the required sample size  $N_s$  is given by

$$N_s = \left[ \frac{\sigma_\ell \times \mu}{(\bar{x}_s - \bar{x})} \right]^2 \text{-----} (3.18)$$

Where  $\mu$  is the standard deviation from the mean and is given by

$$\mu = \sqrt{\frac{\sum_{i=1}^{N_p} (x_i - \bar{x})^2}{N_p - 1}} \text{-----} (3.19)$$

$\bar{x}$  is the mean of the population and is given by

$$\bar{x} = \frac{\sum_{i=1}^{N_p} x_i}{N_p} \text{-----} (3.20)$$

$\sigma_\ell$  is a factor which indicates the confidence that an event will fall within the sample size chosen.

Depending on the accuracy required the term  $(\bar{x}_s - \bar{x})$  may be made as small as desirable. The smaller this term is the more stringent are conditions of tolerance and hence the larger the sample size required. For this investigation



equation 3.18 has been used in the following form

$$N_s = \left[ \frac{\sigma_l \times \mu}{0.01 \bar{x}} \right]^2 \text{-----} (3.21)$$

A program to carry out the above analysis was written and is given in Appendix B.

### 3.4 Liquid Velocity Profile

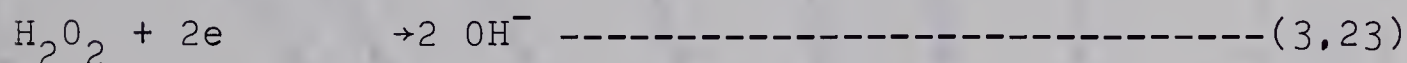
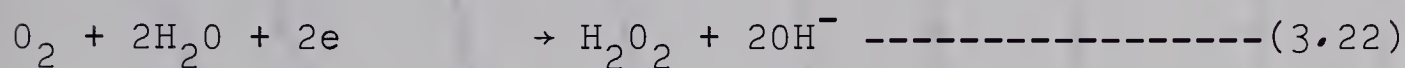
Liquid velocity profiles can be used to characterize the hydrodynamics of the system when mass transfer during bubble formation is measured under conditions of a superimposed liquid velocity. The principle of polarography as applied to electrochemical reactions can be used to measure velocity profiles. This method is also used to measure the instantaneous mass transfer coefficient in electrochemical reactions [66].

When a current is passed through an aqueous solution of a supporting electrolyte, transfer of dissolved oxygen in the water takes place towards the cathode surface. This current which is called cathodic current, increases with applied voltage across the electrodes until the cathode surface becomes completely polarized. Thereafter the current reaches a limiting value called the diffusion current. In this range of applied voltage the transfer of oxygen is diffusion controlled. The magnitude of this current increases with increasing velocity of the liquid.

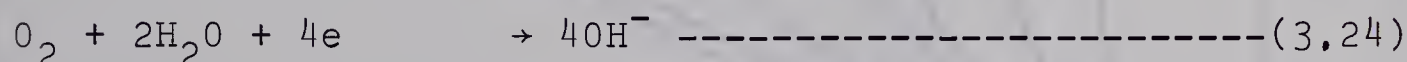


If the applied voltage is maintained at a value corresponding to the diffusion current, point liquid velocities may be measured by following the change in the magnitude of the diffusion current. A sample set of curves for different liquid velocities in the full applied voltage range is given in Figure 4. The chemical reactions that take place at the cathode are as follows:

The cathode reaction is



The overall reaction is



According to Faraday's Law a general relationship may be written for the electrochemical current at a dropping mercury or solid stationary electrode.

$$i = \bar{n}F \frac{dN^*}{dt} \text{-----}(3.25)$$

Where  $i$  is the diffusion current,  $\bar{n}$  the number of electrons taken up (in this case 4) and  $F$  the Faraday Number. Since the current is the diffusion current, the rate of transfer







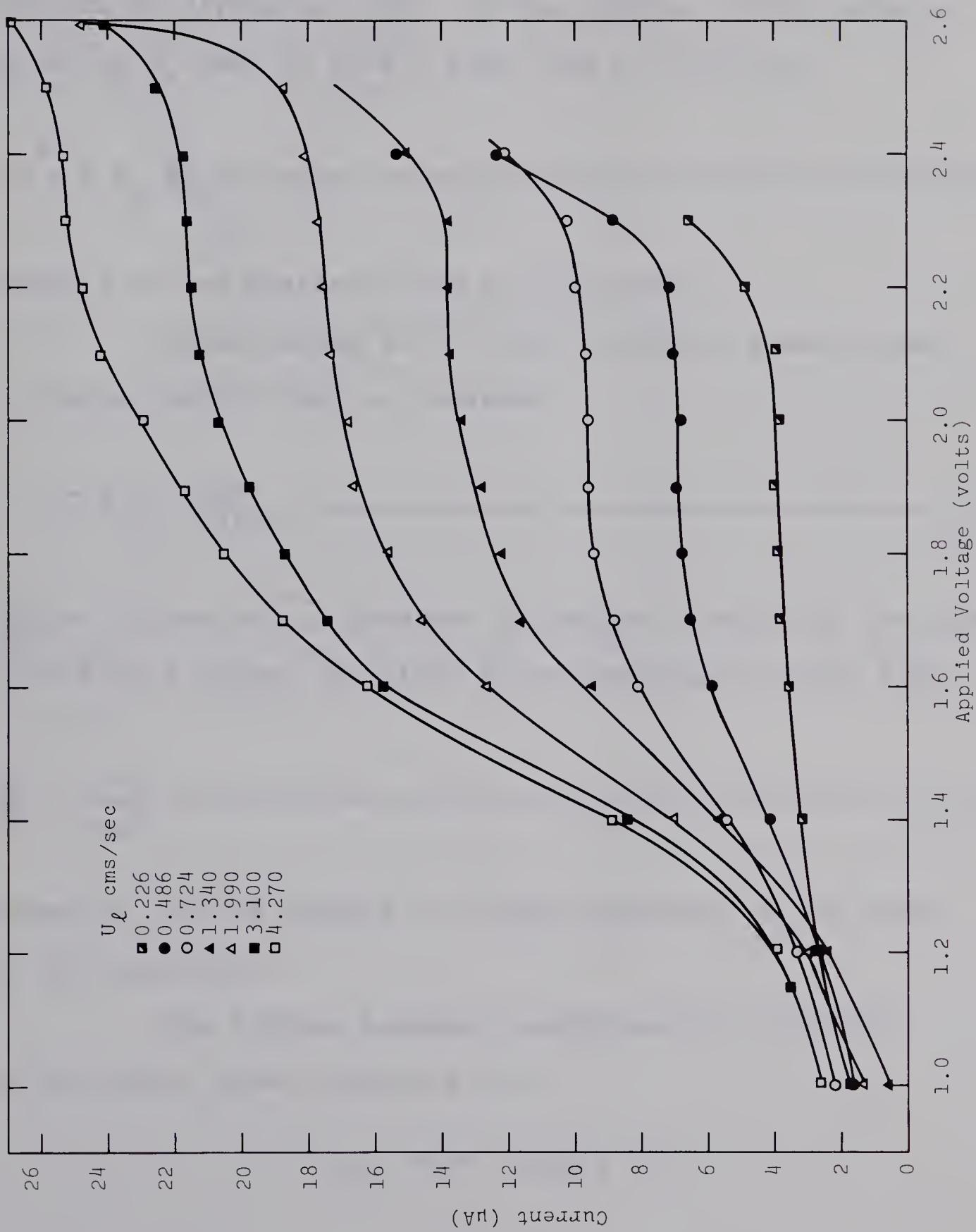


Figure 4: Plot of Polarographic Current vs. Applied Voltage



$\frac{dN^*}{dt}$  is the transfer of the depolarisor per unit area of cathode by diffusion only. If the cathode surface area is given by  $A_e$  then by Fick's first law of diffusion

$$dN^* = D A_e \frac{\partial C}{\partial x} dt \text{ ----- (3.26)}$$

Where  $x$  is the distance from the electrode.

Substituting in 3.25 the following equation for diffusion current may be obtained.

$$i = \bar{n} F A_e D \left( \frac{\partial C}{\partial x} \right)_{x=0} \text{ ----- (3.27)}$$

$\frac{\partial C}{\partial x}$ , the concentration gradient of oxygen in water, is evaluated from Fick's second law given by an expression of the type

$$\frac{\partial C}{\partial t} = D \frac{\partial^2 C}{\partial x^2} \text{ ----- (3.28)}$$

Equation 3.28 is subject to change depending on the shape of the electrode.

The initial boundary conditions for solution of the above given equations are

$$C_{x,t} = C^* \quad \text{for } t = 0$$

$$C_{x,t} = C_o \quad \text{for } t > 0.$$



where  $C^*$  is the concentration of the oxygen in the bulk of the liquid and  $C_0$  is the concentration of oxygen on the cathode surface and is zero for the limiting diffusion current. The final solution is of the form

$$i = \bar{n} F A_e \frac{DC^*}{\sqrt{\pi D t}} = \bar{n} F A_e k_{le} C^* \text{ ----- (3.29)}$$

where  $k_{le}$  is the mass transfer coefficient.

The mass transfer coefficient  $k_{le}$  is a function of the dimensions of the electrode, the properties of the electrode material and of the liquid velocity. For a given electrode the mass transfer coefficient is determined by the value of the liquid velocity, and the limiting diffusion current may therefore be measured as a function of liquid velocity.





## CHAPTER 4

### EXPERIMENTAL

#### 4.1 General Approach

The purpose of this investigation was to measure the liquid phase mass transfer coefficient of carbon-dioxide in water at bubble formation. The method employed was to determine the difference between the volume of gas fed to an orifice and the product of the number of bubbles and their mean detached volume. Due to the fact that the mass transfer from air to water in an air-water system is negligible the difference mentioned above should be essentially zero. The validity and accuracy of the experimental technique was thus determined using the air-water system.

The volumetric flow rate of a gas through the orifice can be related to the bubble volume and frequency by the following equation.

$$G = vV \text{ ----- (4.1)}$$

Where G is the gas flow rate in cc/sec., v the bubble frequency in sec<sup>-1</sup> and V the volume equivalent of one bubble in cc.

For both the carbon-dioxide-water and the air-water



systems, the gas flow rate and bubble frequency were adjusted to the desired value so that stable bubbles were formed at the orifice. High speed motion pictures of the bubbles were then taken during formation. This was done for a range of frequencies. The motion pictures were then analyzed with a digitizer and the surface area and volume determined.

If the volume of the detached bubble evaluated from photographs be designated as  $V^*$  then  $(V - V^*)$  should be zero for the air-water system assuming that the solubility of air in water is negligible. This was the criteria used to ascertain whether or not the experimental techniques used are feasible. For the carbon-dioxide-water system  $(V - V^*)$  gives a measure of the mass transfer to the liquid phase and using this information the mass transfer coefficient can be evaluated.

#### 4-2 Experimental Equipment

A schematic diagram of the experimental set up is given in Figure 5.

Carbon dioxide gas from a high pressure cylinder (1) is saturated with water in a packed saturator (2) and then metered through a soap film meter (3). The gas pressure at the soap film meter is regulated by a pressure regulating valve and recorded on a pressure gauge (5). A micrometer needle valve (4) is installed in the gas line



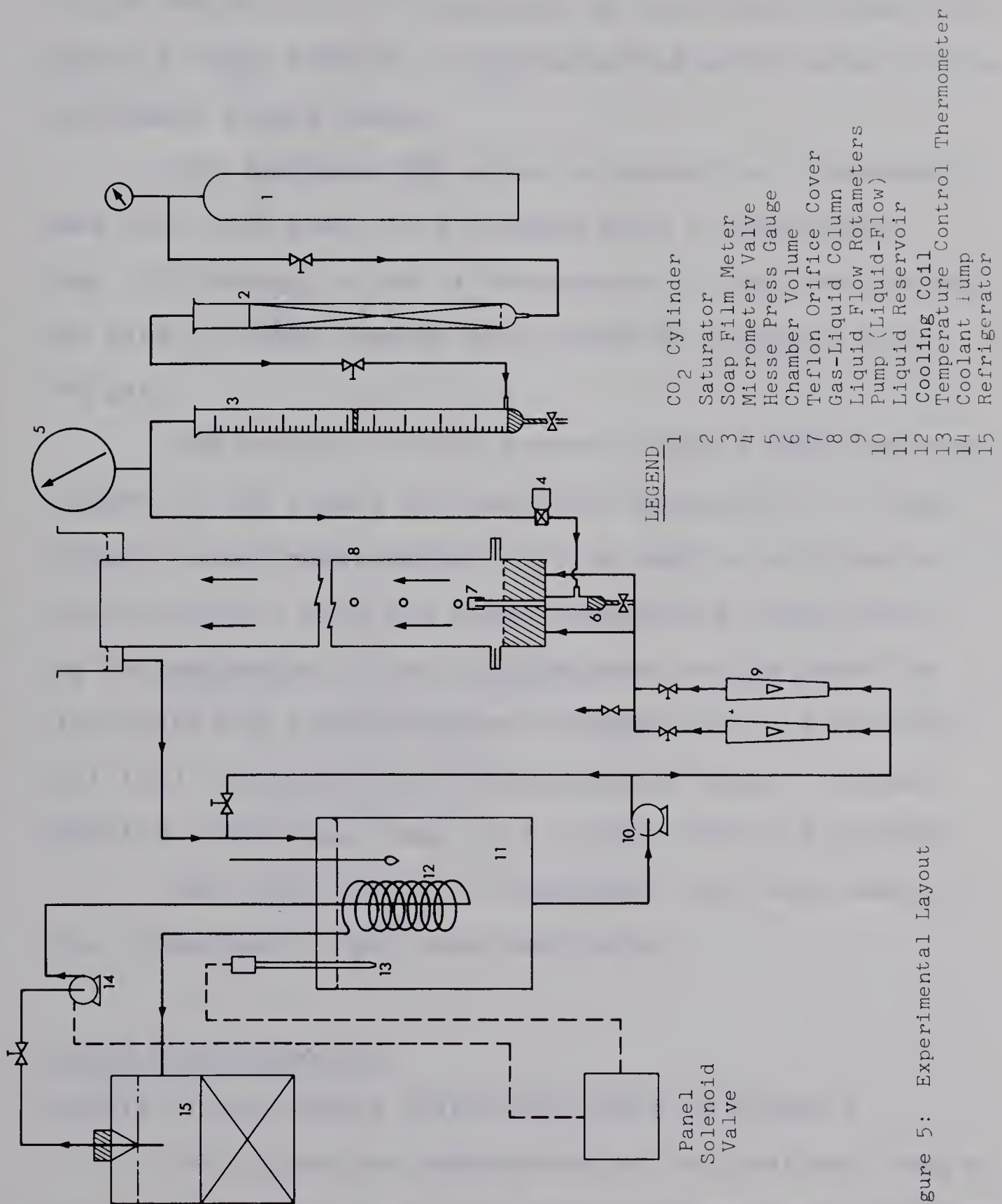


Figure 5: Experimental Layout





so that small gas flow rates may be accurately metered. The gas then passes through an adjustable chamber volume (6) to the orifice (7) installed in the bubble column (8) where it forms bubbles in demineralized water which is the continuous liquid phase.

The demineralized water is stored in a reservoir tank (11) from where it is pumped with a centrifugal pump (10) through a set of rotameters (9) into the column. The flow of water through the column is cocurrent with the gas.

The analysis of the system requires that the temperature of the liquid be controlled accurately. A temperature control thermometer (13) is used to activate a control circuit when the water temperature rises above the desired value. When this happens cooling water is circulated from a refrigerated storage (15) to a cooling coil (12) immersed in the demineralized water. A small capacity centrifugal pump (14) is used for this purpose.

Individual pieces of equipment that were used in this investigation are described below.

### Column and Accesories

Details of the bubble column are given in Figure 6.

The column was constructed in two sections from a lucite pipe of 20.2 cms. I.D. and 0.635 cms. wall thickness with a total height of 100 cms. The two sections of the



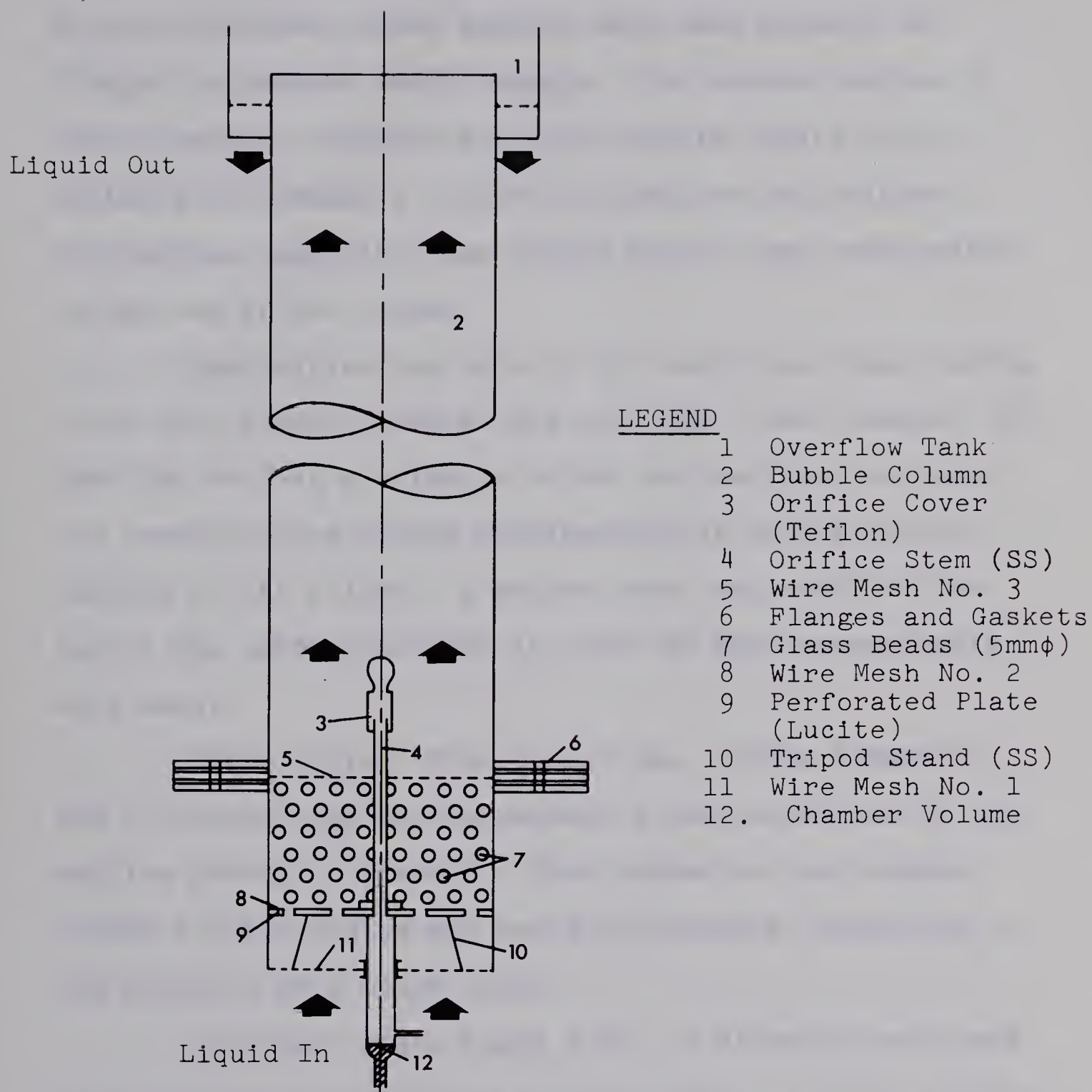


Figure 6: Details of the Experimental Column



FIG. 1. A cross-section of the pump assembly.

column were flanged together with stainless steel bolts. Nylon reinforced rubber gaskets were used between the flanges to prevent water leakage. The bottom section of the column was provided with four liquid inlets and a suitable attachment to secure the orifice in position. An overflow tank with four liquid outlets was constructed on the top of the column.

The orifice was made of 316 stainless steel tubing 0.408 cms. inside diameter and 23.0 cms. total length. To hold the orifice a suitable holder was designed to match the corresponding socket provided for it in the bottom section of the column. A teflon cover was made for the top of the orifice so that it could be made non-wettable with water.

Tygon tubing of about 1.0 cms. inside diameter and 15.0 cms. long was connected to the bottom end of the orifice through a glass T. This served as the chamber volume for the system and could be varied by adjusting the position of a pinch cock.

Spherical glass beads 5 mm. in diameter were used to pack the bottom section of the column. A total packing depth of 16.5 cms. was provided. To support the packing, a circular, perforated lucite plate, three stainless steel wire meshes and a stainless steel wire stand were used. The manner in which the glass beads were supported is shown in Figure 6.







Eight sample points to sample the liquid in the column were constructed by drilling equispaced holes through the column wall at different heights from the flanged end. A liquid height of about 80 cms. could thus be sampled if desired. Special sample points in level with the top edge of the orifice were also constructed.

### Flow Measurement

Rotameters were used to measure liquid flow rates. These were

- (i) Brooks model R13M-25-3 for 0 to 2 litres/sec
- (ii) Brooks model R10M-25-3 for 0 to 0.42 litres/sec.

The floats in both rotameters were made of stainless steel.

A soap film meter was used to measure gas flow rates. It was constructed from a precision 50 cc glass burette. The time taken to displace a given volume of gas through the burette was a measure of the gas flow rate.

### Feed Water Tank

The feed water tank was constructed from 1/2 inch lucite plate to hold a maximum capacity of 100 gallons. Six 3/4 inch openings were provided for lines.



### Connecting Lines

Liquid lines were made from 3/4 inch inside diameter pvc pipe. Three types of lines were used for gas flow. These were, 1/4" inside diameter copper tubing, 1/4" inside diameter polyflow tubing and 3/8 inch diameter tygon tubing.

### Valves and Pumps

Rubber diaphragm valves were used to control liquid flow rates and a Whitey Needle Valve Model 22RS4 316 SS was used to control the gas flow rate.

A centrifugal pump model 882E "Dynapump" manufactured by Crane Co. was used for liquid flow. The pump specifications were stainless steel impellor, carbon steel body, 1/2 HP, 3/4 inch suction and discharge ports.

### Gas Saturators

Two columns were provided for saturating air and carbon-dioxide with water. They were constructed from glass tubes 2.5 inch in diameter and were packed with 5 mm spherical glass beads. The top part of the columns was left unpacked to dampen fluctuations in gas flow. The columns were about three fourths full of water.

### Temperature Control System

In order to maintain a constant temperature of the water used in the bubble column, a temperature control



scheme was used. The layout of this scheme is presented schematically in Figure 5.

The various pieces of equipment that were used to control the water temperature were:

- (1) A refrigerator to maintain the cooling water temperature to about  $0.5^{\circ}\text{C}$ .
- (2) A centrifugal pump for circulation of the cooling water.
- (3) A cooling coil made from 316 stainless steel. This was immersed in the water reservoir.
- (4) A solenoid valve to actuate the pump when the water temperature rose above the set point.
- (5) A Beckmann thermometer to specify the set point and to actuate the solenoid valve when the temperature rose above the desired value.

The temperature of the demineralized water could be controlled within  $\pm 0.05^{\circ}\text{C}$ . by this control scheme.

#### Titration Equipment

All titrations, to standardize solutions and to measure the concentrations of carbon-dioxide in water, were done electrometrically in an atmosphere of nitrogen. The following pieces of equipment were used for the purpose.

- (1) A Coleman Metrion II model 28A AC pH meter
- (2) A Coleman 3-450, shielded glass, heavy duty, screw base, glass electrode





(3) A reference electrode model Coleman, Calomel

3-510, screw base, capillary type liquid function.

A photograph of the titration equipment as set up is given in Figure 7.

#### Water Demineralisers

Demineralised water was used throughout the experimental investigation. The quality of the water was maintained at  $\leq 0.1$  ppm impurity as NaCl. Mixed bed resin cartridges no. 0808 were used in a Double Chamber Type, Model BD-22 Pressure Bantam Demineralizer manufactured by Barnstead still and sterilizer Co.

The demineralizer is shown in Figure 8.

#### Equipment for Measurement of Liquid Velocity Profiles

The electrical circuit required for the measurement of velocity profiles in the column is given in Figure 9.

The magnitude of the diffusion current in electrochemical reactions of the type that occur in this system, is quite small and therefore difficult to measure. In order to facilitate this measurement, a high resistance was installed in series with the cathode and the voltage across this resistance was measured by using a digital voltmeter. The magnitude of this voltage was taken to be a measure of the point liquid velocity in the column. In order to obtain the absolute value of the latter the plat-



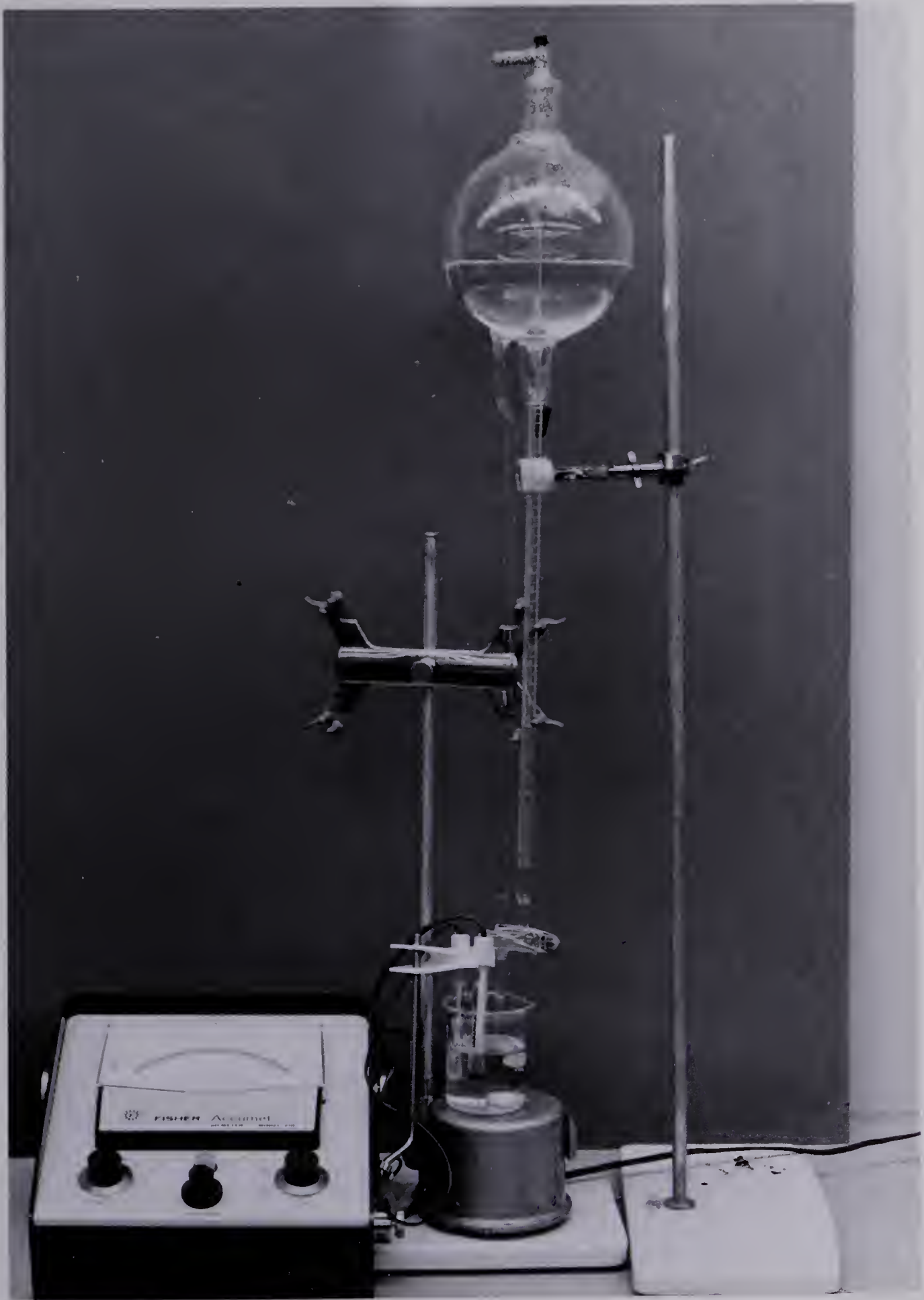


Figure 7: Photograph of Titration Equipment





Figure 8: Photograph of Demineralizer







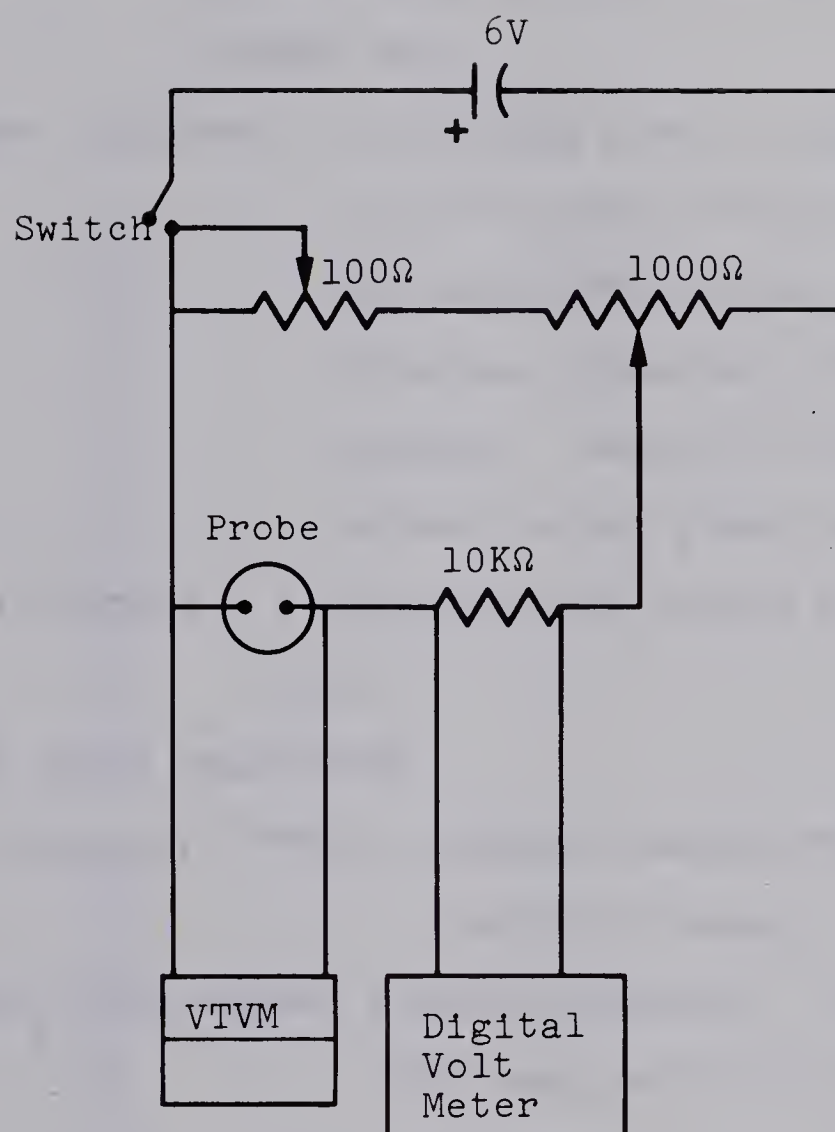


Figure 9: Circuit Diagram for Measurement of Liquid Velocity Profile



inum probes were calibrated to relate the digital voltage with liquid velocity. Details of the equipment used for the measurement of velocity profiles are given below:

Digital voltmeter - Series 4800 digital voltmeter, four figure display made by Non-Linear Systems Inc.

Platinum probe (cathode) - A platinum wire of diameter 0.02184 inches shielded and insulated from outer casing. This was prepared in the laboratory. Details of its construction are given in Figure 10.

Platinum foil (Anode) - A thin one inch square platinum foil.

Dry cells - 6 volts equivalent.

Vacuum tube voltmeter (VTVM) - Heathkit model MM1 - The Heathkit Company.

Set of Variable Resistances (potentionmeters) - 100 ohms, 1000 ohms and 10 kilo ohms.

The platinum probes were calibrated by rotating them in a tank of water at a known velocity and measuring the digital voltage created. The electrical circuit used is given in Figure 9 and details of the tank are shown in Figure 11.



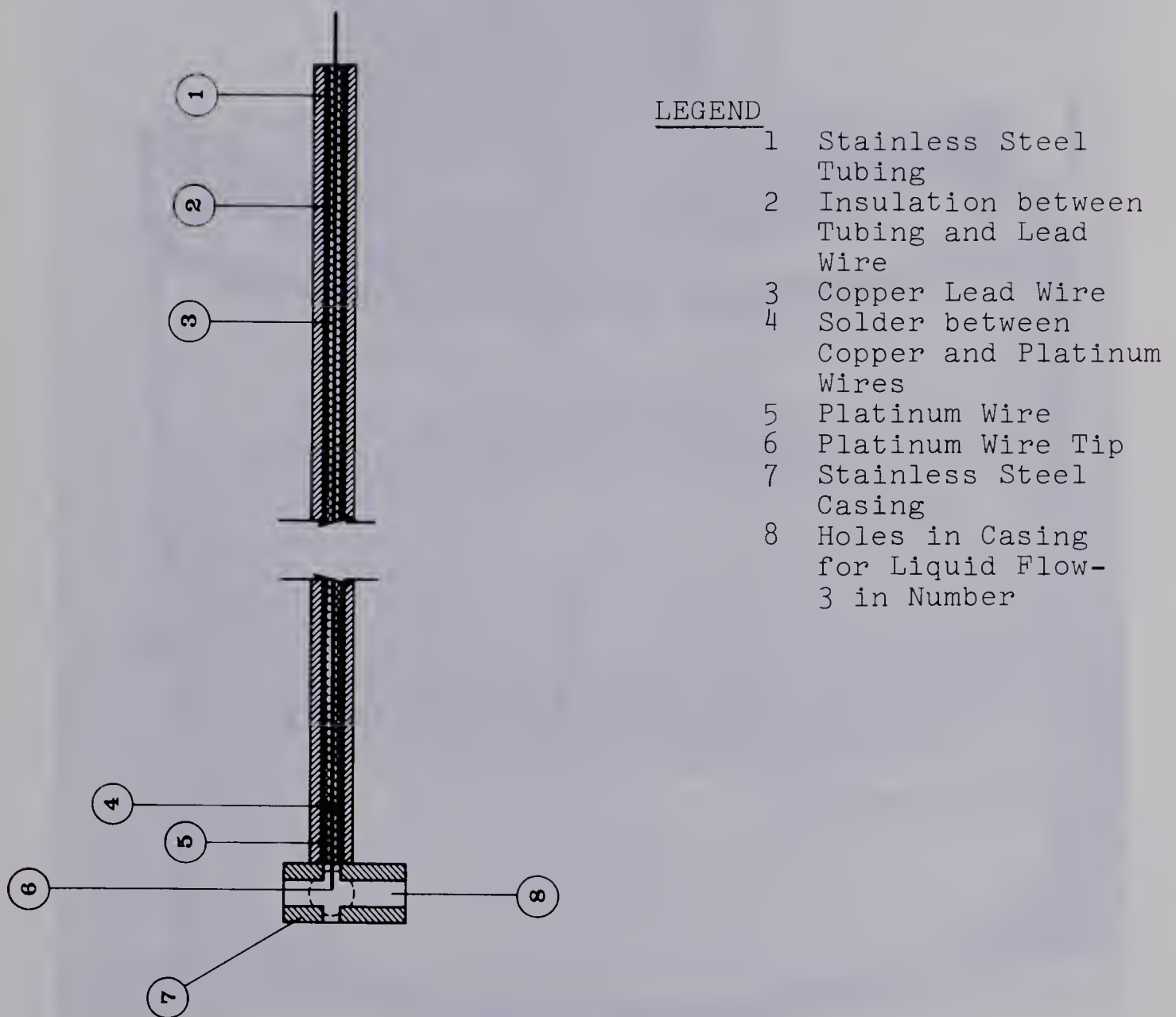


Figure 10: Details of the Platinum Probe





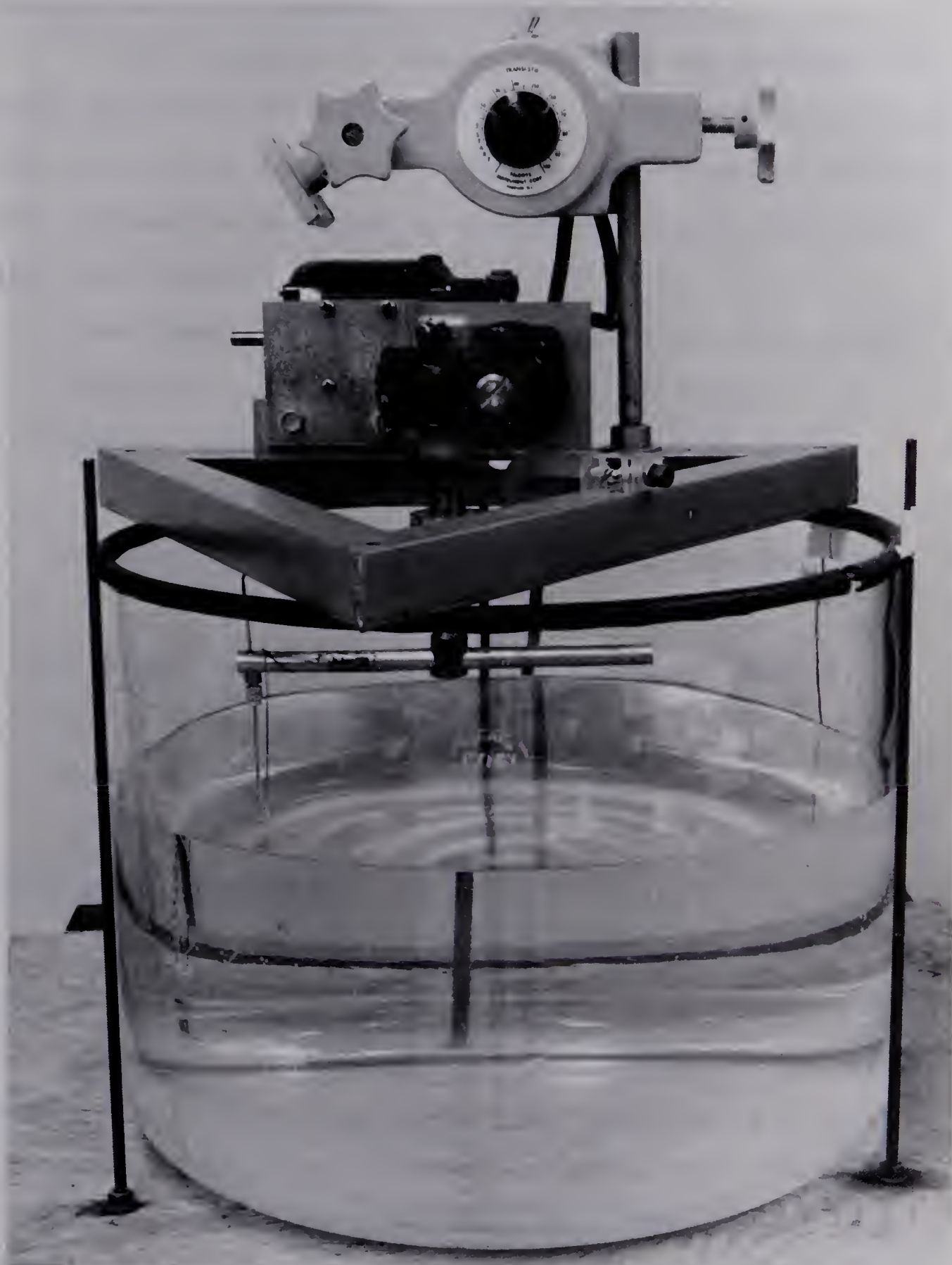


Figure 11: Photograph of the Calibration Tank



### Equipment for Measurement of Bubble Frequency.

The frequency of bubble formation was measured by using an electrical circuit as shown in Figure 12. A laser beam was used to intercept the path of bubbles and a photocell was used to generate an electrical signal. The equipment used included the following.

Laser Beam - Spectra Physics model 130B (ruby laser)

Photocell - Clairex photocell No. CL 707HM

Digital Counter - Universal counter model 361-R,

Transistor Specialities Inc.

Oscilloscope - Heathkit model EUW-25- The Heathkit Company.

Standard Voltage Source - Heathkit model EUW-16

Vacuum tube voltmeter - Heathkit model MM1

Variable resistance - 10 Kilo ohms.

### Photographic Equipment.

A schematic diagram of the photographic set up is given in Figure 13.

The gas bubbles were photographed at camera speeds ranging from 120 to 1200 frames per second using a Hycam high speed motion picture camera model K2004E. This is a 16 mm camera utilizing a rotating prism for optical compensation. It has a film capacity of 400 feet of standard thickness film but adjustments for accomodating 100 feet and 200 feet film spools are also available. The frame



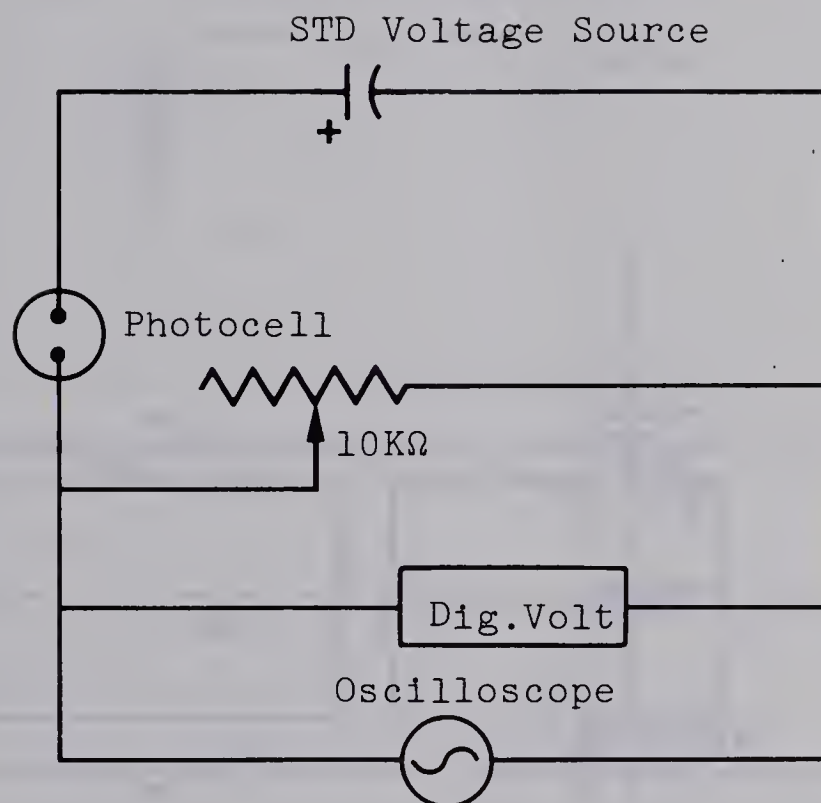
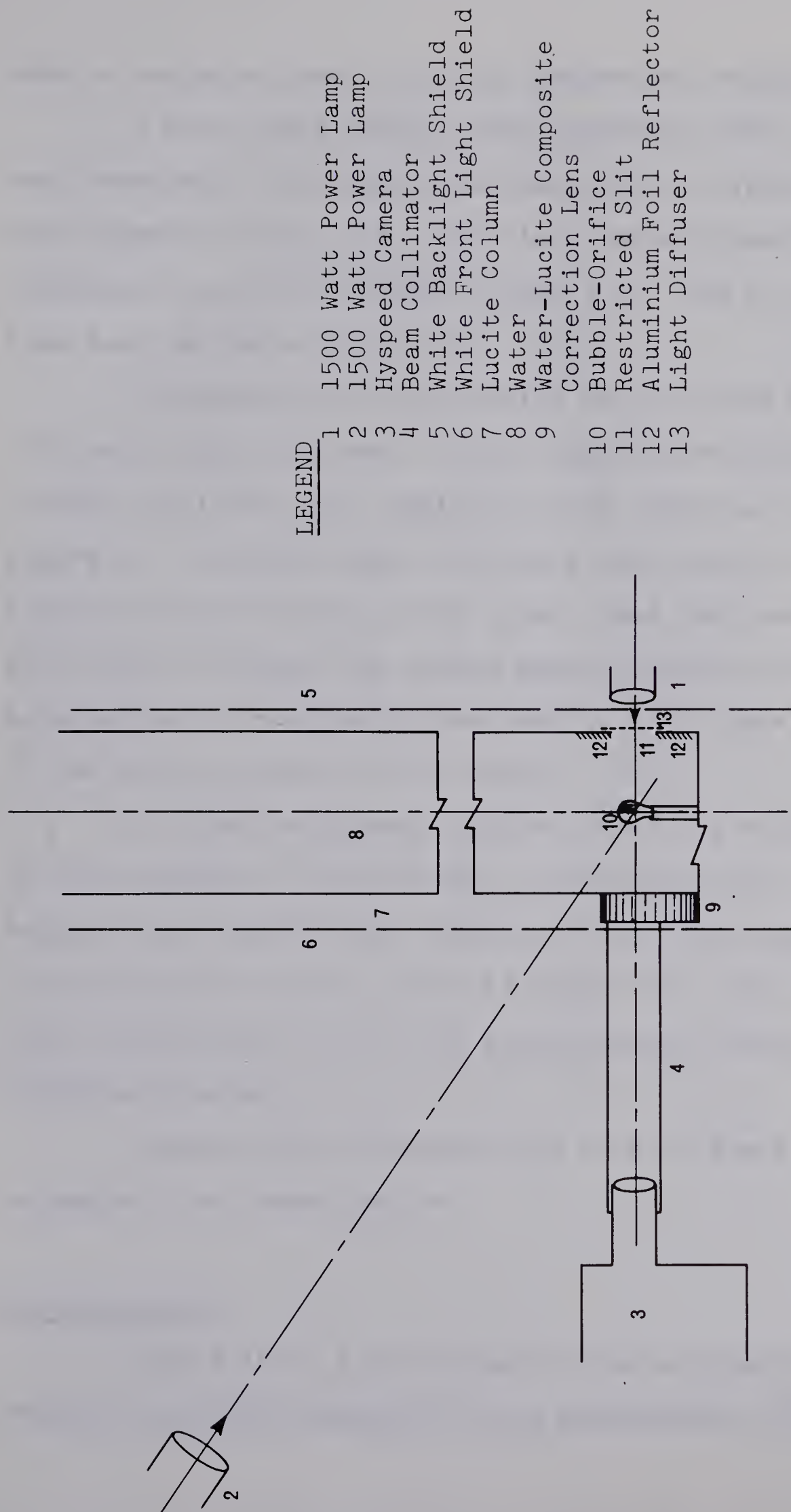


Figure 12: Circuit Diagram for Measurement of Bubble Frequency







LEGEND

- |    |                          |
|----|--------------------------|
| 1  | 1500 Watt Power Lamp     |
| 2  | 1500 Watt Power Lamp     |
| 3  | Hyspeed Camera           |
| 4  | Beam Collimator          |
| 5  | White Backlight Shield   |
| 6  | White Front Light Shield |
| 7  | Lucite Column            |
| 8  | Water                    |
| 9  | Water-Lucite Composite   |
| 10 | Correction Lens          |
| 11 | Bubble-Orifice           |
| 12 | Restricted Slit          |
| 13 | Aluminium Foil Reflector |

Figure 13: Schematic Layout of the Photographic Equipment



rate is variable from 0 to 11000 frames per second.

A Milli-Mite timing light generator model TLG-3 was connected to the camera and was used to determine the exact speeds of the film. This is a battery operated transistorized unit designed to put a 10, 100 to 1000 cycle time base on the moving film.

Illumination of the bubbles was provided with two 1500 watt high spot beams. These lights were placed to provide front and back lighting of the object as shown in Figure 13. Suitable light diffusers were provided to diffuse the light falling on the object, and heat shields were used to protect the column against thermal expansion. An aluminum foil reflector was used to facilitate lighting of the bottom surface of the bubble.

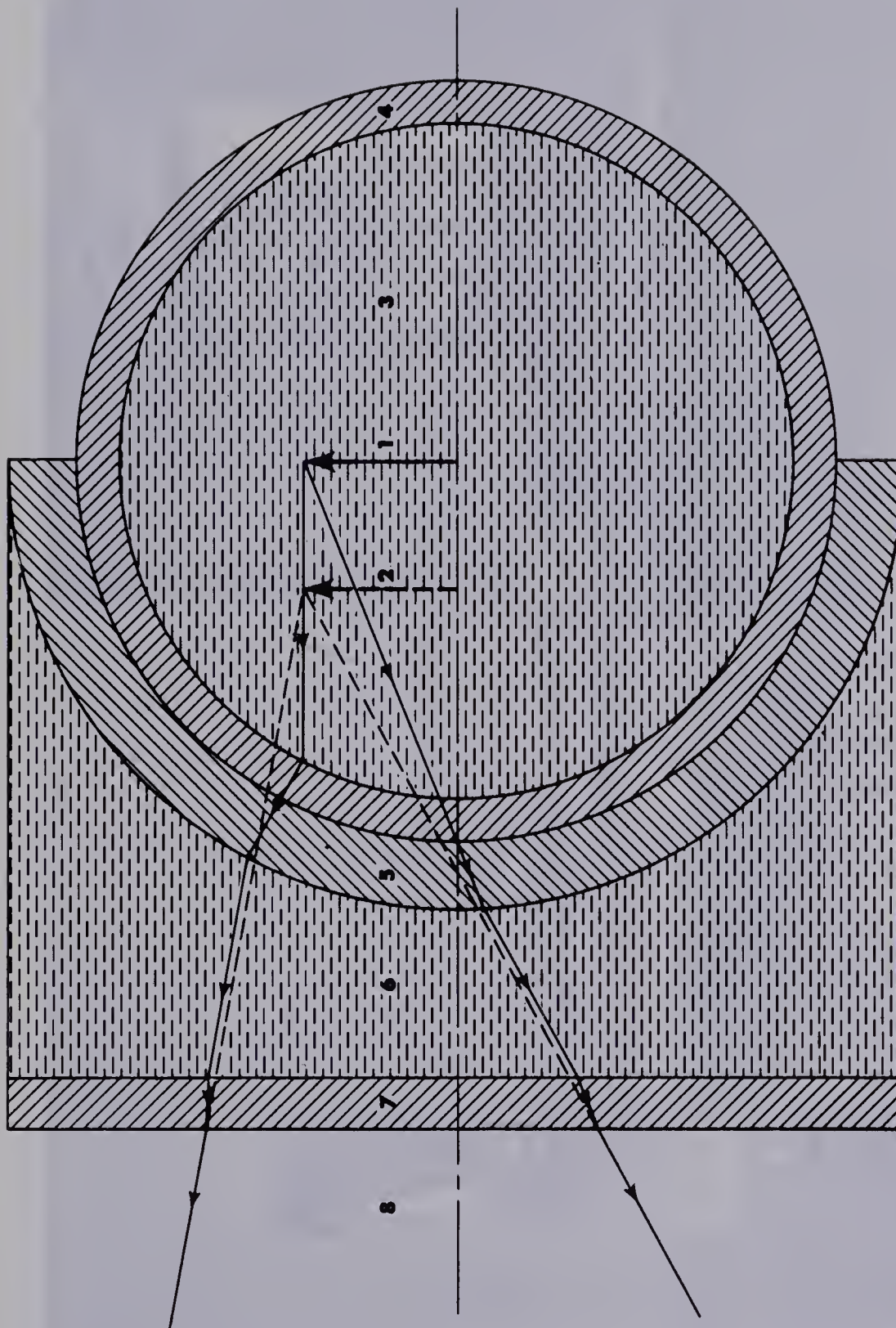
In order to prevent distortion of the bubble due to the curvature of the column, a correction lens was designed and constructed. Details of the ray diagram and the correction lens are given in Figure 14. The lens consists essentially of a hollow plano-concave lucite casing filled with water.

Eastman Tri-X reversal film type 7278 was used throughout the investigation.

#### The Digitizer.

Figure 15 is a photograph of the equipment used to measure the bubble dimensions from photographic film.





LEGEND

- 1 Object
- 2 Image
- 3 Water in Column
- 4 Lucite Column Wall
- 5 Circular Lucite Wall
- 6 Water in Correction Lens
- 7 Flat Lucite Plate
- 8 Air Atmosphere

Figure 14: Ray Line Diagram for the Correction Lens







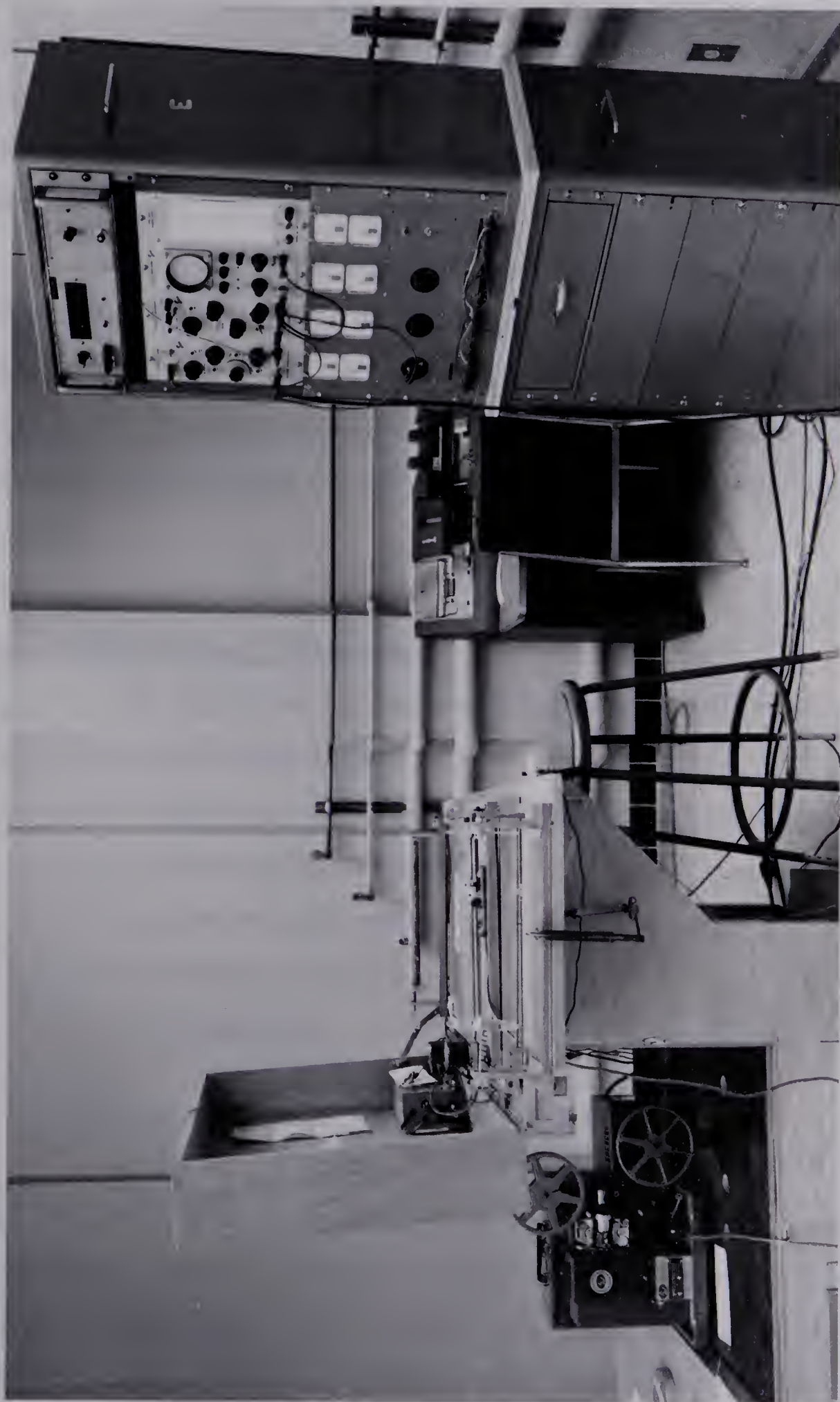


Figure 15: Photograph of the Digitizer



The film is projected on a ground glass screen using a model 224-A LW Photo Optical Data Analyzer. This is a 16 mm stop-start projector with a variable film speed. Its projection speed and stop-start action can be controlled with a remote control panel.

The projected image of the bubble can be scanned manually using a cross wire and any point (x,y) on the bubble periphery can be represented by two voltages for the x and y coordinates respectively. These voltages can be read and punched on computer cards in a pre-determined format.

#### 4.3 Experimental Procedure

The experimental procedure may be discussed under the following subheadings:

- (1) Cleaning and assembly of equipment
- (2) Photographic procedure
- (3) Experimental runs
- (4) Analysis of film
- (5) Precautions

##### 1. Cleaning and assembly of equipment

In order to obtain reliable and reproducible results for both the bubble behaviour and mass transfer it was important that the system be cleaned carefully and thoroughly to avoid contamination. Particular care was taken to avoid any oily material from getting into the system. To do this,





rubber gloves were used to handle all the equipment during the process of cleaning and assembly.

Glass beads used for packing the bottom section of the column were cleaned by immersing them in concentrated chromic acid for at least a period of forty eight hours. They were then rinsed repeatedly with demineralized water and left to dry. The orifice tube, its teflon cover, the rubber gaskets and the wire meshes were washed thoroughly using a detergent and were then rinsed with water and dried with air. In order to improve the non-wetting characteristics of the teflon cover, it was left immersed in acetone for a short period of time. The main column, reservoir tank and connecting lines were cleaned by recycling demineralized water with detergent through the system. A period of about three to four hours was considered to be sufficient for this purpose. Fresh batches of demineralized water were used to rinse the system free of detergent. This was done for as many as ten or fifteen times, and each batch of water was drained after a maximum of one hour.

The importance of careful cleaning cannot be over emphasized. Some runs were conducted where adequate care was not devoted for this purpose and it was found that unstable bubbles were formed at the orifice giving a poor reproducibility of bubble frequency.

Details of the assembly of the column and its accessories are given in Figure 6. Experience with the





system has shown that particular attention should be paid to certain aspects of column assembly. These include the following:

- (a) In order to avoid air entrappment in the packing, the glass beads should be introduced into the column by displacement of water. Entrapped air interferes with measurement of bubble frequency and tends to give a non-uniform liquid velocity profile.
- (b) For the same reason as in (a) the wire meshes should be wetted from the bottom up when the column is filled with water.
- (c) The glass beads should be uniformly distributed through the entire cross-section of the column. This is done to ensure a reasonably flat liquid velocity profile.
- (d) Before the rubber gaskets are placed in position, both flanges should be dried. This prevents water leakage from the flanges.
- (e) A torque wrench should be used to tighten the nuts and bolts holding the two flanges together. Diametrically opposite bolts should be tightened in sequence. This ensures an even pressure on the rubber gaskets and prevents water leakage.

## 2. Photographic procedure.

Figure 13 gives a schematic arrangement of the photographic set up.

The correction lens (9) was secured tightly with



the wall of the column (7) eliminating any air gap between the lens and the column wall as far as possible. The aluminum foil reflector (12) was then wrapped around the base of the column in such a way that the square hole (11) was in line with the top of the orifice and the gas bubble. Two high spot lights (1, 2) were placed in position so as to provide back and front lighting of the gas bubble as shown in Figure 13. A light collimator (4) was adjusted between the high-speed camera (3) and the correction lens so that extraneous light from the environments could be prevented from getting into the camera. The camera was mounted on a suitable stand (not shown in the figure) and its level was adjusted so that the camera lens was in direct line with the object. The camera stand was then locked in that position. Light shields (5,6) and the light diffuser (13) were then provided so as to completely mask the column from direct lighting.

The following procedure was used to photograph the bubbles during the course of an experimental run.

The camera was threaded with a 400 ft. roll of 16 mm film and the millimite cycle timer was hooked into the receptacle provided for it in the camera. The desired timing frequency and the photographing speed were then set on the cycle timer and camera respectively. Both high spot lights were turned on and the light intensity was measured through the collimator by using a suitable exposuremeter.





The camera was then accurately focussed on the orifice keeping the lens aperture wide open and making sure that the correction lens is full of water. The lens aperture was then adjusted according to the reading of the exposure-meter. To prevent any motion of the camera during filming, it was locked in position after the above mentioned setting. After adjusting the variables pertinent to the experiment to their desired values the camera switch was turned on and the desired footage of film was exposed.

### 3. Experimental runs.

To carry out an experimental run with air or carbon dioxide the following steps were followed:

- (a) Admit gas (air or  $\text{CO}_2$ ) into the system through the gas line at a desired gas pressure.
- (b) Admit water into the column and adjust the rate of flow of water.
- (c) Control liquid temperature to the desired value.
- (d) Adjust the gas flow rate and obtain a constant bubble frequency.
- (e) Make final adjustments of the gas pressure.
- (f) Analyse liquid samples of  $\text{CO}_2$ -water runs only.
- (g) Take photographs.

The supply gas pressure was adjusted to the desired value and the gas was admitted into the saturator (see Figure 5) slowly and intermittently to prevent a surge of





liquid through the gas line. The control valve in the gas line was set to give the desired pressure of the gas at the soapfilm meter, and the micrometer needle valve was opened to let the gas into the column through the orifice.

Any air in the water lines and rotameter tubes was then expelled from the system through the air vent. To do this, the water inlet ports to the column were closed and air was displaced through the vent by pumping water through the lines. The column was then filled with water at a very low flow rate and the latter was adjusted to the desired value once the column was full.

The set point of the Beckman Thermometer was fixed at the desired temperature and the temperature control circuit was turned on. The flow of cooling water through the cooling coil was adjusted till the on-off control was set in operation. The liquid temperature was thus controlled within a limit of  $\pm 0.05^{\circ}\text{C}$ .

In order to measure bubble frequencies, a laser beam and photocell were used. The electrical circuit for this measurement is given in Figure 12. The position of the laser beam was adjusted such that the bubble intercepted the beam after detachment from the orifice. In order to avoid erroneous measurements at high gas flow rates due to incipient coalescence, the laser beam position was adjusted away from the central axis of the bubble. Every interruption of the laser beam was measured as a discrete signal by



the photocell and was recorded on a universal counter. An oscilloscope was used to display a waveform which was indicative of the stability of bubble formation.

The gas needle valve and the gas pressure were adjusted alternately till the desired bubble frequency and gas pressure were obtained.

For mass transfer runs with  $\text{CO}_2$ -water system, the continuous water phase has to be analysed for the amount of dissolved  $\text{CO}_2$ . This is necessary to determine the driving force for mass transfer.

The analysis of  $\text{CO}_2$  in water was done by back titrations. A blank titration with  $\text{Ba}(\text{OH})_2$  against  $\text{HCl}$  in an atmosphere of nitrogen was done for each experimental run. To titrate the water sample, a known volume of it was added to a known volume of  $\text{Ba}(\text{OH})_2$  solution and the mixture was titrated with  $\text{HCl}$  to a green end point of Bromo Thymol Blue indicator. A nitrogen atmosphere was used throughout the titration. The concentration of  $\text{CO}_2$  in water could then be determined by calculation as indicated in Appendix C. The water sample was titrated either immediately before or immediately after photographing the bubbles.

The bubbles were then photographed by using the procedure outlined in section 2. The values of all the variables pertinent to the experiment were recorded before and after filming. In order to determine the number of bubbles to be analysed to obtain a reliable value of bubble





surface and volume, it was necessary to record a representative population of bubble frequency during each experimental run.

#### 4. Analysis of films.

The films of gas bubbles taken during the experimental runs were analysed in the following fashion.

- (a) Film Editing
- (b) Determination of the number of data points per bubble.
- (c) Analysis of detached bubbles.
- (d) Analysis of bubbles during formation.

Before any data could be taken from the films, they were screened to determine the quality of the pictures obtained. A given film was accepted only if it conformed to the following specifications.

- (i) The orifice should have sharp well defined edges.
- (ii) The bubble should be sharp and completely in focus at each stage of formation.
- (iii) There should be a deep contrast of the orifice and bubble with its background.
- (iv) There should be no light reflections on the bubble edges at any time during formation and detachment.

If the pictures failed to meet any one of the above conditions, it was discarded and the experimental run was repeated.

The total number of bubbles photographed during a run were then counted and a given number of them, as required





by the statistical sample size, were isolated. A reference mark was made on the film at a position corresponding to the first bubble to be analysed. This was done so that the frame counter on the film projector could be set at zero.

In order to obtain reliable results of bubble surface area and volume it was necessary to decide on the number of data points to be taken from the periphery of one bubble. This was done by a trial and error procedure. The number of data points taken from a given bubble were increased for each trial till the bubble surface area and volume evaluated for two consecutive trials did not differ by more than an acceptable tolerance. This analysis was done for detached bubbles only. For forming bubbles the number of data points had to be increased as the bubble grew larger. The maximum number of data points were taken just prior to detachment.

Analysis of detached bubbles involved taking data from a single frame corresponding to the bubble in its detached position. This was done for each bubble of a given sample size. In order to obtain surface area and volume as a function of time, however, different frames of the same bubble were analysed at various stages of formation. Analysis of all bubbles in a given sample size would therefore require taking data from a prohibitively large number of frames. To avoid this, a representative bubble from a



sample was selected and the surface area as a function of time evaluated from it was used to determine the mass transfer coefficient.

Data from the bubble periphery was taken with the digitizer. Taking the data consisted of reading the coordinates of points on the periphery and punching these on computer cards in a pre-determined format.

## 5. Precautions.

Careful experimental work is prerequisite to obtaining reliable data from an experimental program. Success of the experimental work invariably depends on the care taken in observing a number of precautions pertinent to a particular system. Some precautions that should be observed while performing an experiment such as outlined here, are reiterated below:

### (a) Cleaning and assembly of equipment.

- (1) The quality of the demineralised water should not fall below the desired value.
- (2) Handling the components inside the column with bare hands should be avoided.
- (3) If the system is washed with detergent, adequate care should be taken to wash all the detergent away.
- (4) Some extraneous material can sometimes collect in the orifice passage. This situation should be avoided. The orifice cover should be finally cleaned with acetone.





(5) The rubber gaskets and wire meshes should be dried with air before being used.

(6) Glass beads should be evenly packed in the base of the column taking care to avoid entrapped air bubbles.

(7) The column flanges should be evenly tightened to avoid liquid leakage.

(b) Photographic Procedure.

(1) The column should be kept well shielded from direct light.

(2) The camera should be focussed on the object, with the lens aperture fully open to take full advantage of the light. The desired aperture for filming should subsequently be adjusted.

(3) Care should be taken to ensure that there is water in the correction lens before filming the bubbles.

(c) Experimental Run.

(1) The experimental run should be performed as soon as the system is cleaned and assembled to avoid deviations in data resulting from a change in the surface age of the orifice.

(2) All gas leaks in the gas line should be completely eliminated before starting a run. Any gas leak could be interpreted as additional mass transfer and this could jeopardise the purpose of the investigation.

(3) Thermal effects to the column from its surroundings should be minimised by adequate shielding.





- (4) The flow of gas through the orifice should be started before the column is filled with the liquid.
- (5) Care should be taken to avoid moving any gas lines during the experiment. This affects bubble frequency.
- (6) To prevent desorption of  $\text{CO}_2$  from the water sample, the pipette tip should dip into the  $\text{Ba}(\text{OH})_2$  solution before the sample is discharged.

(d) Analysis of films.

- (1) Film editing should be done very critically before deciding to take data.
- (2) The number of points read from the bubble periphery should be evenly distributed for good results.
- (3) All instructions for proper use of the digitizer should be closely followed.



## CHAPTER 5

### RESULTS

#### 5.1 General

The results of this investigation are subdivided as follows:

- (i) Liquid Velocity Profiles
- (ii) Air-Water System
- (iii) Mass transfer during bubble formation with the CO<sub>2</sub> water system.

#### 5.2 Liquid Velocity Profiles

The glass bead packing and the stainless steel wire meshes in the bottom section of the column were intended to provide a flat liquid velocity profile in the column. It was found, however, that due to varying degrees of channelling from different sections of the packing, the velocity profile was different across different diameters of the column. Measurements of point velocities were thus made to select the diameter along which minimum deviation from a flat profile could be obtained. Thereafter, velocity measurement were made along the selected diameter at different average liquid velocities, so as to select the liquid velocity which gave the most flat profile. These measurements were made for an orifice size of 2.1 mm, and



bubble frequencies ranging from 0 to 25 per second. All measurements were made using the air-water system. The velocity profiles obtained for average velocities of 1.0 and 2.0 cms/sec are given in Figures 16, 17 & 18. The data is reported in Appendix C.

### 5.3 Air-Water System

The air-water system was used to investigate the following:

(i) The inter-relationship of orifice diameter, bubble frequency, gas flow rate and bubble diameter. This may also be referred to as a study of bubble phenomena.

(ii) An evaluation of the technique used to measure mass transfer during bubble formation.

(iii) An observation of bubble behaviour during bubble formation.

Investigations of the effect of orifice diameter, bubble frequency, gas flow rate and bubble diameter on bubble phenomena have been carried out by a number of previous investigators. A further investigation was warranted here in order to establish a conformity of fundamental bubble behaviour with previous work in the field.

The range of experimental conditions for the air-water system are given in Table 1.





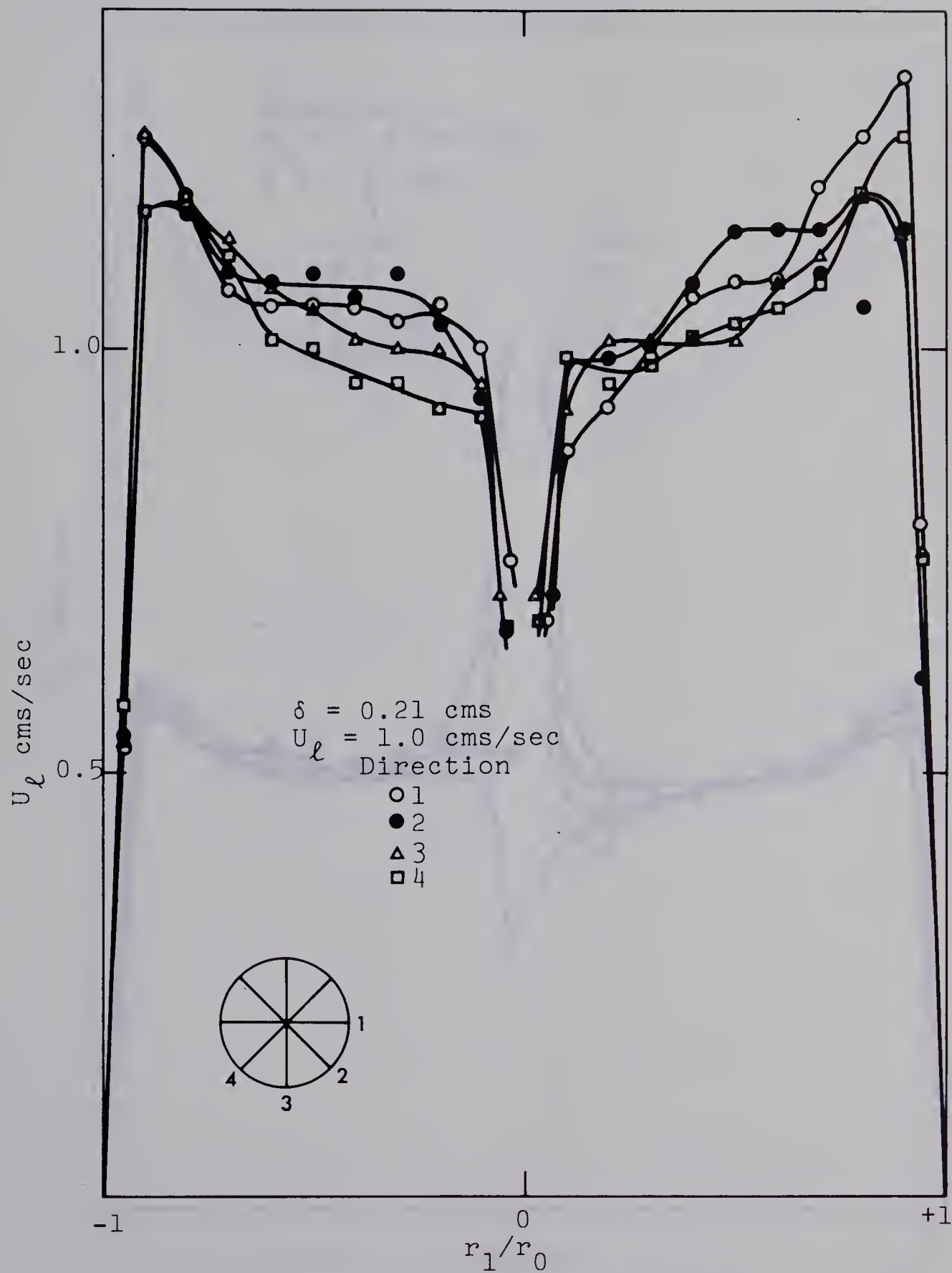


Figure 16: Plot of Liquid Velocity Profiles at Different Diametric Orientations



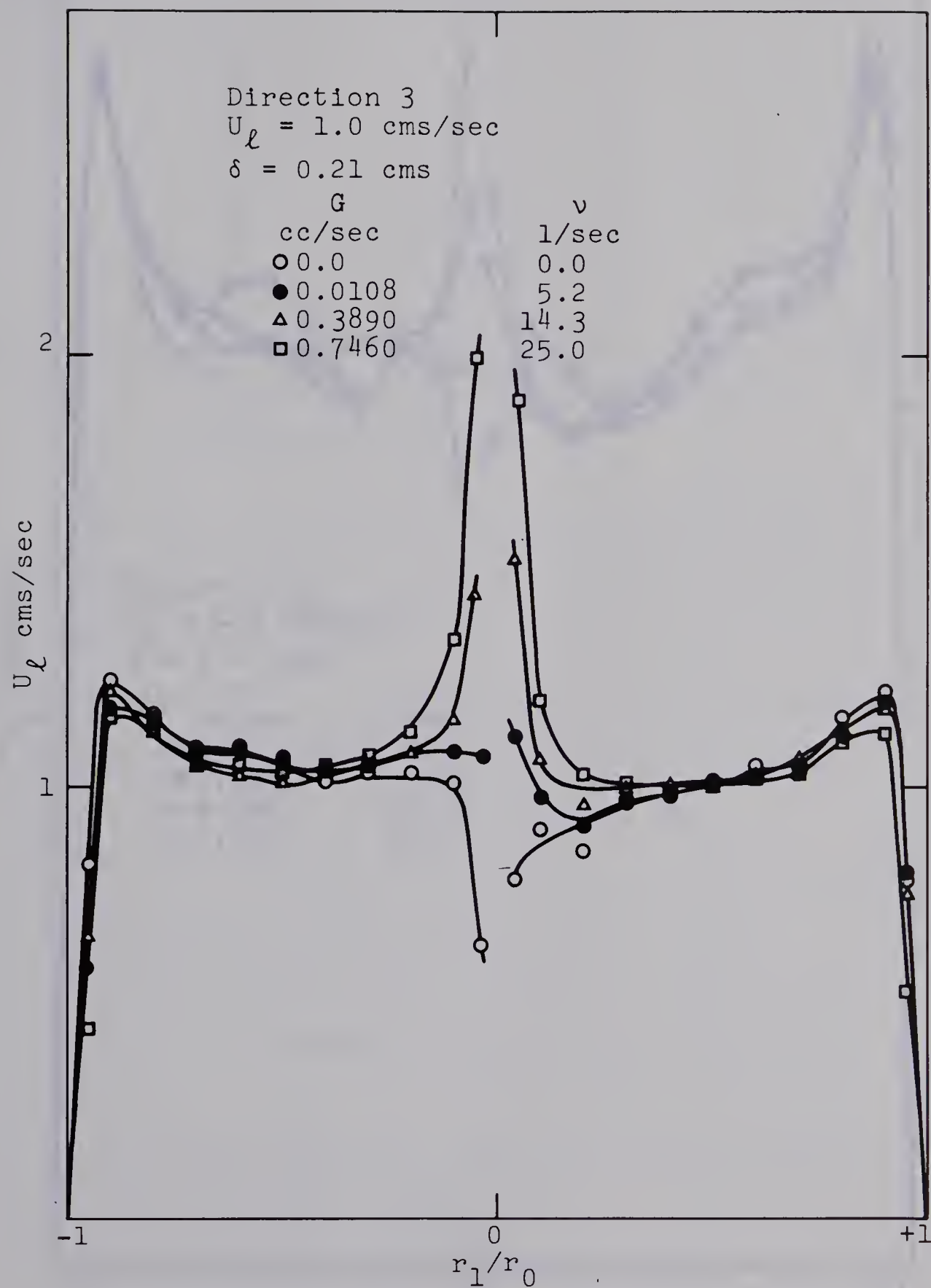


Figure 17: Liquid Velocity Profiles at Different Bubble Frequencies for an average liquid velocity of 1.0 cms/sec.



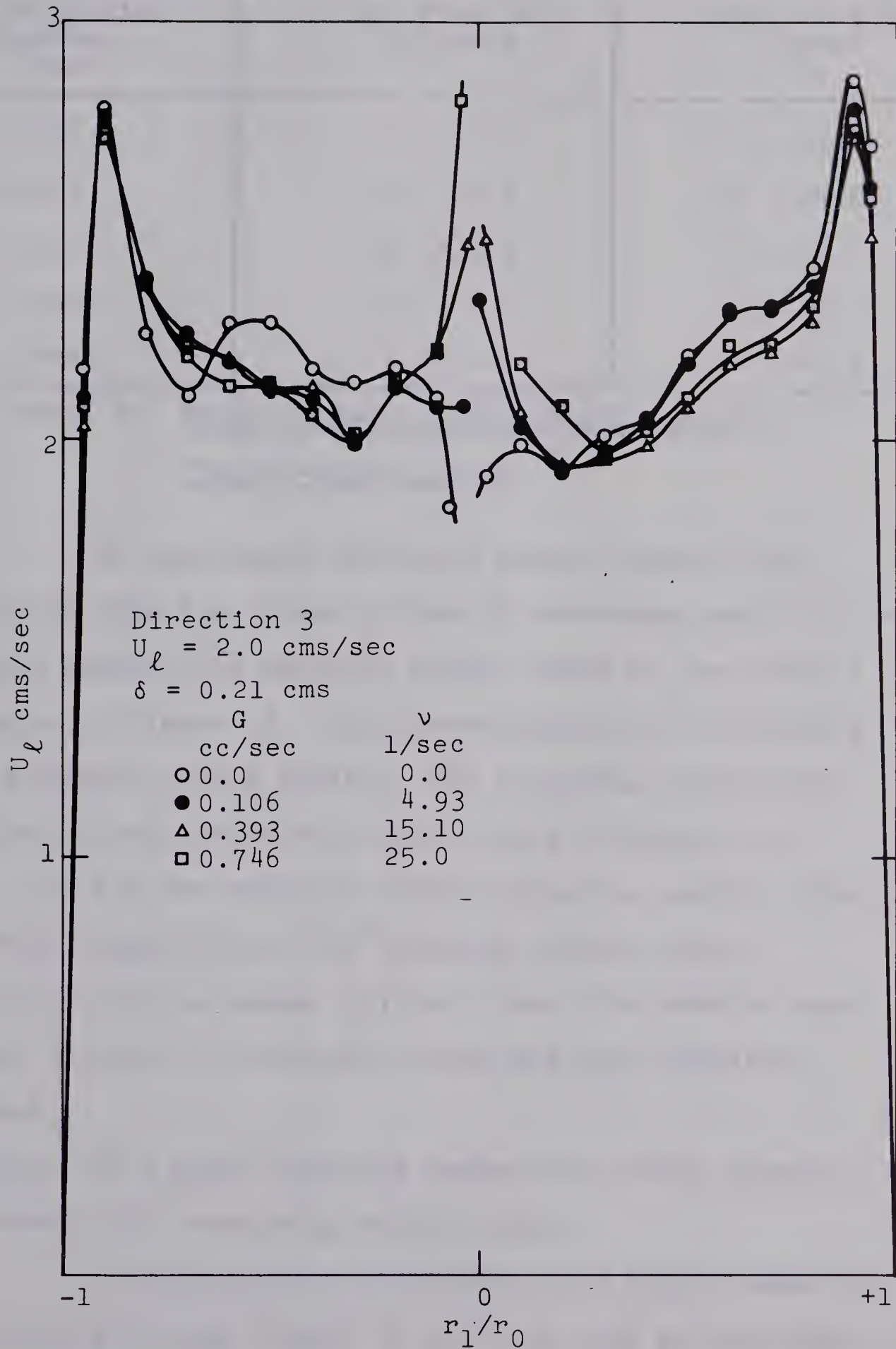


Figure 18: Liquid Velocity Profiles at different Bubble Frequencies for an average liquid velocity of 2.0 cms/sec.





Inside Orifice Diameter (cms)	Gas Flow Rate (cc/sec)	Bubble Frequency (1/sec)
0.804	0 → 14.0	0 → 14.0
0.408	0 → 50.0	0 → 25.0
0.210	0 → 11.0	0 → 26.0
0.0936	0 → 2.0	0 → 28.0
0.0485	0 → 1.0	0 → 45.0

Table 1: Range of Experimental Conditions for  
The Air-Water System

An equivalent spherical bubble diameter was evaluated from the bubble volume at detachment and this is plotted against the Reynolds number based on the orifice diameter in Figure 19. This investigation was conducted in a stagnant liquid medium. The following significant conclusions may be drawn from the data of Figure 19.

(i) For the smallest orifice size the bubble formation occurred completely in the constant volume region.

(ii) For the larger orifice sizes, the bubbles were formed in both the constant volume and the transition regions.

(iii) At a given Reynolds number the bubble diameter increased with increasing orifice size.

The existence of the transition region cannot be established through Figure 19 only but must be confirmed by reference to Figure 20 also. This is due to the fact



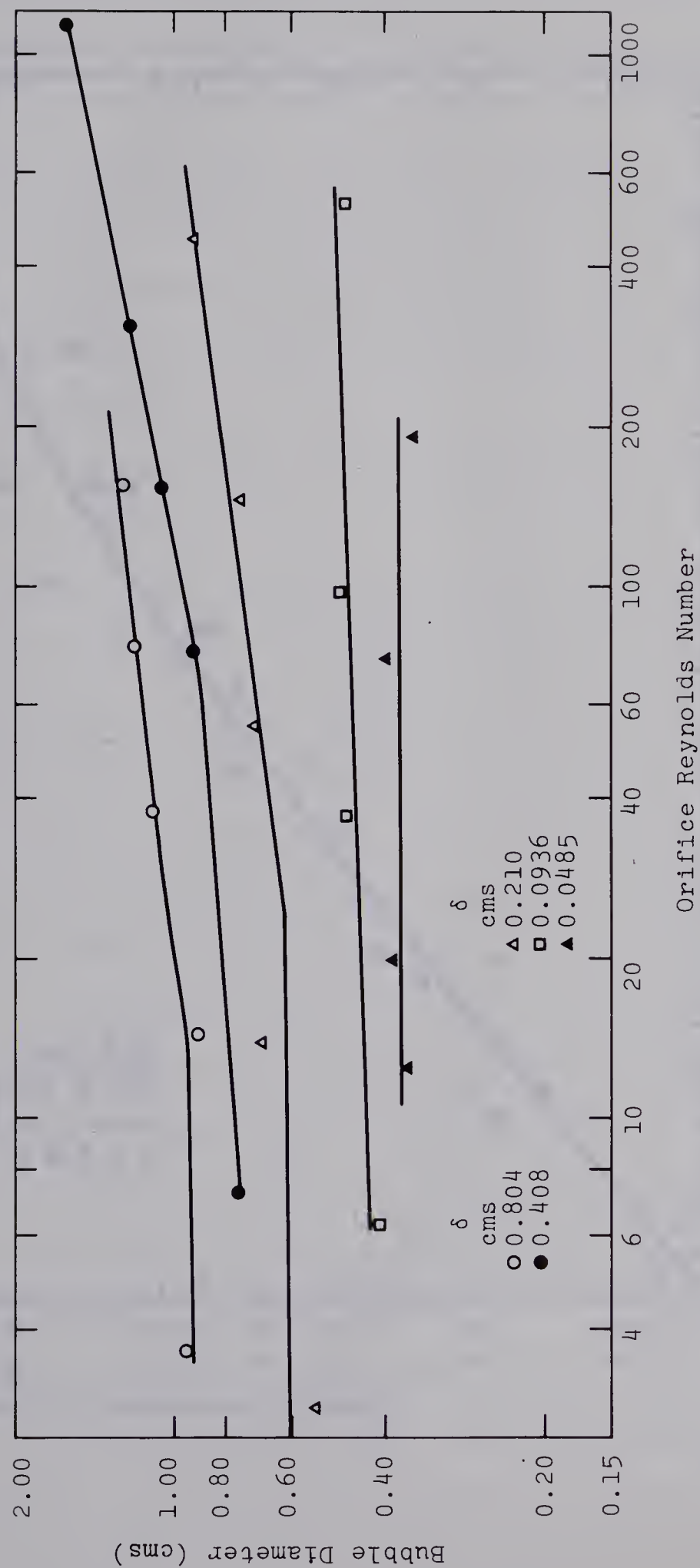


Figure 19: Plot of Bubble Diameter vs. Orifice Reynolds Number



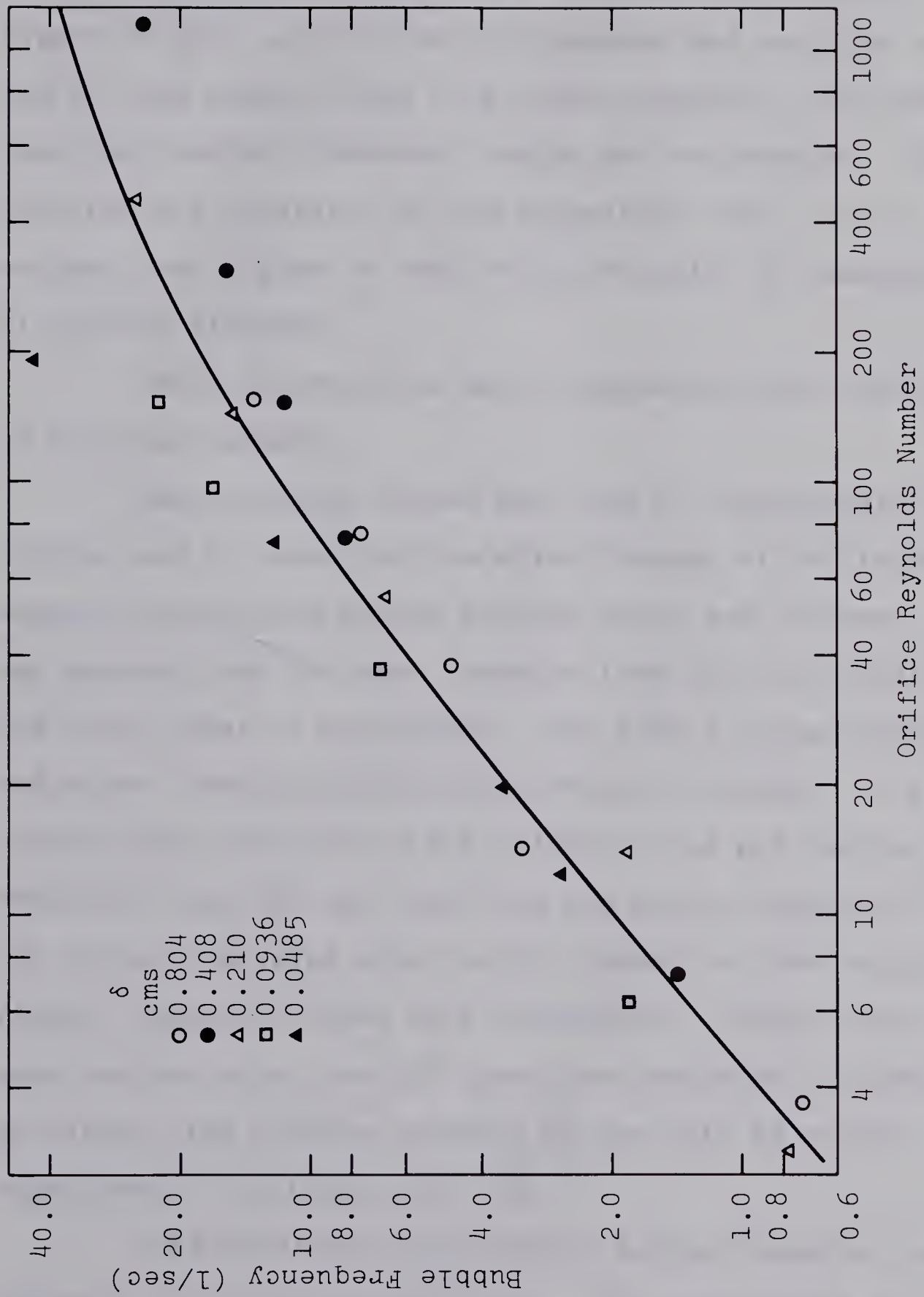


Figure 20: Plot of Bubble Frequency vs. Orifice Reynolds Number





that bubble volume increases with increasing gas flow rate in the constant frequency and the transition regions.

Figure 20 is a plot of bubble frequency and Reynolds number and for the range of gas flow rates studied it indicates that the constant frequency region was not reached. This confirms the existence of the transition zone. It is also evident from Figure 20 that the correlation is independent of orifice diameter.

These observations are in agreement with the work of previous authors.

The air-water system was used to characterize the orifice and to establish the effectiveness of the technique adopted to evaluate bubble surface areas and volumes. It was assumed that the mass transfer from the air bubble to the water phase is negligible. The bubble volume before and after formation should thus remain unchanged. A comparison was made between the volume of the air bubbles as evaluated from the gas flow rate and bubble frequency with the volume evaluated after bubble formation from photographic films. Figure 21 shows this comparison. Though there is some scatter about the  $45^\circ$  line, the variation is distributed on either side and the accuracy of the data is within experimental limitation of  $\approx 2\%$ .

The behaviour of gas bubbles during formation was observed from photographic films. The photographs of Figure 22 show a typical bubble during its various stages



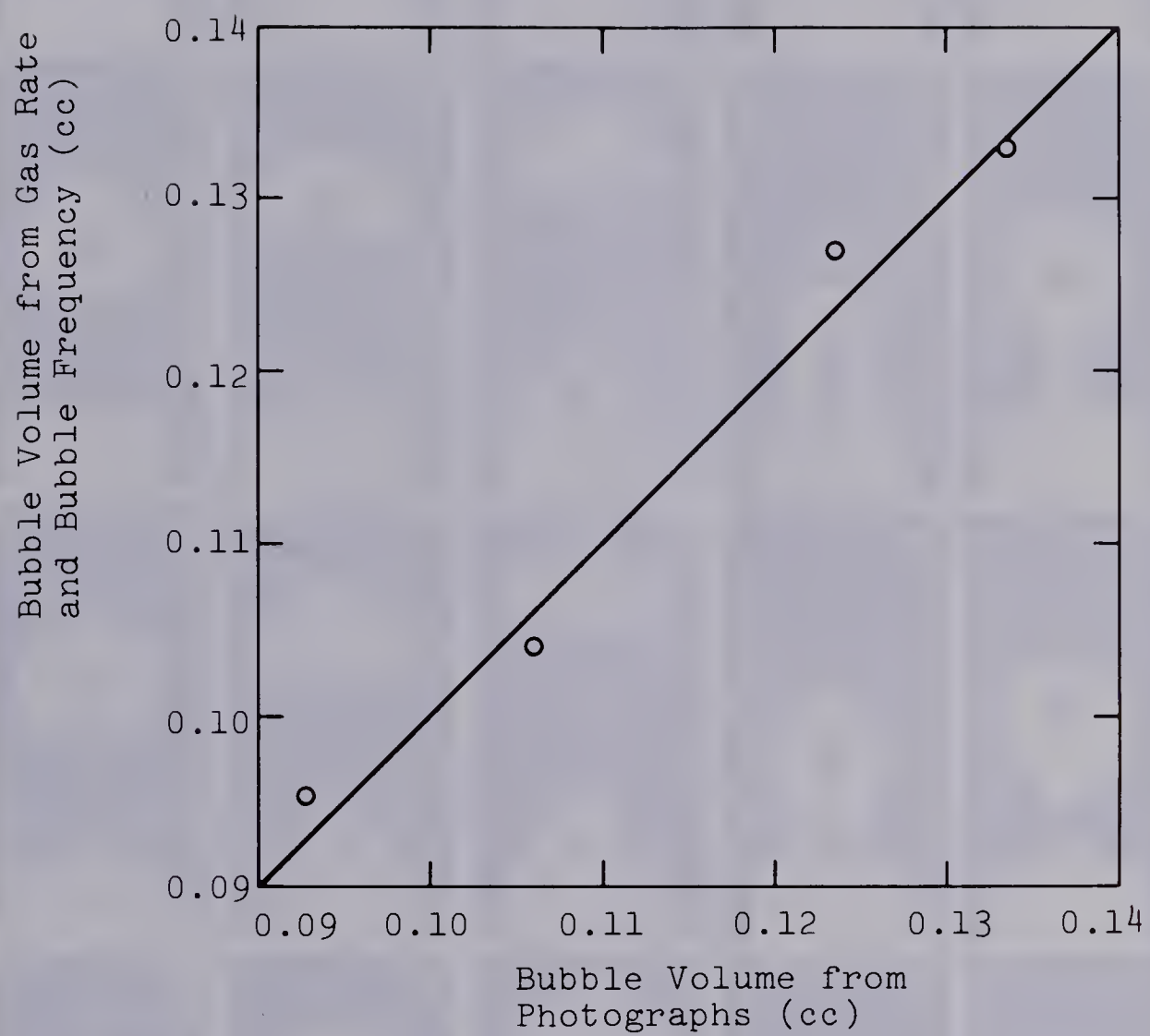


Figure 21: Comparison of Bubble Volume from Gas flow rate and bubble frequency with Bubble volume from Photographs





Figure 22: Photographs of Bubble Behaviour







of formation.

In its initial stages of formation, the gas bubble experiences a mechanical oscillation in the axial direction resulting from an equal and opposite reaction due to the break off of the previous bubble. These oscillations cease fairly quickly and the bubble grows steadily and uniformly in an almost spherical pattern. This growth occurs till the volume of the bubble approaches a limiting value determined by an equilibrium between the surface and gravitational forces. A neck then develops and the bubble begins oscillating in its axial direction. The neck becomes thinner with each oscillation but the bubble volume keeps on increasing. The bubble eventually breaks off from the orifice and this creates an imbalance in the forces acting on the bubble. This effect, which is sometimes referred to as a kinetic impingement, is responsible for the initial oscillations of the oncoming bubble and for severe rippling on the surface of the detached bubble. On detachment, the bubble undergoes violent deformations in addition to surface rippling till finally it assumes an oblate spheroidal shape which is deformed only by its spiral motion up the liquid column.

#### 5.4 Mass Transfer During Bubble Formation: $\text{CO}_2$ -Water System

Experiments were carried out to measure the amount of mass transfer during bubble formation for the absorption



of  $\text{CO}_2$  in water. The following conditions were used:

Orifice Inside Diameter = 0.408 cms.

Liquid Average Velocity = 1.0 cms/sec.

Bubble Frequencies = 0.5, 1.0, 5.0 and 10.0 bubbles/sec.

The 0.408 cms. diameter orifice was chosen in preference to the others from its overall performance during studies with the air-water system. Bubble formation was more stable for this orifice size. The sets of experimental conditions used for individual runs are given in Table 2.

Run No.	Gas Rate cc/sec	Bubble Frequency (1/sec)	Average Liquid Velocity (cms/sec)
M1	0.1011	1.0190	1.0
M2	0.5008	5.008	1.0
M3	1.3298	10.002	1.0
M4	0.0850	1.0269	1.0
M5	0.4846	4.996	1.0
M6	1.2441	9.883	1.0
M7	0.0483	0.5014	1.0

Table 2: Experimental Conditions used for  $\text{CO}_2$ -Water Runs

The surface area and volume of bubbles determined as a function of time from photographs is shown in Figures 23 to 28. In evaluating bubble area and volume, corrections were incorporated to account for the rest bubble which is



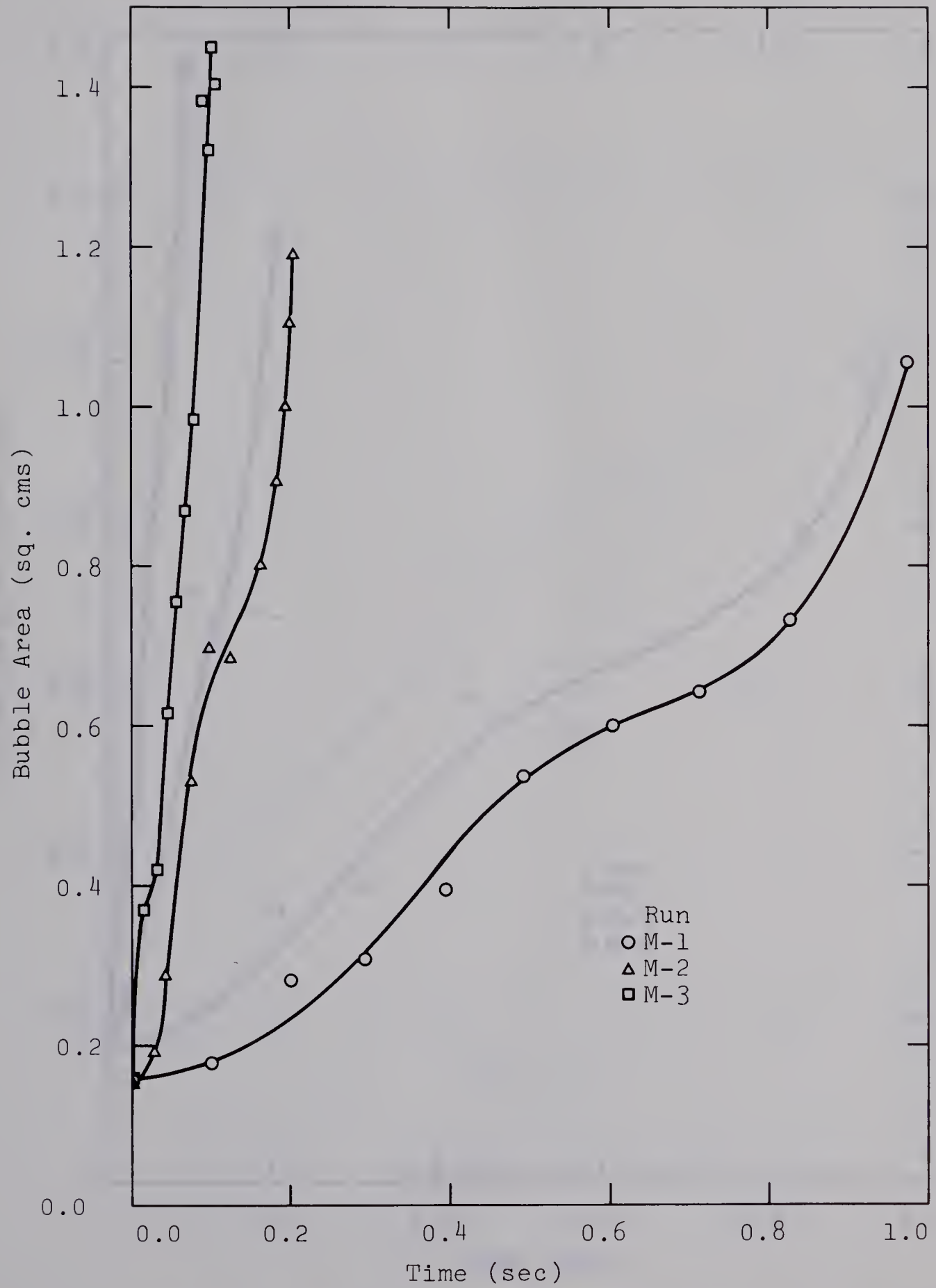


Figure 23: Plot of Bubble Surface Area vs. Time for Runs M-1, M-2 and M-3





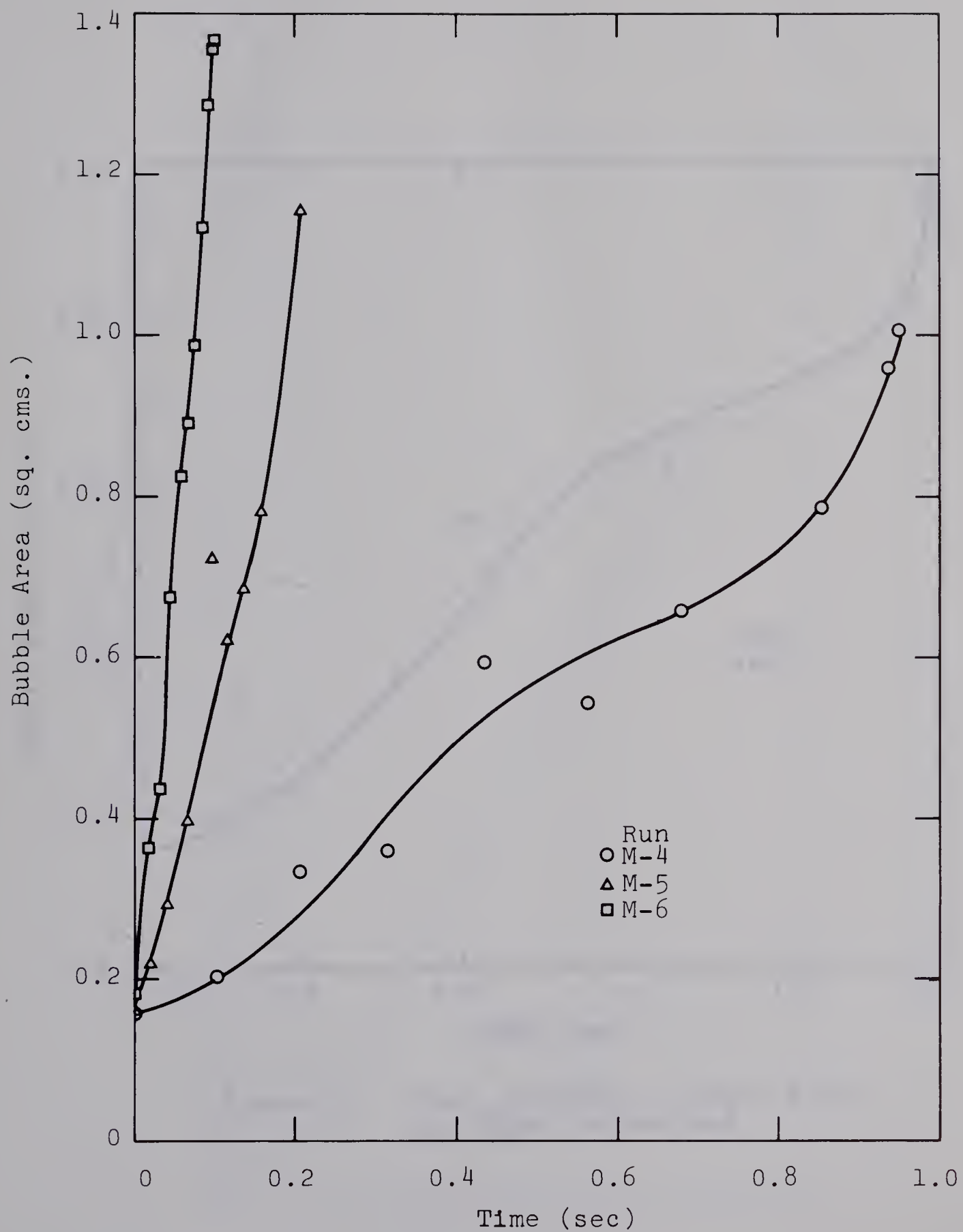


Figure 24: Plot of Bubble Surface Area vs. Time for Runs M-4, M-5 and M-6



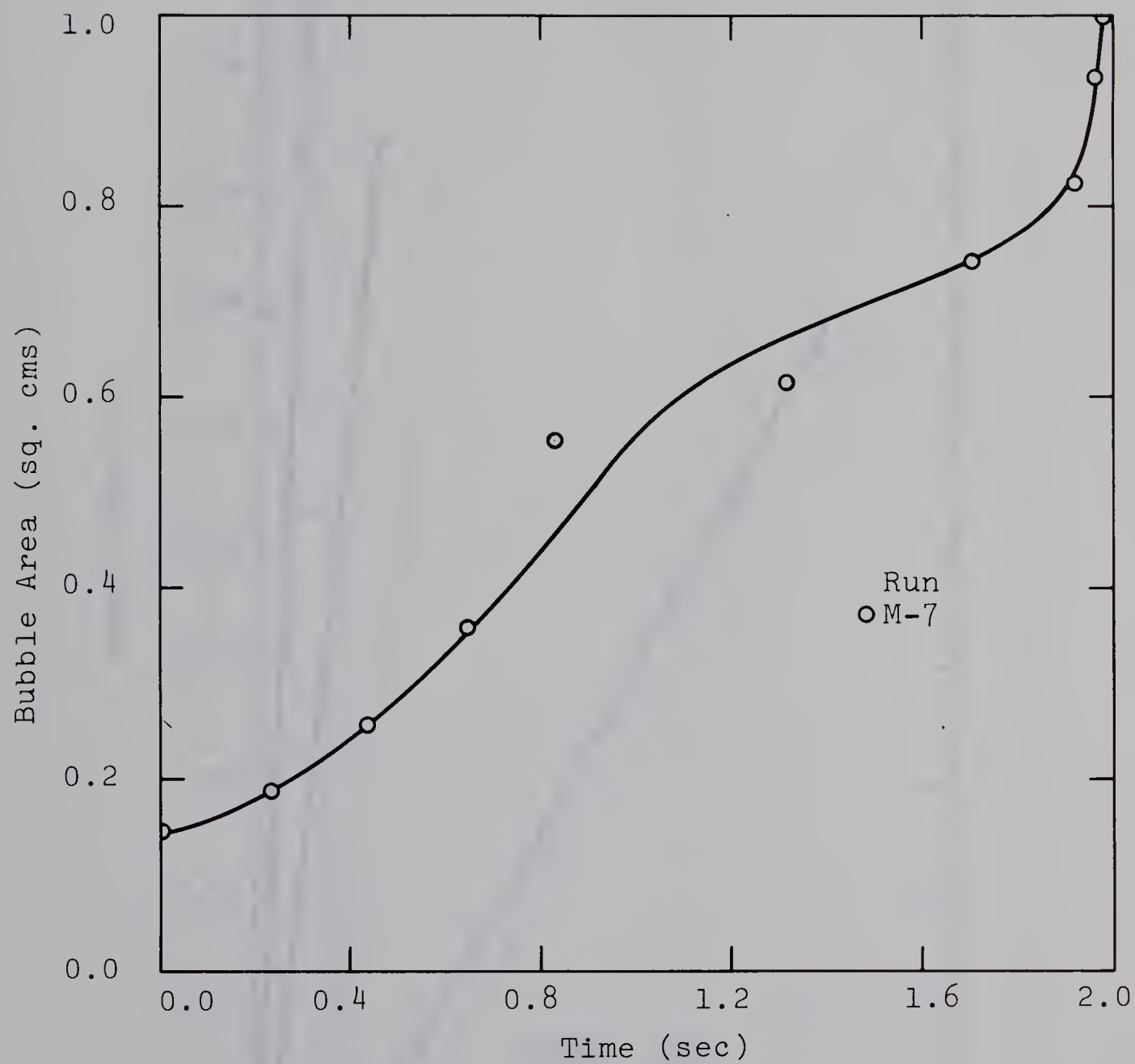


Figure 25: Plot of Bubble Surface Area vs. Time for Run M-7



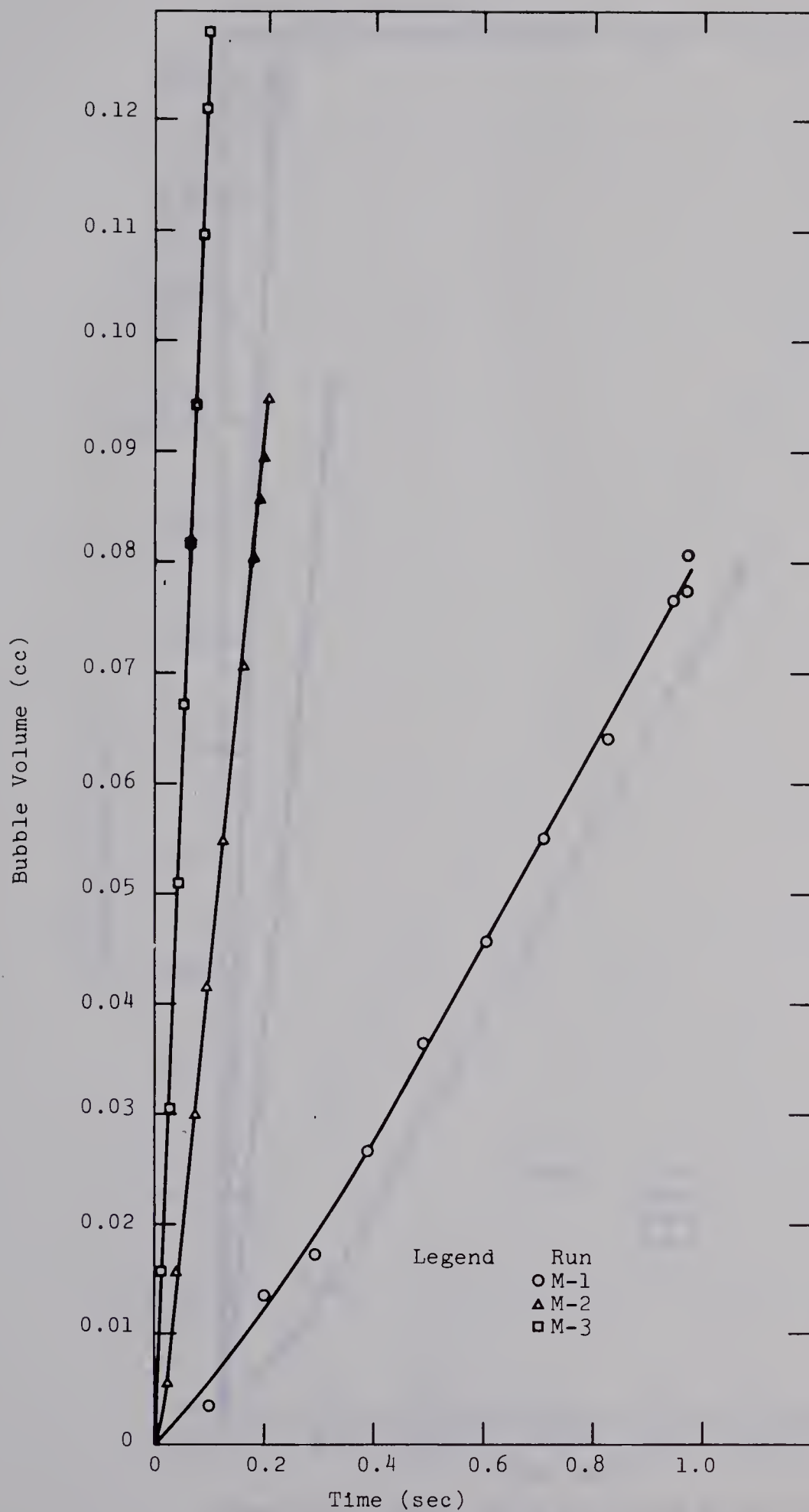


Figure 26: Bubble Volume vs. Time for Runs M-1, M-2 and M-3





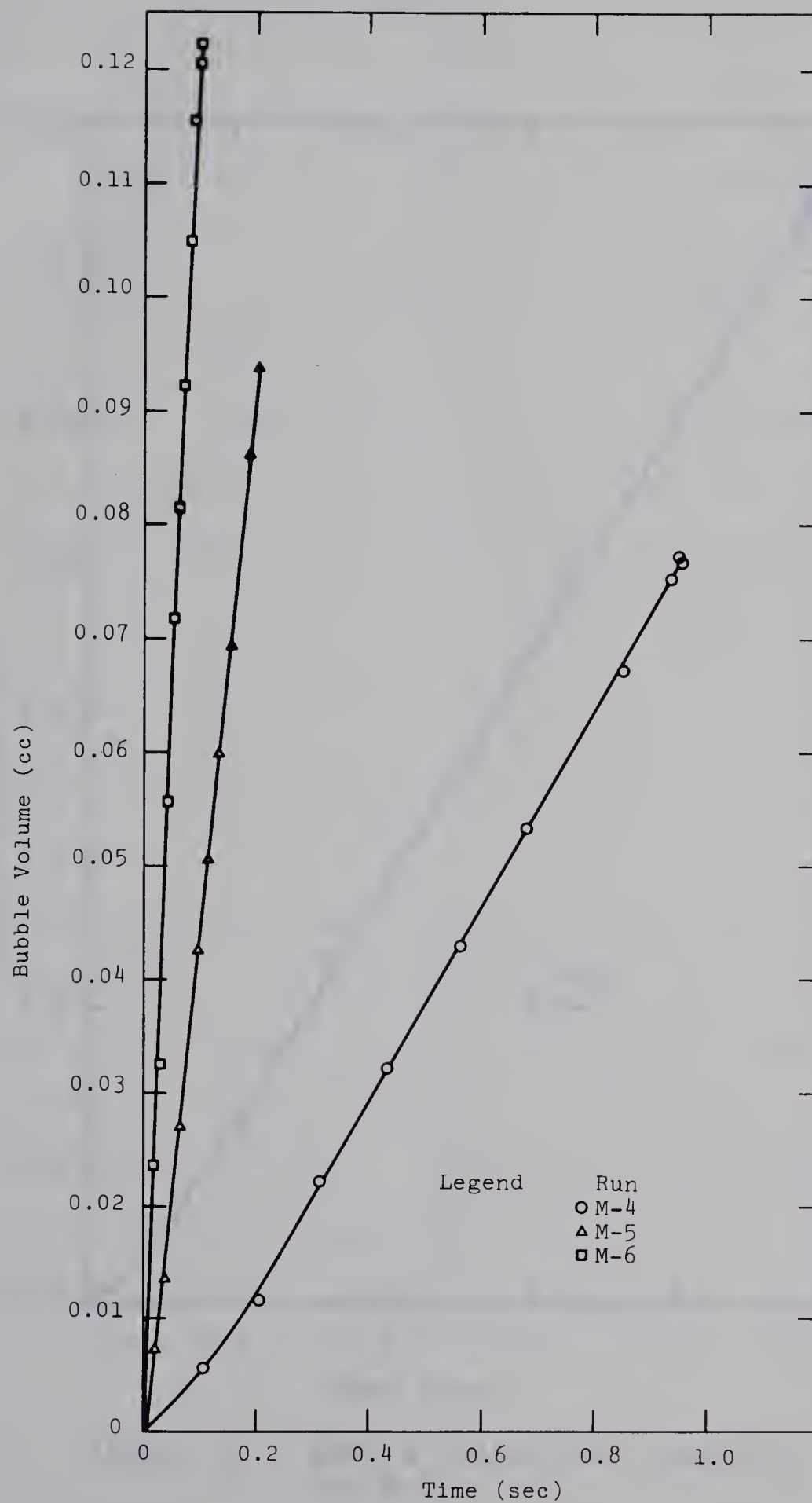


Figure 27: Bubble Volume vs. Time for Runs M-4, M-5 and M-6



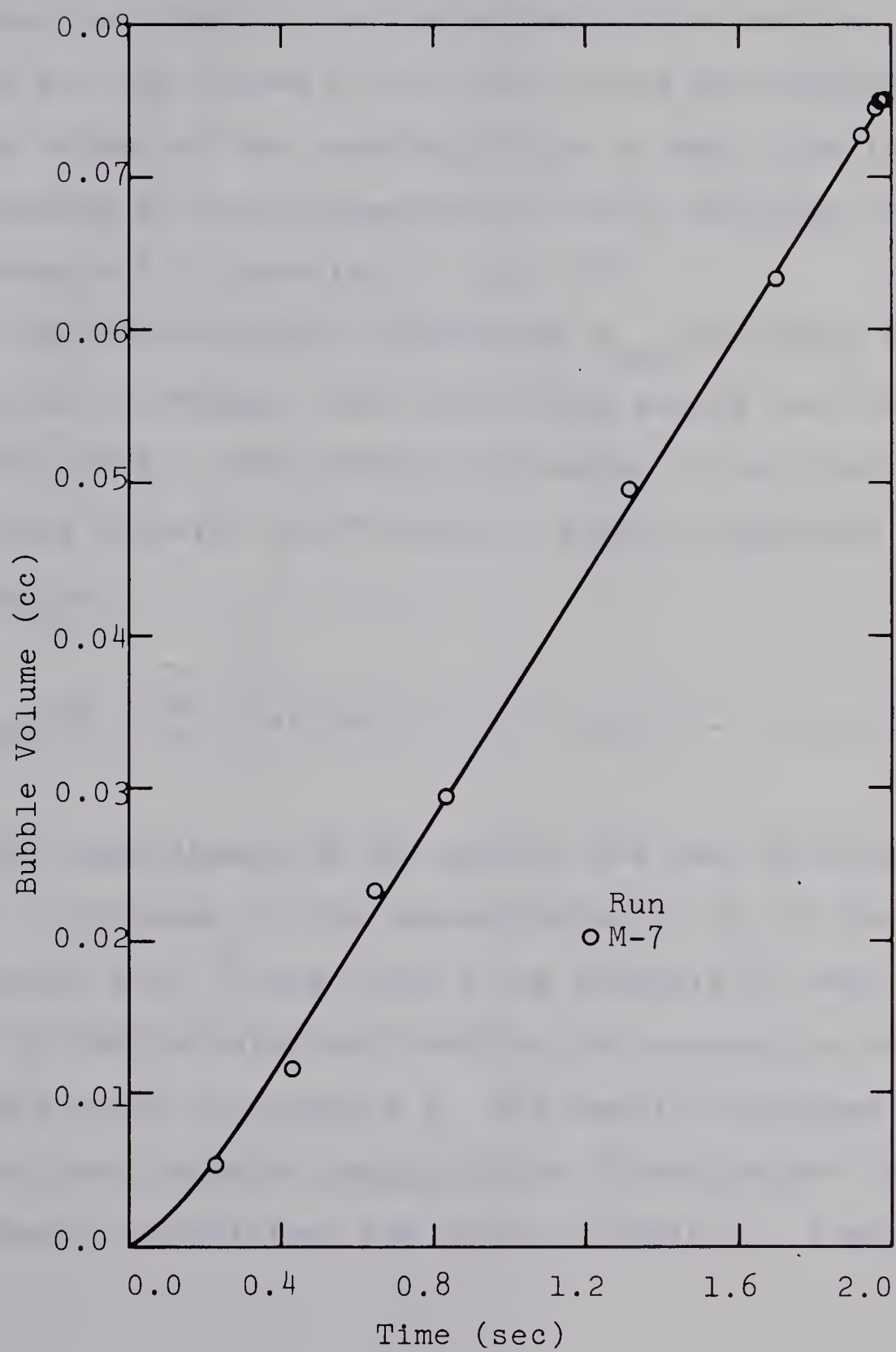


Figure 28: Bubble Volume vs. Time for Run M-7



that part of the bubble left behind on the orifice after detachment. The surface area corresponding to the rest bubble was included in the evaluation of the area vs. time integral and the volume of the rest bubble was deducted from the volume of the oncoming bubble at each time interval. The necessity of this correction to obtain reliable results was pointed out by Heertjes et. al. [67].

The mass transfer coefficient  $k_{Lav}$  evaluated from the data is an average value determined during the time of formation  $0 \leq t \leq T_f$ . The general expression for evaluation of the mass transfer coefficient is given by equation 3.3 expressed as

$$N_A = k_{Lav} (C_A^s - C_A^b) \int_0^{T_f} A(t) dt \text{-----} (3.3)$$

where the significance of the symbols has been previously defined. The value of the concentration of  $CO_2$  in the bulk liquid phase i.e.  $C_A^b$  was found to be essentially zero.

Details of the calculations involved for evaluation of  $C_A^s$  and  $C_A^b$  are given in Appendix D. The results obtained for amount of mass transfer during bubble formation and the mass transfer coefficient are given in Tables 3, 4 and 5.





Run No.	Atm. Press $P_a$ (psia)	Water Head (cm)	$P_{H_2O}$ Water (psia)	$P_a + P_{H_2O}$ (psia)	$P_o$ -Operating Press (psig)	$P_o$ (psia)	Atm. Temp. $^{\circ}C$	Water Temp. $^{\circ}C$	$V_1$ =Gas flow at meter $cm^3/sec.$	$V_2$ =Gas flow at nozzle $cm^3/sec.$
M-1	13.50	91.7	1.3	14.80	17.40	30.90	25.2	25.0	0.0484	0.10105
M-2	13.50	91.7	1.3	14.80	17.50	31.00	25.3	25.0	0.2391	0.5008
M-3	13.50	91.7	1.3	14.80	17.48	30.98	25.3	25.0	0.6353	1.3298
M-4	13.56	91.7	1.3	14.86	17.40	30.96	27.7	25.0	0.0464	0.0967
M-5	13.56	91.7	1.3	14.86	17.48	31.04	28.04	25.0	0.2320	0.4846
M-6	13.56	91.7	1.3	14.86	17.50	31.06	27.04	25.0	0.5928	1.2441
M-7	13.62	91.7	1.3	14.92	17.40	31.02	25.56	25.0	0.0233	0.0483

Table 3:  $CO_2$ -Water Mass Transfer Run Data.



Run No.	Nozzle size (cm) (ID)	Gas Flow Rate at Nozzle (cm <sup>3</sup> /sec)	Bubble Freq. (1/sec.)	Bubble Volume V <sub>O</sub> (cm <sup>3</sup> )	Bubble volume after detachment V <sub>F</sub> (cm <sup>3</sup> )	% Absorption $\frac{V_O - V_F}{V_O} \times 100$	Date
M-1	0.408	0.10105	1.01896	0.09917	0.0808	18.54	31-1-68
M-2	0.408	0.5008	5.0081	0.09999	0.0952	4.80	31-1-68
M-3	0.408	1.3298	10.0017	0.13296	0.1295	2.63	31-1-68
M-4	0.408	0.0967	1.0269	0.09417	0.0764	18.89	1-3-68
M-5	0.408	0.4846	4.9960	0.09700	0.0930	4.12	1-3-68
M-6	0.408	1.2441	9.8827	0.12589	0.1224	2.77	1-3-68
M-7	0.408	0.0483	0.5014	0.09640	0.0736	22.86	20-4-68

Table 4: Mass Transfer Data CO<sub>2</sub>-Water System.



Run No.	Gas Pressure at Orifice (psia)	Atm. Pressure (psia)	Gm. Molecular Volume (cc)	Value of Area Integral (cm <sup>2</sup> sec)	Dissolved Volume during formation (cc)	Mass Transfer Coefficient (cm/hr)
M1	14.8	13.50	22303.5	0.5110	0.01837	161.6
M2	14.8	13.50	22303.5	0.1199	0.00480	180.0
M3	14.8	13.50	22303.5	0.0699	0.00346	222.4
M4	14.86	13.56	22312.2	0.5034	0.01777	158.6
M5	14.86	13.56	22312.2	0.1202	0.00400	149.4
M6	14.86	13.56	22312.2	0.0731	0.00349	214.5
M7	14.92	13.62	22320.8	1.0025	0.02204	98.7

Temperature of system =  $25 \pm 0.05^{\circ}\text{C}$

Table 5: Mass Transfer Coefficient for CO<sub>2</sub>-Water System.





## CHAPTER 6

### DISCUSSION

#### 6.1 Air-Water System.

The variation of bubble frequency with Orifice Reynolds number as shown in Figure 20 indicates that the correlation is independent of orifice diameter in the constant volume and transition regions. At high Reynolds numbers it is seen that the curve levels off to some extent indicating the approach of the constant frequency region. Davidson et. al. [16] indicated that the maximum bubble frequency corresponding to the constant frequency region is a function of the orifice diameter and is given as

$$\eta_m \propto \frac{1}{d^{0.33}}$$

where  $\eta_m$  is the maximum frequency attained. This effect can be seen in Figure 20 at high Reynolds numbers where the frequency curve tends to level off at different values for different orifice diameters.

#### 6.2 CO<sub>2</sub>-Water System

The interpretation of the results obtained for the CO<sub>2</sub>-water system may be subdivided into the following sections:



- (i) Variation of Surface Area and Volume with time of bubble formation.
- (ii) Mass transfer during bubble formation.

During a study of mass transfer at bubble formation Popovich et. al. [57] assumed that the surface area of the growing bubble or drop may be represented by the equation

$$A = k_1 t^{n_1} \text{-----}(2.19)$$

$$\text{or } \ln A = \ln k_1 + n_1 \ln t \text{-----}(6.1)$$

If the bubble is assumed to grow as a sphere then  $n_1 = 2/3$ .

The surface area of the bubbles obtained in this investigation is plotted according to equation 6.1 in Figures 29, 30 and 31. It is seen from these figures that  $(\ln A)$  is not linear with  $(\ln t)$  throughout the period of formation as indicated by equation 6.1. A departure from linearity is observed in each case, resulting in a sharp rise of surface area and examination of photographic films indicated that the non-linear portion of the curve corresponds to bubble necking and subsequent bubble break-off. It may be concluded from this that during neck formation and bubble breakoff the surface area of the bubbles rises at a faster rate than predicted by equations 2.19 or 6.1.

Calderbank et. al. [8] suggested that the bubble area as a function of time could be represented by equation



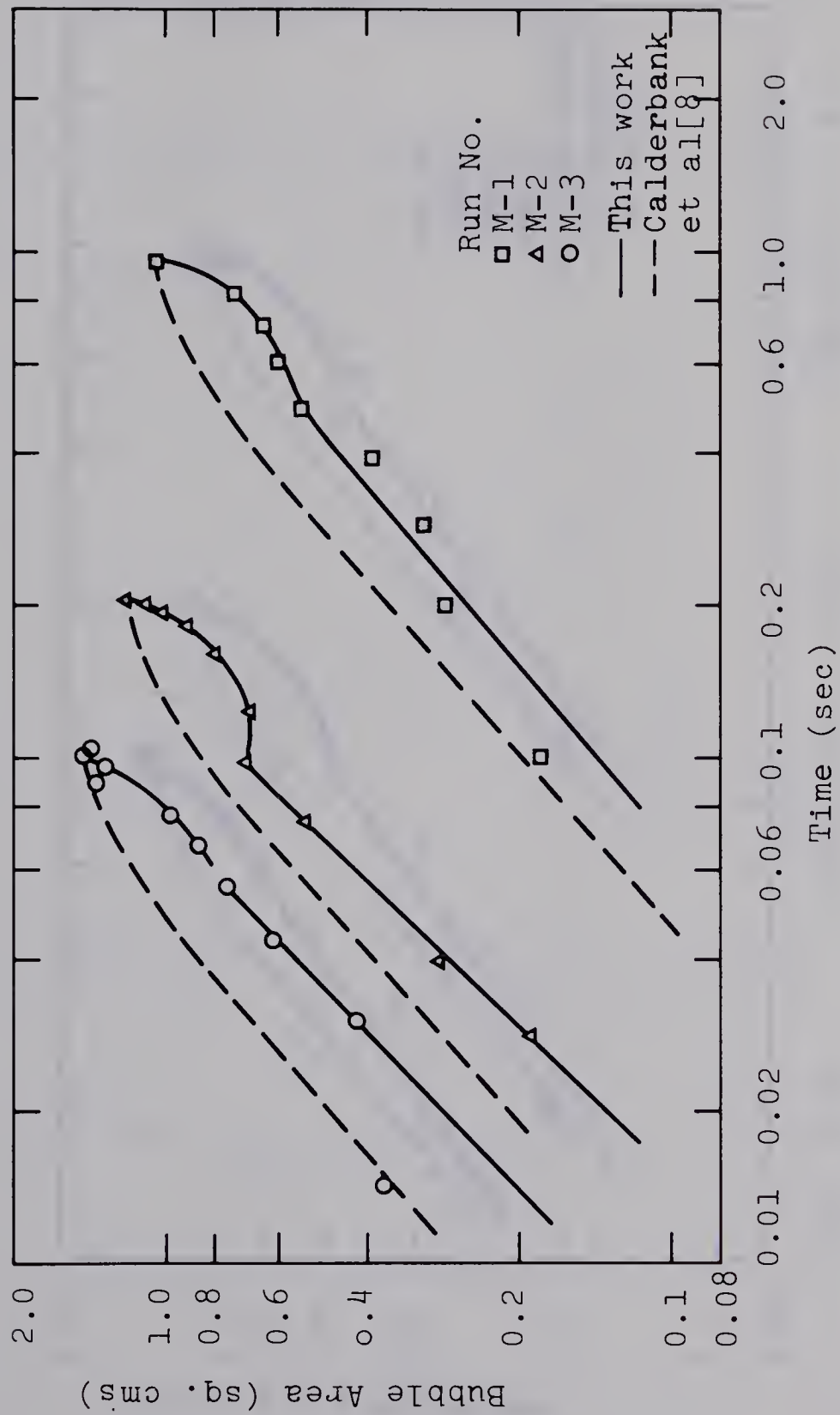


Figure 29: Log-Log Plot of Bubble Area vs. Time for Runs M-1, M-2 and M-3





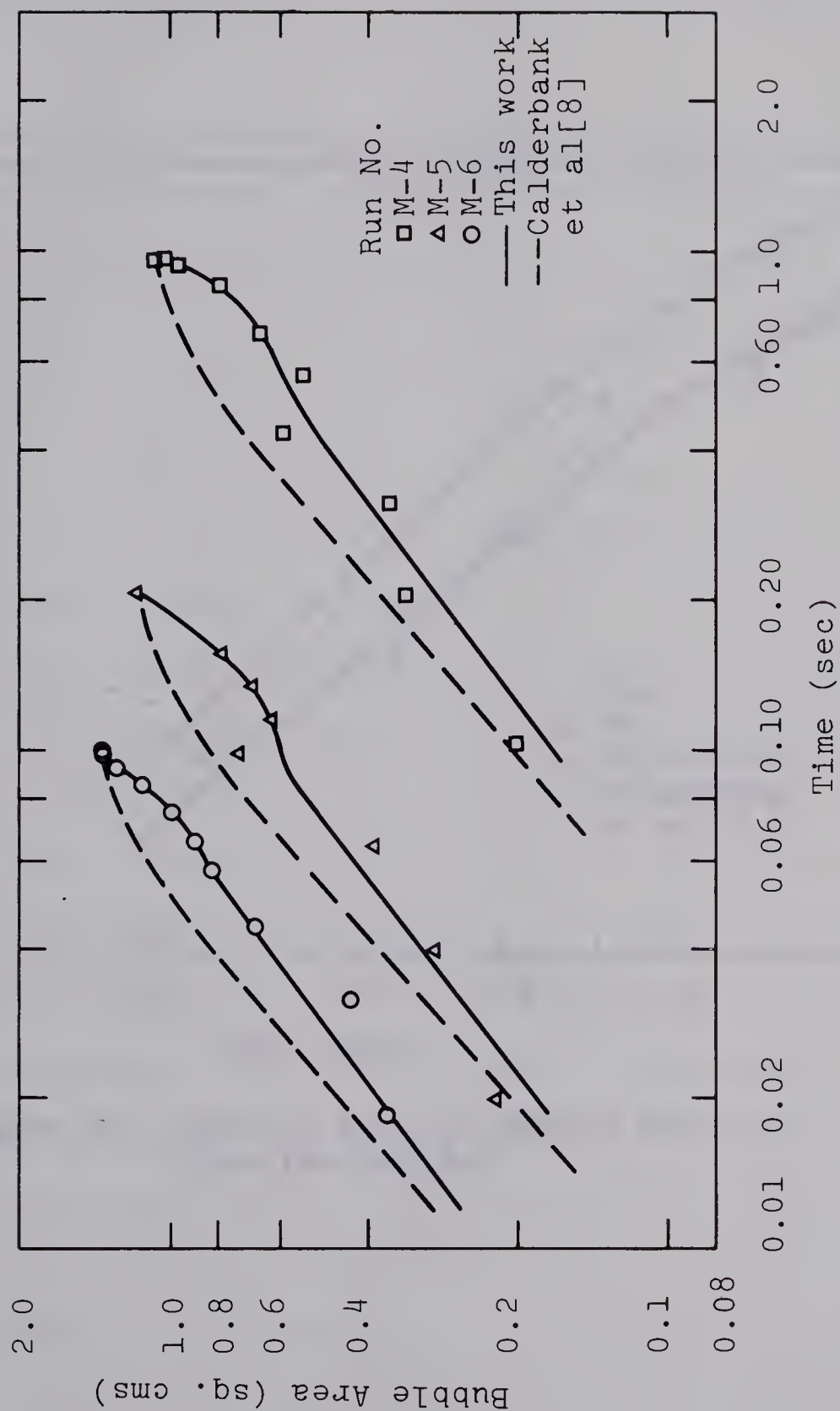


Figure 30: Log-Log Plot of Bubble Area vs. Time for Runs M-4, M-5 and M-6



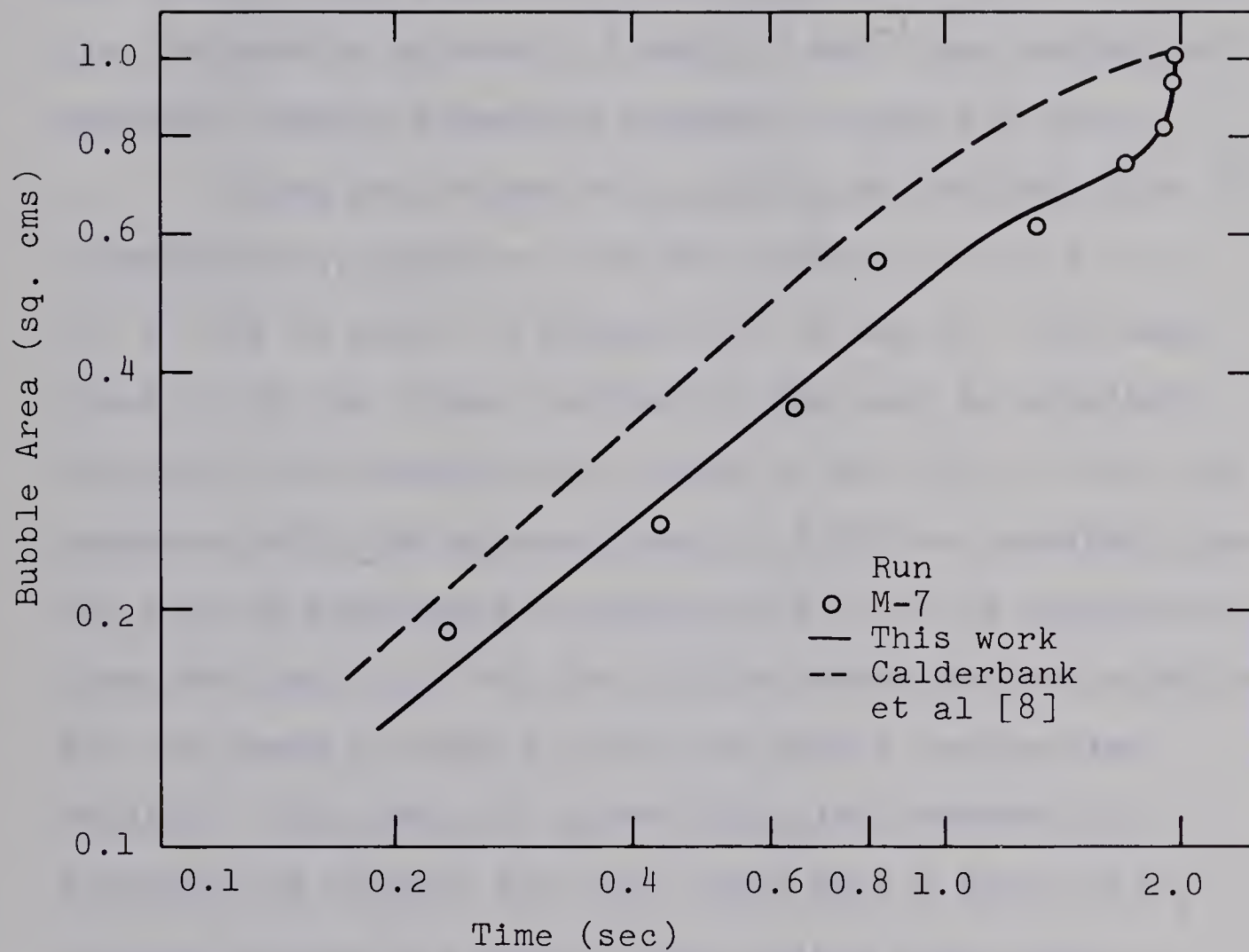


Figure 31: Log-Log Plot of Bubble Area vs. Time for Run M-7



2.26 which is given as follows:

$$\frac{A}{A_m} = 1 - \left[ \frac{(T_f - t)}{T_f} \right]^{n_2} \text{-----} (2.26)$$

The value of the exponent  $n_2$  was reported as 1.86 for bubble frequencies between 0.2 and 2.0  $\text{sec}^{-1}$  and equivalent spherical bubble diameters between 0.5 and 1.0 cms.

Using the values of  $A_m$  and  $T_f$  as obtained from this investigation, equation 2-26 was plotted as  $(\ln A)$  vs.  $(\ln t)$  and is given in Figures 29, 30 and 31. The mean slope  $n_1$  of the linear portion of the plot as obtained from this investigation was found to be 0.850. This value compares well with a mean slope of 0.875 as obtained from the plot of Calderbank's equation [8]. It is possible to conclude from this that the bubble growth was not spherical for the range of bubble sizes and bubble frequencies studied. Non spherical growth was also observed by Poutanen and Johnson [68] who found that a value of  $n_1$  varying between 2/9 and 5/9 best suited their data.

When plotted on linear coordinates the sharp rise in bubble area at necking is represented by a pronounced inflection as shown in Figures 23 to 25. This effect though present at all frequencies cannot be clearly seen at higher frequencies from Figures 23 and 24 because of the scale chosen. It is interesting to plot bubble area vs. time on transformed time coordinates taking the time axis





to be  $(T_f - t)$  where  $T_f$  is the total formation time. This affords a comparison with the work of Poutanen and Johnson [68]. The inflection region is fairly conspicuous from this plot also as is shown in Figure 32, but the work of Poutanen and Johnson [68] indicates no such observation. This difference may be due to the different techniques used to evaluate bubble surface area during formation. Poutanen et. al. represented the bubble profile by an empirical equation of the form

$$r^{n^*} \theta = 1 \text{ -----} (6.2)$$

where  $r$  and  $\theta$  are polar coordinates and  $n^*$  is an exponent determined from some shape factors evaluated using specific bubble dimensions. The expressions for bubble surface area and volume were determined explicitly in a manner similar to the one used in this study to derive expressions given by equations 3.16 and 3.17. The area and volume of the elongated neck during bubble necking was evaluated assuming the neck to be made up of frustra of right cones. In this study, however, the numerical approach was used in preference to the continuous function approach because the neck could be accurately represented by actual data points before evaluating the surface and volume and also because this procedure was thought to give more reliable results.

The variation of bubble volume with time was found



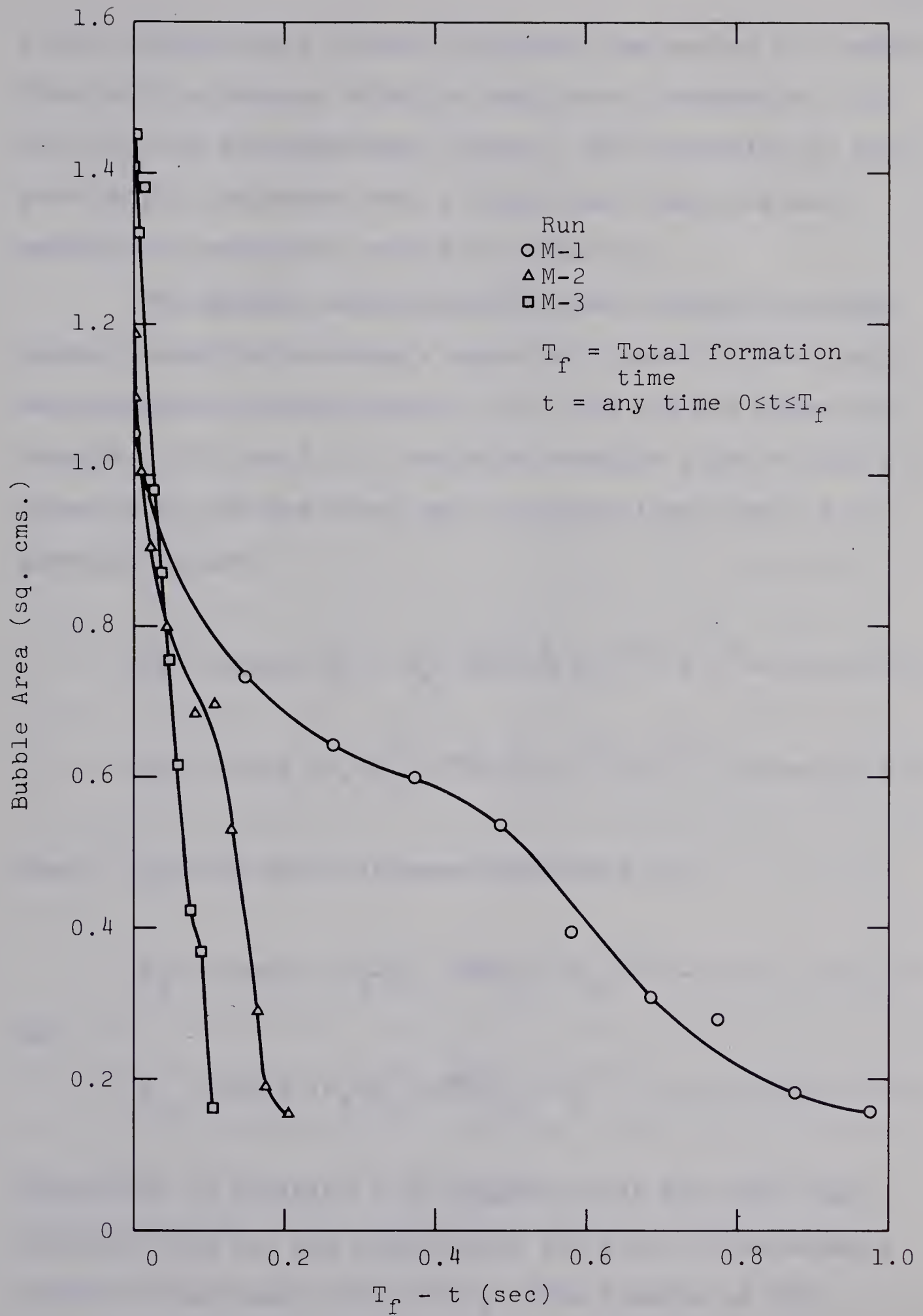


Figure 32: Plot of Bubble Area vs. Time on transformed Time Coordinates



to be substantially linear throughout the period of formation. This is in agreement with the results of Poutanen et. al. [68] for the Nitrogen-Water System. The linearity of this plot merely indicates that a steady gas flow rate was maintained during the period of formation.

The general expressions for mass transfer during bubble formation assuming a spherical growth of the bubble were suggested by Popovich et. al. [57] and are given by equations 2.22 to 2.25. The mass transfer flux at time  $t$  given by  $N_A'$  and the total mass transfer from time 0 to  $t$  given by  $N_A$  are

$$N_A' = \text{const} (C_A^s - C_A^b) \sqrt{D\Pi} d_f^2 T_f^{-2/3} t^{1/6} \text{-----} (2.22)$$

$$N_A = \text{const} (C_A^s - C_A^b) \sqrt{D\Pi} d_f^2 T_f^{-2/3} t^{7/6} \text{-----} (2.23)$$

When  $t = T_f$  the above expressions reduce to

$$N_A' = \text{const} (C_A^s - C_A^b) \sqrt{D\Pi} d_f^2 T_f^{-1/2} \text{-----} (2.24)$$

and

$$N_A = \text{const} (C_A^s - C_A^b) \sqrt{D\Pi} d_f^2 T_f^{1/2} \text{-----} (2.25)$$

Inspection of equation 2.25 suggests that the total mass transfer from the gas bubble upto the point of detachment varies as the square root of  $T_f$ . The results of this





study indicate that this is not so. A plot of total mass transfer vs. time of formation is shown in Figure 33 and the slope of a least square line through the data was found to be 0.685 indicating that the exponent on  $T_f$  is 0.685 and not 0.50 as suggested by equation 2.25.

This difference can be explained by the fact that the growth of the bubble in this study was not spherical whereas this is implicitly assumed in equation 2.25. Popovich et. al. [57] confined their work to liquid drops of approximately 0.2 to 0.4 mm diameter and spherical growth of the drop for small drop sizes is reasonable. The equivalent bubble diameters in this investigation, however, were in the range of 5.2 to 6.3 mm and an assumption of spherical growth for these sizes is not justified. In addition to this the variation of bubble surface area with time was not represented by equation 2.19 throughout the period of bubble growth and this too has been assumed in deriving equation 2.25.

Bowman et. al. [3] conducted some work with  $\text{CO}_2$ -water and reported the variation of mass transfer coefficient with bubble frequency during the bubble rise period. Their results indicated that mass transfer coefficient increases with bubble frequency and the results of this study indicated that this was true during bubble formation also. A comparison of the results of Bowman et. al. [3] and this work is presented in Figure 34.



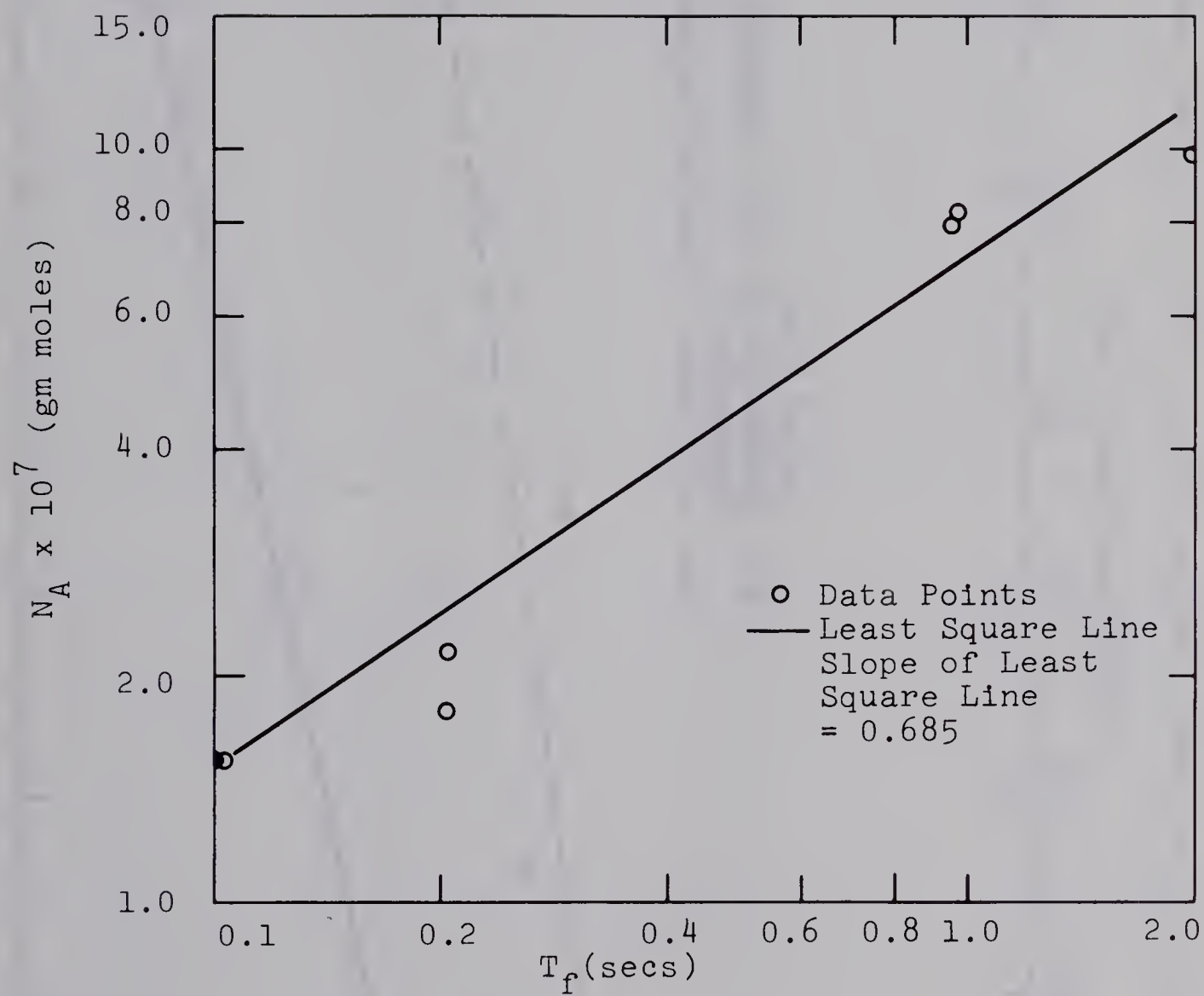


Figure 33: Plot of Total Mass Transfer vs. Total Bubble Age



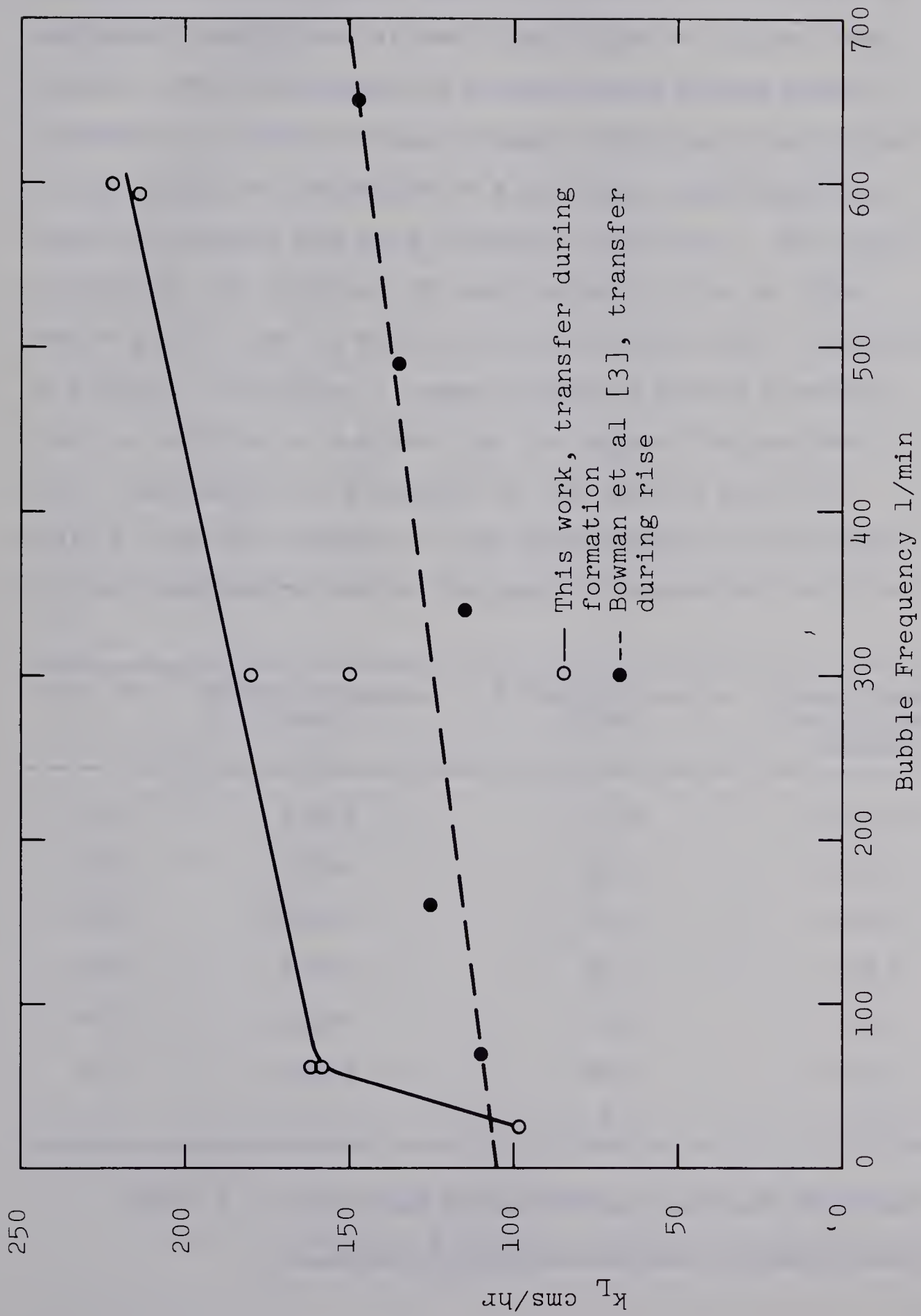


Figure 34: Plot of Mass Transfer Coefficient vs. Bubble Frequency





An increase of mass transfer coefficient with increasing bubble frequency can be explained on the basis of increased disturbances in the liquid phase at higher frequencies. The development of a neck during bubble growth followed by a bubble breakup causes considerable turbulence in the liquid in the region of the orifice mouth and this tends to increase the mass transfer coefficient. For lower frequencies the fraction of neck formation time to total bubble growth time is smaller than that for higher frequencies. In addition, there are a larger number of bubble breakoffs from the orifice in a given time for higher frequencies. These statements are supported by the results shown in Table 6, and the increase of the mass transfer coefficient with an increase of bubble frequency is therefore justified.

Run No.	Bubble Frequency (1/sec)	% Neck Formation Time	Mass Transfer Coefficient cms/hr.
M1	1.019	11.2	161.6
M2	5.008	19.6	180.0
M3	10.002	24.6	222.4
M4	1.027	11.7	158.6
M5	4.996	15.6	149.4
M6	9.883	25.1	214.5
M7	0.5014	6.7	98.7

Table 6: Percentage Neck Formation Time in Relation to Bubble Frequency and Mass Transfer Coefficient



As seen from Figure 34, the mass transfer coefficient obtained during bubble formation is of the same order of magnitude as that obtained during bubble rise. The former is, however, greater in absolute value. Calderbank and Patra [8] reported that the mass transfer coefficient during bubble formation is lower than that during bubble rise but their investigation was limited to a stagnant liquid phase. The higher value of mass transfer coefficient during bubble formation obtained in this study may be attributed to a superimposed liquid velocity on the forming bubble. This is supported by the fact that higher mass transfer coefficients during bubble rise due to a moving liquid phase have also been reported by Himmelbau et. al. [52].

Figure 35 presents the results of the mass transfer coefficients during bubble formation obtained in this study as a comparison with the mass transfer coefficients obtained during free bubble rise for the  $\text{CO}_2$ -water system by other authors. The plot presents the mass transfer coefficient vs. the equivalent spherical bubble diameter at bubble detachment from the orifice.

It is interesting to note the wide disparity in the results obtained by different authors for the same system during bubble rise. Bogandy et. al. [69] and Leonard [70] indicate an increase in the mass transfer coefficient with increasing bubble diameter while Himmelbau et. al. [52],



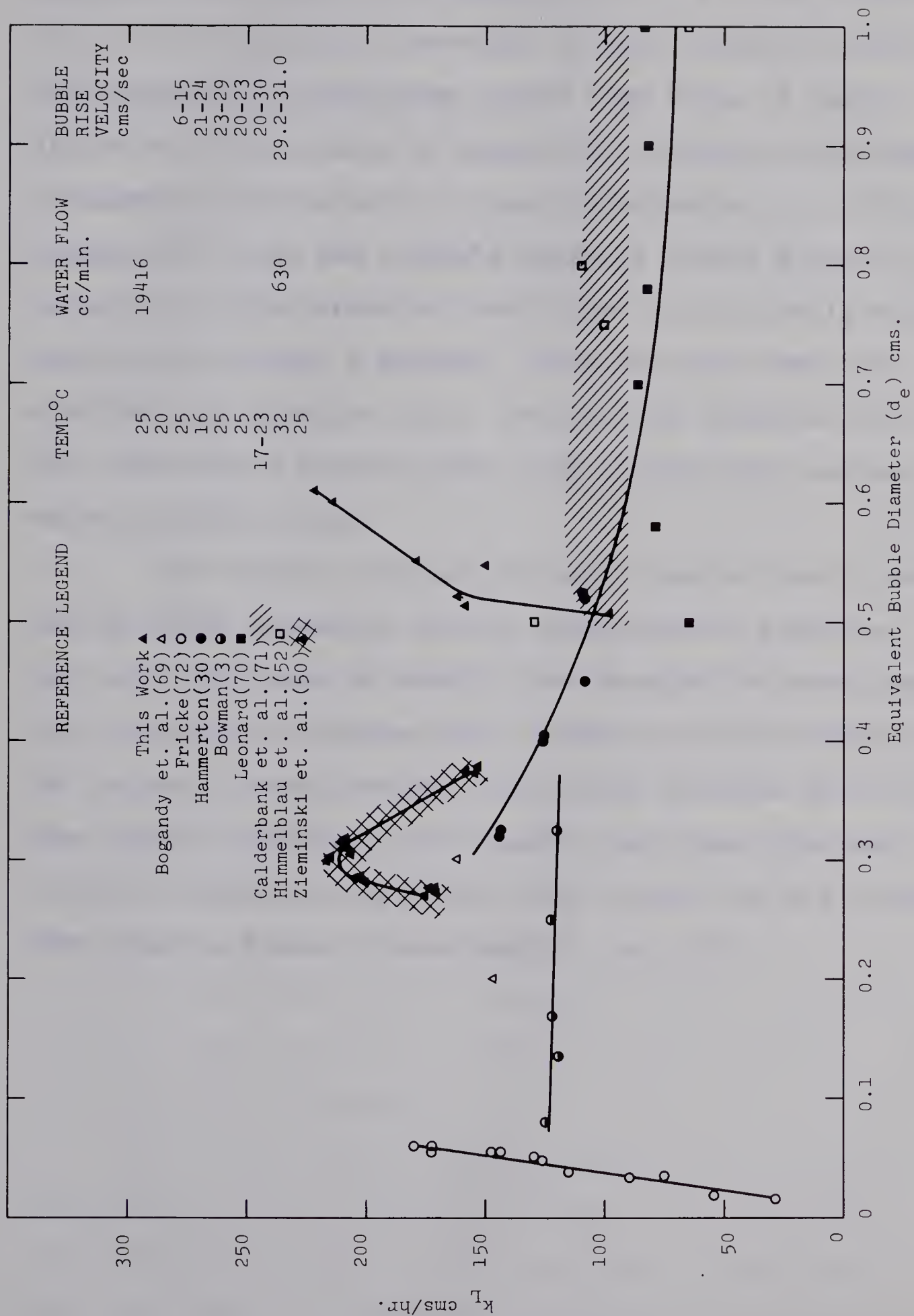


Figure 35: Plot of Mass Transfer Coefficient vs. Equivalent Bubble Diameter







Hammerton and Garner [30], Bowman et. al. [3] and Calderbank et. al. [71] indicate a decrease in mass transfer coefficient with increasing bubble size in the same range of bubble diameters. The results of Fricke [72] together with those of Hammerton and Garner [30] and Calderbank et. al. [71] suggest that over the complete range of bubble sizes the curve of the mass transfer coefficient during bubble rise should pass through a maximum. This fact has been substantiated by Siddique [51]. The work of Zieminski et. al. [50] indicates a similar trend over a relatively narrow range of bubble sizes.

The results obtained for mass transfer coefficients during bubble formation in this investigation indicate that over the range of bubble sizes studied the mass transfer coefficient increases with increasing bubble diameter. The values of mass transfer coefficient obtained are of the same order of magnitude, but higher than those obtained by other authors during bubble rise studies and are in the same range as those of Zieminski et. al. [50].



CHAPTER 7CONCLUSIONS AND RECOMMENDATIONS

From the study of mass transfer during bubble formation and the analysis of the data obtained in this investigation using the  $\text{CO}_2$ -water system, the following conclusions may be made.

- (1) The total mass transfer during formation depends on  $T_f^{0.685}$  where  $T_f$  is the time of formation of the bubble. This fact does not correspond to the equations proposed by Popovich et. al. [57] wherein the mass transfer varies as  $T_f^{0.5}$ .
- (2) The mass transfer coefficient increases with increasing bubble frequency in the range of frequencies investigated. This is supported by the work of Bowman et. al. [3].
- (3) The mass transfer coefficient during bubble formation with a superimposed liquid velocity is higher than the mass transfer coefficient (i) during bubble rise in a stagnant liquid (ii) during bubble rise in a moving liquid (iii) during bubble formation in a stagnant liquid. The mass transfer coefficients in all the above given cases are of the same order of magnitude.
- (4) With a superimposed liquid velocity the mass transfer coefficient during formation increases with increase of the equivalent spherical bubble diameter at detachment over the range of bubble sizes examined.



(5) The bubble surface area during growth follows the relationship  $A = k_1 t^{n_1}$  up to the point where the bubble develops a neck. Subsequent to this the surface area increases sharply with time till bubble break-off. The average value of  $n_1$  found in the investigation was 0.850. The growth of the bubble is therefore not spherical.

(6) The volume of the gas bubble increases linearly with time throughout the period of formation.

(7) The surface area and volume of the bubble could be evaluated at detachment with sufficient accuracy using the computer program based on the continuous function approach. The continuous function was a modification of the equation of a cardioid.

(8) The computer program based on the numerical approach gives much more flexibility of analysis in that it can be used to evaluate surface area and volume of the bubble as a function of time during bubble formation. It can also be used to evaluate the area and volume of the detached bubble.

The following conclusions could be made from the air-water runs conducted to characterize the system.

(1) The correlation of the frequency of bubble formation with orifice Reynolds number is independent of orifice size. The frequency increases with gas flow rate up to an orifice Reynolds number of about 500 after which it increases with gas flow rate at a decreasing rate. The maximum







bubble frequency is an inverse function of orifice size.

(2) Bubble volume increases with orifice diameter at a given gas flow rate.

(3) The bubble volume is essentially constant at low gas flow rates but increases during the transition region with increase of gas flow rate. The extent of the constant volume region and transition region from a point of view of orifice Reynold's numbers is a function of orifice size. Essentially constant bubble volume is obtained below Reynolds numbers of 30 for all orifice sizes investigated. This limit is higher for smaller orifice sizes.

On the basis of the results obtained during this investigation the following recommendations for future studies in the field can be made.

(1) Additional data should be obtained using the same orifice size but different liquid velocities to substantiate the effect of liquid velocity on mass transfer coefficient. This should be extrapolated to zero liquid velocity to compare the results with mass transfer studies in stagnant liquids conducted by previous authors.

(2) Mass transfer data could be obtained using different size orifices to study the effect of orifice size on mass transfer coefficient. This would help in optimum system design.

(3) More information is necessary on the effect of small amounts of surfactants in the system being investigated.



(4) Immediately after detachment, the gas bubble undergoes rapid changes in shape constantly renewing its surface area. The mass transfer coefficient in this region is likely to be high. It is suggested that attempts be made to measure the mass transfer coefficient during this period.



NOMENCLATURE

- a = Constant in equation of the Cardioid and subsequent equations presented in Chapter 3, and Appendix A.
- $a_1$  = Lower limit of the surface and volume integrals given by equations 3.4 and 3.5.
- A = Surface area of the bubble or drop ( $\text{cm}^2$ ).
- $A_e$  = Cathode surface area ( $\text{cm}^2$ ).
- $A_m$  = Maximum surface area of bubble ( $\text{cm}^2$ ).
- $b_1$  = Upper limit of the surface and volume integrals.
- c = Acoustic velocity in the gas (cm/sec).
- C = Concentration of oxygen in water at a given position in the column.  $(\frac{\text{gms or gm moles}}{\text{cc}})$  or  $(\frac{\text{gms or gm moles}}{\text{litre}})$ .
- $C^*$  = Concentration of oxygen in the bulk water phase  $(\frac{\text{gms or gm moles}}{\text{cc}})$  or  $(\frac{\text{gms or gm moles}}{\text{litre}})$ .
- $C_o$  = Concentration of oxygen on the cathode surface  $(\frac{\text{gms or gm moles}}{\text{cc}})$  or  $(\frac{\text{gms or gm moles}}{\text{litre}})$ .
- $C_A$  = Concentration of diffusing solute 'A'.  $(\frac{\text{gms or gm moles}}{\text{cc}})$  or  $(\frac{\text{gms or gm moles}}{\text{litre}})$ .
- $C_A^b$  = Concentration of the solute 'A' in the bulk liquid phase.  $(\frac{\text{gms or gm moles}}{\text{cc}})$  or  $(\frac{\text{gms or gm moles}}{\text{litre}})$ .
- $C_A^s$  = Concentration of solute 'A' in the liquid phase at saturation.  $(\frac{\text{gms or gm moles}}{\text{cc}})$  or  $(\frac{\text{gms or gm moles}}{\text{litre}})$ .
- $d_e$  = Bubble equivalent spherical diameter (cms.).
- $d_f$  = Final equivalent spherical diameter of the bubble at formation (cms.).
- D = Diffusivity of the solute in the liquid phase ( $\text{cm}^2/\text{sec}$ ).





$D_{ik}$  = Function in expression for derivative by Lagrangian Interpolation. Given by equation A.19.

$e_c$  = Eccentricity of bubble ( =  $\frac{\text{Maximum Width}}{\text{Maximum Height}}$  ).

$f(v)$  = Function describing bubble periphery i.e. abscissa of a point on the bubble periphery (cms).

$f'(v)$  = Derivative of  $f(v)$  with respect to  $V$ .

$F$  = Faraday Number.

$g(v)$  = Function defined as  $[f(v) \sqrt{1+f'(v)^2}]$ .

$G$  = Gas flow rate through the orifice ( $\frac{cc}{sec}$ ).

$h$  = Spacing interval in Newton Cotes integration formula.

$H$  = Henry's Law constant.

$i$  = Diffusion current ( $\mu A$ ).

$k$  = Constant in equations for bubble periphery given as 3.7 through 3.12, 3.16 and 3.17.

$k_1$  = Constant in equation 2.19 for surface area of a bubble as a function of time.

$k_L$  = Instantaneous liquid phase mass transfer coefficient.  
( $\frac{cms}{sec}$ ) or ( $\frac{cms}{hr}$ ).

$k_{Lav}$  = Average liquid phase mass transfer coefficient during bubble formation. ( $\frac{cms}{sec}$ ) or ( $\frac{cms}{hr}$ ).

$k_{Lav}^1$  = Average liquid phase mass transfer coefficient during bubble rise period. ( $\frac{cms}{sec}$ ) or ( $\frac{cms}{hr}$ ).

$k_{Le}$  = Mass transfer coefficient of oxygen in water.  
( $\frac{cms}{sec}$ ) or ( $\frac{cms}{hr}$ ).

$K^*$  = A function of bubble eccentricity used in equation 2-15.



$n$  = Exponent for equations representing models of the bubble periphery (equations 3.8, 3.9, 3.16 and 3.17).

$n_1$  = Exponent of time in equation 2.19 for variation of bubble area with time.

$n_2$  = Exponent of dimensionless time in surface area equations 2.26.

$n^*$  = Exponent of polar coordinate 'r' in equation 6.2.

$\bar{n}$  = Number of electrons taken up during the electrochemical reaction.

$N$  = Normality of  $\text{Ba}(\text{OH})_2$  solution.

$N_1$  = Normality of  $\text{HCl}$  solution.

$N_{\text{CO}_2}$  = Normality of carbon-dioxide in solution.

$N^*$  = Mass transfer of oxygen in water to the cathode.  
(gms or gm moles).

$N_A$  = Total mass transfer in time 't' (gms or gm moles).

$N'_A$  = Mass Transfer rate at time 't' ( $\frac{\text{gms or gm moles}}{\text{sec}}$ ).

$N_c$  = Capacitance Number ( $= \frac{4g(\rho_c - \rho_d)V_c}{\pi \delta^2 \rho_d c^2}$ ).

$N_p$  = Total number of data points in a given population i.e. size of the population.

$N_s$  = Representative sample size for a given population.

$p_A$  = Partial pressure of 'A' in the gas phase (mm.Hg).

$Pe$  = Peclet Number of bubble or drop ( $= \frac{d_e U}{D}$ ).

$P_i(x)$  =  $i^{\text{th}}$  Lagrangian polynomial in x.

$P_j(x)$  = Polynomial of degree j ( $j=0,1,\dots,m$ ).

$r$  = Polar coordinate of bubble periphery.



$r_o$  = Radius of the column (cms).

$r_l$  = Any radial position in the column from the centre line (cms).

$r_e$  = Radius of a sphere of volume equivalent to the axis-symmetric body of revolution (cms).

$Re$  = Orifice Reynolds Number ( $= \frac{\rho_d U_g \delta}{\mu_c}$ ).

$S$  = Surface area of revolution of a body ( $\text{cm}^2$ ).

$Sc$  = Schmidt Number ( $= \frac{\mu_c}{\rho^c D}$ ).

$Sh$  = Sherwood Number ( $= \frac{k_L^c d_e}{D}$ ).

$t$  = Time (sec).

$t_e$  = Time taken by bubble to rise a distance equal to its equivalent spherical diameter at its vertical rise velocity. (sec).

$T_f$  = Total time of formation of bubble (sec).

$U_l$  = Average liquid velocity in the column (cms/sec).

$U_g$  = Velocity of the gas at the orifice (cms/sec).

$U$  = Free rising or falling velocity of bubble or drop (cms/sec).

$v$  = Vertical height of the bubble or the ordinate of a point on the bubble periphery (cms.).

$V$  = Volume of revolution of a body or volume of a bubble (cc).

$V_1$  = Volume of  $\text{HCl}$  used to neutralize a given volume of  $\text{Ba(OH)}_2$  solution in a blank titration (cc).

$V_2$  = Volume of  $\text{HCl}$  used at the end of the first stage of the back titration (cc).

$V^*$  = Volume of a detached bubble estimated from photographs (cc).







$V_c$  = Chamber Volume (cc).

$x$  = Distance from the electrode (cms).

$\bar{x}$  = Mean of the sample.

$x_i$  = Value of the individual data point in a given population.

$\bar{x}_s$  = Mean of the sample.

$X^*$  = Characteristic length for platinum probe 1 (mm).

$X_A$  = Moles of solute 'A' per mole of  $\text{CO}_2$ -Water Solution.

$y_j$  = Value of a function of 'x' at  $x=x_j$ .

$Y^*$  = Characteristic length for platinum probe 2 (mm).

### Greek Symbols

$\alpha_j$  = Factor in Forsythe polynomial given by equation A.16.

$\beta_j$  = Factor in Forsythe polynomial given by equation A.17.

$\delta$  = Orifice diameter (cms).

$\theta$  = Polar coordinate for bubble periphery and an axis-symmetric body of revolution.

$\mu$  = Standard deviation of the individual data point from the mean of the population.

$\mu_c$  = Viscosity of the continuous phase ( $\frac{\text{gm}}{\text{cm sec}}$ ).

$\rho_c$  = Density of the continuous phase (gms/cc).

$\rho_d$  = Density of the dispersed phase (gms/cc).

$\nu$  = Frequency of bubble formation ( $\text{sec}^{-1}$ ).

$\eta_m$  = Maximum frequency of bubble formation attained in the constant frequency region ( $\text{sec}^{-1}$ ).

$\sigma_\ell$  = Cut off limits or sigma limits on a given distribution



of individual data points for a given level of confidence.

$\Phi_m(x)$  = Function for a polynomial fit.

$\Phi_n(x)$  = Function given by equation A.21.



REFERENCES

- (1) Calderbank, P.H., Trans. Inst. Chem. Engrs., 34, 79, (1956).
- (2) Haselden, G.G., and Thorogood, R.M., Trans. Inst. Chem. Engrs., 42, 81, (1964).
- (3) Bowman, C.W., and Johnson, A.I., Can. J. Chem. Eng., 40, 139, (1962).
- (4) Licht, W., and Conway, J.B., Ind. Eng. Chem., 42, 1151, (1950).
- (5) Licht, W., and Pansing, W.F., Ind. Eng. Chem., 45, 1885, (1953).
- (6) Dixon, B.E., and Swallow, J.E.L., J. Appl. Chem., 4, 86, (1954).
- (7) Dixon, B.E., and Russell, A.A.W., J. Soc. Chem. Inc. Lond., 69, 284, (1950).
- (8) Calderbank, P.H., and Patra, R.P., Chem. Eng. Sci., 21, 719, (1966).
- (9) Higbie, R., Trans. A.I.Ch.E. Journal, 31, 365, (1953).
- (10) Van Krevelin, D.W., and Hoftijzer, P.J., Chem. Eng. Progr., 46, 29, (1950).
- (11) Quigley, C.J., Johnson, A.I., and Harris, B.L., Chem. Eng. Progr. Sym. Ser., No. 16, 51, 31, (1955).
- (12) Hughes, R.R., Handlos, A.E., Evans, H.D., and Maycock, R.L., Chem. Eng. Progr., 51, 557, (1955).





- (13) Coppock, P.D., and Meiklejohn, G.T., Trans. Inst. Chem. Engrs., 21, 75, (1951).
- (14) Leibson, I., Holcomb, E.G., Cacosso, A.G., and Jacmic, J.J., A.I.Ch.E. Journal, 2, 296, (1956).
- (15) Data, R.L., Napier, D.M., and Newitt, D.M., Trans. Inst. Chem. Engrs., 28, 14, (1950).
- (16) Davidson, L., Amick, E.H. Jr., A.I.Ch.E. Journal, 2, 337, (1956).
- (17) Benzing, R.J., and Myers, J.E., Ind. Eng. Chem., 47, 2087, (1955).
- (18) Valentin, F.H.H., "Absorption in Gas Liquid Dispersions", 1<sup>st</sup> Ed., Chapter 2, Spon's Chem. Eng. Series, 1967.
- (19) Davidson, J.F., and Schüller, B.O.G., Trans. Inst. Chem. Engrs., 38, 144, (1960).
- (20) Eversole, W.G., Wagner, G.H., and Stackhouse, E., Ind. Eng. Chem., 33, 1459, (1941).
- (21) Calderbank, P.H., Brit. Chem. Eng., 1, 206 and 267, (1956).
- (22) Seimes, W., Chem. Ing. Techn., 26, 479, (1954).
- (23) Rennie, J., and Evans, F., Brit. Chem. Eng., 7, 498, (1962).
- (24) Hayes, W.B., Hardy, B.W., and Holland, C.D., A.I.Ch.E. Journal, 5, 319, (1959).
- (25) Mahoney, J.F. Jr., and Wenzel, L.A. A.I.Ch.E. Journal, 9, 641, (1963).



- (26) Towell, G.D., Strand, C.P., and Ackerman, G.H.,  
A.I.Ch.E. - I. Chem. E., Sym. Ser., No. 10, 97,  
(1965).
- (27) Leonard, J.H., and Houghton, G., Chem. Eng. Sci., 18,  
133, (1963).
- (28) Calderbank, P.H., Chem. Engr., Review Series, No. 3,  
209, Oct. 1967.
- (29) Locheil, A.C., Ph.D. Thesis, Department of Chemical  
Engineering, University of Edinburgh, 1963.
- (30) Hammerton, D., and Garner, F.H., Trans. Inst. Chem.  
Engrs. Supplement, 32, 18, (1954).
- (31) Baird, M.H.I., and Hamielec, A.E., Can. J., Chem.  
Eng., 40, 164, (1962).
- (32) Friedlander, S.K., A.I.Ch.E. Journal, 7, 347, (1961).
- (33) Calderbank, P.H., and Moo-Young, M.B., Chem. Eng.  
Sci., 16, 39, (1962).
- (34) Ward, D.M., Trass, O., and Johnson, A.I., Can. J.  
Chem. Eng. 40, 164, (1962).
- (35) Aksel'Rud, G.A., Zh.fiz.Khim., 27, 1445, (1953).
- (36) Tomotika, S., A.R.C. Rep. Ser., No. 1678, (1953).
- (37) Froessling, N., Beitr, Geophys., 32, 170, (1938).
- (38) Hadamard, J., Dokl, Akad. Nauk, SSSr, 152, 1735,  
(1911).
- (39) Rybczynsky, W., Bull. Acad. Sci. Cracovie (A), 40,  
(1911).
- (40) Chao, B.T., Physics Fluid, 5, 69, (1962).
- (41) Griffith, R.M., Chem. Eng., Sci., 12, 198, (1960).



- (42) Heertjes, P.M., Holve, W.A., and Talsma, H., Chem. Eng. Sci., 3, 122, (1954).
- (43) Stefan, M.J., Sitz, Acad. Wiss. Wien., 77, 371, (1878).
- (44) Boussinesq, M.J., Compt. Rend. (Paris), 156, 1124, (1913).
- (45) West, F.B., Ind. Eng. Chem. ind. (int.) Edn., 43, 234, (1951).
- (46) Ruckenstein, E., Chem. Eng., Sci., 19, 131, (1964).
- (47) Zahm, A.F., NACA Rep., No. 253, 517, (1926).
- (48) Rosenberg, B., Report No. 727, (1950), (Washington D.C.: The David Taylor Model Basin).
- (49) Takadi, T., and Maeda, S., Chem. Eng. Toyko, 25, 254, (1961).
- (50) Zieminski, S.A. and Raymond, D.R., Chem. Eng. Sci., 23, 17, (1968).
- (51) Siddique, Q.M., Ph.D. Thesis, Department of Chemical Engineering, University of Birmingham, 1963.
- (52) Himmelblau, D.M., and Takayuki, N., A.I.Ch.E. Journal, 13, 697, (1967).
- (53) Groothuis, H., and Kramers, H., Chem. Eng. Sci., 4, 17, (1955).
- (54) Ilkovic, D., Coll. Czech. Chem. Commun., 6, 498, (1934).
- (55) Ilkovic, D., J. Chim. Phys., 35, 129, (1938).
- (56) Michels, H.H., Ph.D. Thesis, Department of Chemical Engineering, University of Delaware, 1960.







- (57) Popovich, A.T., Jervis, R.E., and Trass, O., Chem. Eng., Sci., 19, 357, (1964).
- (58) Hu, S., and Kintner, R.C., A.I.Ch.E. Journal, 1, 42, (1955).
- (59) Zieminski, S.A., Maurice, M.C., and Robert, B.B., I & E C Fundamentals, 6, 233, (1967).
- (60) Baird, M.H.I., and Davidson, J.F., Chem. Eng. Sci., 17, 87, (1962).
- (61) Houghton, G., Ritchie, P.D., and Thomson, J.A., Chem. Eng. Sci., 17, 221, (1962).
- (62) Lapidus, L., "Digital Computation for Chemical Engineers", Chapter 7, McGraw Hill Publication, 1962.
- (63) Charmonman, S., Department of Computing Science, University of Alberta, Edmonton, Alberta, Personal Communication.
- (64) Lapidus, L., "Digital Computation for Chemical Engineers", Chapter 2, McGraw Hill Publication, 1962.
- (65) Lapidus, L., "Digital Computation for Chemical Engineers", Chapter 2, McGraw Hill Publication, 1962.
- (66) Reiss, L.P., and Hanratty, T.J., A.I.Ch.E. Journal, 8, 245, (1962).
- (67) Heertjes, P.M., de Nie, L.H., Chem. Eng. Sci., 21, 755, (1966).
- (68) Poutanen, A.A., and Johnson, A.I., Can. J. Chem. Eng., 38, 93, (1960).



- (69) Bogandy, L., von Rutsch, W., and Stranski, I.N.,  
Chem. Ing. Tech., 31, 580, (1959).
- (70) Leonard, J.H., Ph.D. Thesis, Department of Chemical  
Engineering, University of Pittsburgh, Pa., 1961.
- (71) Calderbank, P.H., and Locheil, A.C., Chem. Eng. Sci.,  
19, 485, (1964).
- (72) Fricke, R., Z. Phys. Chem., 104, 363, (1923).
- (73) Perry, J.H., "Chemical Engineers Handbook", 4<sup>th</sup> Ed.,  
Section 14-4, McGraw Hill Publication, 1963.
- (74) Perry, J.H., "Chemical Engineers Handbook", 4<sup>th</sup> Ed.,  
Section 3-43, McGraw Hill Publication, 1963.



APPENDICESAppendix AEvaluation of Bubble Surface and Volume for Program I

With reference to Figure 2

$$S = 2\pi \int_{a_1}^{b_1} f(v) \sqrt{1+f'(v)^2} dv \text{ -----A-1}$$

$$r = a(k+\cos^n \theta) \text{ -----A-2}$$

$$f(v) = r \sin \theta = a(k+\cos^n \theta) \sin \theta = ak \sin \theta + a \sin \theta \cos^n \theta \text{ -----A-3}$$

$$f'(v) = \frac{df(v)}{d\theta} \frac{d\theta}{dv} \text{ -----A-4}$$

$$v = r \cos \theta = a(k+\cos^n \theta) \cos \theta = ak \cos \theta + a \cos^{n+1} \theta \text{ -----A-5}$$

$$dv = a \sin \theta (k+(n+1) \cos^n \theta) d\theta \text{ -----A-6}$$

$$\frac{d\theta}{dv} = - \frac{1}{a \sin \theta (k+(n+1) \cos^n \theta)} \text{ -----A-7}$$

also

$$\frac{df(v)}{d\theta} = ak \cos \theta - an \sin^2 \theta \cos^{n-1} \theta + a \cos^{n+1} \theta \text{ -----A-8}$$

substituting in A-4 we get





$$f'(v) = \frac{n \sin^2 \theta \cos^{n-1} \theta - k \cos \theta - \cos^{n+1} \theta}{\sin \theta (k + (n+1) \cos^n \theta)} \text{-----A-9}$$

Substituting for  $f(v)$  and  $f'(v)$  and  $dv$  in A-1 we get

$$S = 2\pi \int_{\pi/2}^0 -a^2 \sin \theta (k + \cos^n \theta) [\sin^2 \theta (k + (n+1) \cos^n \theta)^2 + (n \sin^2 \theta \cos^{n-1} \theta - k \cos \theta - \cos^{n+1} \theta)^2]^{1/2} d\theta \text{-----A-10}$$

The volume is evaluated as shown below:

$$V = \pi \int_a^b f(v) dv \text{-----A-11}$$

substituting for  $f(v)$  from A-3 and for  $dv$  from A-6 we get

$$V = \pi \int_{\pi/2}^0 -a^3 \sin^3 \theta (k + \cos^n \theta)^2 (k + (n+1) \cos^n \theta) d\theta \text{-----A-12}$$

### Equations Used for development of Program II

#### Forsythe Orthogonal Polynomial

The Forsythe Orthogonal Polynomial combined with the least square criterion is used in this investigation to smoothen the raw data obtained from photographic films. The maximum order permitted is 12. The standard deviation is of the order of  $10^{-4}$ . The program terminates when either of the two limits specified above is first achieved.



The equations are given as follows:

$$\Phi_m(x) = \sum_{j=0}^{j=m} b_j P_j(x) \text{ -----A-13}$$

Where  $\Phi_m(x)$  is the representation of the discrete data points in the form of a polynomial fit where  $P_j(x)$  is a polynomial of degree  $j$ . The Forsythe orthogonal polynomials are given by

$$P_{-1}(x) = 0$$

$$P_0(x) = 1$$

$$P_1(x) = (x - \alpha_1)P_0(x) - \beta_0 P_{-1}(x) \text{ -----A-14}$$

‘  
‘  
‘

$$P_{j+1}(x) = (x - \alpha_{j+1})P_j(x) - \beta_j P_{j-1}(x)$$

where  $\beta_0 = 0$ . The values of  $\alpha$  and  $\beta$  are chosen in such a way that

$$\sum_{i=1}^n P_j(x_i) P_k(x_i) = 0 \quad j \neq k \text{ -----A-15}$$

In general

$$\alpha_{j+1} = \frac{\sum_{i=1}^n x_i P_j(x_i)^2}{\sum_{i=1}^n P_j(x_i)^2} \text{ -----A-16}$$

and



$$\beta_j = \frac{\sum_{i=1}^n x_i P_{j-1}(x_i) P_j(x_i)}{\sum_{i=1}^n P_{j-1}(x_i)^2} \text{-----A-17}$$

### Evaluation of the Derivative at discrete points Using Lagrangian Interpolation

The equation used to evaluate the derivative  $\frac{dy}{dx}$  at a point  $(x_k, y_k)$  is given by

$$Y'|_{x_k} = \left\{ \sum_{\substack{i=0 \\ i \neq k}}^n \frac{y_i}{D_{ik}} \left( \prod_{\substack{j=0 \\ j \neq k}}^n (x_k - x_j) \right) + y_k \sum_{\substack{j=0 \\ j \neq k}}^n \left( \frac{1}{x_k - x_j} \right) \right\} \text{-----A-18}$$

Where  $D_{ik}$  is given by

$$D_{ik} = (x_k - x_i) P_i(x_i) \text{-----A-19}$$

and

$$P_i(x_i) = \prod_{\substack{j=0 \\ j \neq i}}^n (x_i - x_j) \text{-----A-20}$$

$P_i(x_i)$  is the Lagrangian Polynomial at  $x_i$ .

### Lagrangian Interpolation Formula

This is implicitly stated in the previous section  
i.e.





$$\Phi_n(x) = \sum_{i=0}^n \frac{P_i(x)}{P_i(x_i)} y_i \text{ -----A-21}$$

$$\text{where } P_i(x) = \prod_{\substack{j=0 \\ j \neq i}}^n (x-x_j) \text{ -----A-22}$$

### Newton Cotes 4<sup>th</sup> order integration Formula with 'm' subintervals

The integration formula for five evaluation points

$x_0, x_1, \dots, x_4$  is given by

$$\int_{x_0}^{x_4} f(x)dx = \frac{2h}{45} (7y_0 + 32y_1 + 12y_2 + 32y_3 + 7y_4) - \frac{8h^7}{945} f^{[6]}(\epsilon) \text{ ---A-23}$$

Where 'h' is the interval spacing. This formula may be applied repeatedly to cover more than 5 points, e.g.

$$\int_{x_0}^{x_9} f(x)dx = \int_{x_0}^{x_4} f(x)dx + \int_{x_4}^{x_9} f(x)dx \text{ and so on.}$$

In general, if this is applied 'm' times in succession the equation is given by

$$\int_{x_0}^{x_{4m}} f(x)dx = \frac{2h}{45} [7y_0 + 32(y_1 + y_3 + y_5 + \dots + y_{4m-1}) + 12(y_2 + y_6 + \dots + y_{4m-2}) + 14(y_4 + \dots + y_{4m-4}) + 7y_{4m}] \text{ -----A-24}$$



Appendix BProgram I

The program is entitled PROG 1 and consists of the mainline program five subroutines and two function subprograms. The subroutines are entitled PRELIM, LSQFIT, GAUSS, STD and GAQ10; the function subprograms are called FCT1 and FCT2.

Input to the program is done completely in the mainline and includes the following sequence of cards.

(1) NN, M1 where NN is the total number of data points minus one and M1 is the number of functions of x involved in the least square fit routine LSQFIT.

(2) XL, SV:- The lower and upper limits of integration respectively. These are used in the routine GAQ10. For this investigation  $XL = \pi/2$  and  $SV = 0$ .

(3) NUMRUN which indicates the total number of separate runs being analysed.

(4) L1:- The Total number of bubbles being analysed in any given run.

(5) G,U,SP,D where G is the gas flow rate in cc/sec, U is the liquid velocity in cms/sec, SP is the film speed in frames/sec and D is the outside orifice diameter in cms.

(6) M which indicates the frame number of the bubble being analysed. This is indicated on the film projector.

(7) OR1 (I),  $I=1,4$  :- These are four numbers representing the x and y coordinates of the two edges of the orifice to



give the orifice size on the projected film. These numbers are obtained from the photographic film of the bubble with the aid of the digitizer. The Y coordinate should precede the X coordinate in all cases.

(8) Data points from the bubble periphery:- These are obtained with the digitizer. A format of (16I5) is specified indicating a maximum of 16 numbers or 8 points on the bubble periphery per card. The sequence in which the bubble periphery should be traversed is shown in Figure 36. The total number of cards used up with this data depends on the total number of points taken on the bubble periphery.

(9) NAPEXV, NAPEXF:- These are the Y and X coordinates respectively of the apex of the bubble i.e. corresponding to point 17 in Figure 36. This is read separately from the rest of the data so that the same data deck could be used for Program II.

For each bubble belonging to the same run, cards corresponding to sections 6 through 9 above must be included. For each run, cards corresponding to sections 4 through 9 should be included.

The operations performed by different parts of the program are as follows:

Mainline Program:- (i) Inputs all the data mentioned above.  
 (ii) Transforms the data of the bubble periphery so that the bubble is symmetrical above the







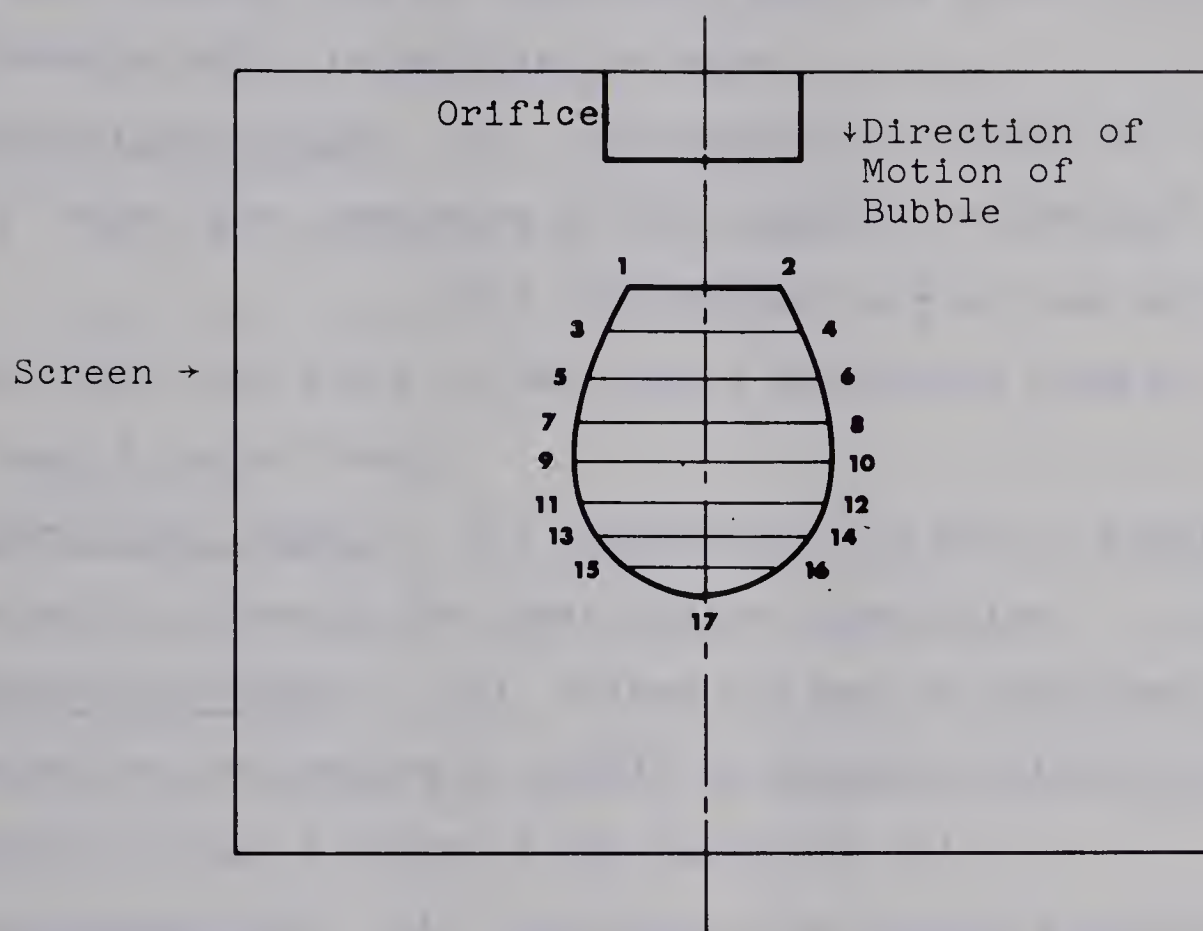


Figure 36: Sequence of Reading the Bubble Periphery



central axis.

(iii) Converts the digitized data to actual bubble size by comparison with the actual orifice diameter which is supplied as data.

Subroutine PRELIM:- (i) Determines the values of 'a' and 'k' which are parameters of the equation  $r=a(k+\cos\theta^n)$

(ii) Determines  $\ln(\frac{r}{a}-k)$  and  $\ln(\cos\theta)$  for each data point on the bubble and stores them as vectors Y and X respectively.

Subroutine LSQFIT:- (i) Determines the set of simultaneous equations through the least square formulation

Subroutine GAUSS:- (i) Solves the set of simultaneous equations determined in LSQFIT by Gaussian Elimination Method to get a value of the parameter 'n'.

Subroutine STD:- (i) Determines the standard deviation of the least square fit.

Subroutine GAQ10:- (i) Integrates the functions for bubble volume and surface derived in Appendix "A" by a ten point Gaussian Quadrature formula.

Function Subprogram FCT1:- (i) Defines the function for bubble surface.

Function Subprogram FCT2:- (i) Defines the function for bubble volume.

The output from the program includes a listing of the following:

- (i) The run number being considered.
- (ii) The number of the bubble being analysed.



- (iii) The frame number the bubble corresponds to
- (iv) The gas and liquid flow rates, the film speed and the orifice outside diameter .
- (v) The standard deviation of the least square fit to determine the parameter 'n'.
- (vi) The bubble surface in  $\text{cm}^2$ .
- (vii) The bubble volume in  $\text{cm}^3$ .

## Program II

The program is entitled "FORMING" and is used to evaluate the bubble surface and volume using a numerical procedure. It consists of the mainline program and four subroutines which are entitled FORSYT, LADERI, LAGINT and NCOTES.

The input to the program is done in the mainline program only and consists of the following sequence of cards:

- (1) ERROR:- This is a specification of the upper bound on the variance in the Forsythe Orthogonal Polynomial fit used to smoothen the raw data.
- (2) NUMRUN:- Indicates the total number of runs analysed.
- (3) G,U,SP,D,TIMER,(C(I),I=1,4):- The variables are defined as
  - (i) G = Gas flow rate in cc/sec
  - (ii) U = Liquid velocity in cm/sec
  - (iii) SP= Film speed in frames/sec
  - (iv) D = Outside orifice diameter





- (v) TIMER = The cycle timer frequency in cycles/sec. This variable is not used in the program but could be output if required and is useful to check on the film speed SP.
- (vi) C(I), I=1,4 = These are four coefficients used in the fourth order Newton Cotes integration formula. The coefficients are 7.0, 32.0, 12.0 and 14.0.
- (4) L1:- The total number of bubbles to be analysed.
- (5) M1:- The total number of frames per bubble. This is used for cases where surface area is desired as a function of time for any one given bubble during the period of formation.
- (6) N,N1:- N is the total number of points on the bubble periphery excluding the apex of the bubble e.g. with reference to Figure 36, N=16. N1 is the number of intervals the total bubble height has been divided into upto the value of N. i.e.
- $$N_1 = \left[ \frac{N}{2} - 1 \right].$$
- With reference to Figure 36, N1=7.
- (7) L2(M):- The frame number of the frame being analysed.



(8) The data subsequent to section (7) above includes the same deck as indicated in sections (7), (8) and (9) of Program I. Even though both coordinates of the apex point are supplied, the program reads only the Y coordinate and generates the X coordinate itself.

If the program is being used for analysis of bubble formation, then  $M1 > 1$ . Cards corresponding to sections 6, 7 and 8 above must therefore be supplied for each frame analysed. If more than one bubble is being analysed in a given run, cards corresponding to sections 5 through 8 must be included for each bubble.

The complete set of data excluding the cards 1 and 2 for the ERROR and NUMRUN respectively, must be included for each run being analysed if the total number of runs is greater than 1.

The function of the subroutines used in the program is as follows:

Main Line Program:- The operation of the mainline in this program is identical to that in Program I.

Subroutine FORSYT:- Smoothens the data obtained from photographs by using the Forsythe Orthogonal Polynomials.

Subroutine LADERI:- Evaluates the derivative  $f'(v)$  at each of the smoothed data points. The Lagrangian interpolation formula is used.

Subroutine LAGINT:- Generates equispaced data for  $f(v)$  and for  $f(v) \sqrt{1 + f'(v)^2}$  using a third order Lagrangian Inter-



potation formula.

Subroutine NCOTES:- Integrates the functions  $f(v)^2$  and  $f(v)\sqrt{1+f'(v)^2}$  with respect to 'v' by a fourth order 'K' panel Newton Cotes formula. The number of panels K are determined by the total number of points on the bubble periphery. This number is generated in the main line program.

If detached bubbles are being analysed the output from the program includes the following:

- (i) The run number being considered
- (ii) The number of bubble being considered
- (iii) The gas flow rate in cc/sec and the liquid velocity in cms/sec
- (iv) The frame number and the cumulative time in seconds determined by the ratio  $\frac{\text{Frame Number}}{\text{Film Speed}}$ .
- (v) The bubble surface in  $\text{cm}^2$ .
- (vi) The bubble volume in  $\text{cm}^3$ .
- (vii) The number of panels used in the Newton Cotes integration formula.

If different frames from a single bubble are analysed to obtain surface area and volume as a function of time of formation, the output in sections (iv) through (vii) appears as a matrix in which each row corresponds to a frame analysed.







Program III

The program is called "SAMPLE" and is used to estimate the sample size from a given population of bubbles so that the bubble area and volume evaluated from the sample is representative of the total population.

The program input consists of the following sequence of cards.

- (1) M1,K1:- These are identification numbers for the run being investigated.
- (2) N,UP:- N is the total population size and UP is the sigma limit for a given level of confidence.
- (3) X(I),I=1,N:- These are the N actual data points from which the sample size is to be evaluated.
- (4) L1:- This indicates the total number of runs being analysed. This card is required only if L1>1 and is included after the data of the first run.

The output from the program includes the following:

- (i) The identification numbers of the orifice, liquid velocity and the number of the run.
- (ii) The individual data points X(I),I=1,N.
- (iii) The mean value of the variable 'X' from the total population.
- (iv) The standard deviation from the mean for the data.



It is defined as

$$\text{STDEV} = \sqrt{\frac{\sum_{I=1}^n (X(I) - \bar{X})^2}{N-1}}$$

where  $\bar{X}$  is the mean of the population.

(v) The sample size required.

The source listing of the three programs is included.



## - PROG 1 -

## - PROG 1 -

```

REAL FV(50),V(50),R(50),COSTA(50),X(50),Y(50),Q(25,50)
1,QT(50,25),C1(25),D2(25,25),P(25),DAUG(25,25),DEV(50),
2OR(4),SD,AC,ACP1,A,C,S,VOL,INT1,INT2,G,U,SP,D,D1,XL,
3XU,X1(50,25),Y1(50)
INTEGER FV1(50),V1(50),OR1(4),N,M,NM1,L,L1,M1,M2,IM1,
1IP1,M3,KP1,N1
EXTERNAL FCT1,FCT2

```

C THE PROGRAM EVALUATES THE SURFACE AND THE VOLUME OF GAS  
 C BUBBLES THAT HAVE BEEN JUST DETACHED FROM THE ORIFICE.  
 C THE TOTAL NUMBER OF BUBBLES AND THE GAS AND LIQUID FLOW  
 C RATES AND THE ORIFICE SIZE WILL BE READ IN AND PRINTED  
 C OUT. THE BUBBLES HAVE BEEN PHOTOGRAPHED BY A HIGH SPEED  
 C CAMERA AND DIGITAL DATA OF THE BUBBLE PERIPHERY IS TAKEN  
 C BY A DIGITISING MACHINE. THE FOLLOWING EQUATION HAS BEEN  
 C FOUND TO FIT THE BUBBLE PERIPHERY CLOSELY AND WILL BE USED  
 C IN THIS PROGRAM AS A BASIS.  $R=(A)*(K+\cos(\theta))^P$  WHERE  
 C P IS AN EXPONENT TO BE DETERMINED.

```

      READ(5,94)NN,M1
94  FORMAT(I3,I2)

```

C NN IS THE TOTAL NUMBER OF POINTS MINUS ONE.  
 C M1 IS THE NUMBER OF FUNCTIONS OF X INVOLVED IN THE FIT.  
 C I.E. IF  $Y=A+A1U1(X)$  THEN  $M1=1$ ; IF  $Y=A+A1U1(X)+A2U2(X)$  THEN  
 C  $M1=2$  ETC.  
 C THE BOTTOM APEX POINT IS OMITTED SO THAT THE  
 C DATA MAY BE MADE CONFORMABLE TO A NUMERICAL PROGRAM  
 C WRITTEN FOR A SIMILAR PURPOSE. N WILL BE SUBSEQUENTLY  
 C DEFINED AS  $NN+1$ .

```

      READ(5,96) XL,XU
96  FORMAT(2F12.8)
      READ(5,91)NUMRUN
91  FORMAT(I4)
      NRUN=1
90  L=1
      READ(5,99)L1
99  FORMAT(I4)
      READ(5,98)G,U,SP,D
98  FORMAT(F10.5,F10.5,F9.2,F9.5)
100 READ(5,93)M
93  FORMAT(I5)
      READ(5,101)(OR1(I),I=1,4)
101 FORMAT(4I5)
      READ(5,95)(V1(I),FV1(I),I=1,NN)
95  FORMAT(16I5)
      READ(5,92)NAPEXV,NAPEXF
92  FORMAT(2I5)

```





## - PROG 1 -

```

N=NN+1
V1(N)=NAPEXV
FV1(N)=NAPEXF

```

```

C THE ABOVE STATEMENTS SUPPLY ALL THE DATA.N=NO.OF DATA
C POINTS M=FRAME NO.G=GAS FLOW RATE U=LIQUID FLOW RATE
C SP=FRAME SPEED FV,V=DATA COORDINATES AND D=ORIFICE SIZE.
C THE DATA WILL NOW BE TRANSFORMED THROUGH AN AXIS SHIFT
C AND CORRECTED FOR MAGNIFICATION AND DISTORSION.
C FLOATING DIGITAL DATA

```

```

      DO 97 I=1,N
      FV(I)=FLOAT(FV1(I))
      V(I)=FLOAT(V1(I))
97  CONTINUE
      DO 50 I=1,4
      OR(I)=FLOAT(OR1(I))
50  CONTINUE
      D1=OR(4)-OR(2)
102 DO 103 I=1,N
      FV(I)=FV(I)*D/D1
      V(I)=V(I)*D/D1*3.48/3.42
103 CONTINUE

```

```

C EVALUATING THE MEAN 'Y' COORDINATE FOR TWO DATA POINTS IN
C THE SAME HORIZONTAL LEVEL.CONSIDERING THE TOTAL NUMBER OF
C POINTS TO BE ALWAYS ODD.

```

```

      NM1=N-1
      DO 104 I=2,NM1,2
      IM1=I-1
      V(I)=(V(I)+V(IM1))/2.0
      V(IM1)=V(I)
104 CONTINUE

```

```

C TRANSFORMING COORDINATES BY AXIS SHIFT

```

```

      SHIFT=V(1)
      SHIFT1=(FV(2)+FV(1))/2.0
      DO 105 I=1,N
      FV(I)=FV(I)-SHIFT1
      V(I)=V(I)-SHIFT
105 CONTINUE

```

```

C THE ABOVE TRANSFORMATION GIVES A POSITIVE AND A NEGATIVE
C VALUE OF FV FOR EACH VALUE OF V.THE VALUES MUST BE OF THE
C SAME ABSOLUTE MAGNITUDE.

```

```

      DO 106 I=2,NM1,2
      IM1=I-1

```



- PROG 1 -

```

SUM=(ABS(FV(I))+ABS(FV(IN1)))/2.0
FV(I)=+SUM
FV(IN1)=-SUM
106 CONTINUE

C SINCE COS(THETA) IS POSITIVE IN THE FIRST AND FOURTH
C QUADRANTS WE NEED TO CONSIDER ONLY HALF THE GIVEN POINTS.

CALL PRELIN(FV,V,R,COSTA,Y,X,AC,ACP1,A,C,N,NM1)
N1=(NM1/2)
INDEX=2
DO 120 I=1,N1
X1(I,1)=X(I+INDEX)
Y1(I)=Y(I+INDEX)
INDEX=INDEX+1
120 CONTINUE
CALL LSQFIT(X1,Y1,Q,QT,C1,D2,P,N1,M1,M2)
CALL GAUSS (X1,Y1,Q,QT,C1,D2,P,DAUG,N1,M1,M2)
CALL STD(P,Y1,QT,DEV,SD,N1,M2)
CALL GAQ10(XL,XU,FCT1,INT1,A,C,P)

C THE REQUIRED FUNCTION HAS NOW BEEN INTEGRATED AND THE
C SURFACE MAY BE EASILY EVALUATED.

S=2.0*3.1415926*INT1

C AREA OF THE CIRCULAR FLAT REGION AT THE BOTTOM IS GIVEN BY

S1=3.1415926*(AC**2)
S=S+S1

C EVALUATION OF VOLUME REQUIRES ANOTHER INTEGRATION OF A
C DIFFERENT FUNCTION.

CALL GAQ10(XL,XU,FCT2,INT2,A,C,P)
VOL=3.1415926*INT2
IF(L.GT.1) GO TO 121
WRITE(6,119)NRUN
119 FORMAT('1',20X,'RESULTS FOR RUN NO. P=',I3)
121 WRITE(6,107)L
107 FORMAT('1',20X,'DATA AND RESULT FOR BUBBLE NO.=',I4)
WRITE(6,108)
108 FORMAT('0',10X,'G CC/SEC',5X,'U CM/SEC',5X,'SP F/SEC',
15X,'D CM',7X,'M')
WRITE(6,109)G,U,SP,D,M
109 FORMAT(' ',7X,F10.5,3X,F10.5,4X,F9.2,3X,F9.5,2X,I6)
WRITE(6,115)SD
115 FORMAT(' ',10X,'STANDARD DEVIATION OF FIT = ',E20.8)
WRITE(6,116)S,VOL
116 FORMAT(' ',10X,'BUBBLE SURFACE IN SQ.CMS = ',E16.8,/)

```



## - PROG 1 -

```
110X,'BUBBLE VOLUME IN CC = ',E16.8)
  IF(L.GE.L1)GO TO 117
  L=L+1
  GO TO 100
117  IF(NRUN.GE.NUMRUN) GO TO 122
     NRUN=NRUN+1
     GO TO 90
122  STOP
     END
```





## SUBROUTINE PRELIM

```

SUBROUTINE PRELIM(FV,V,R,COSTA,Y,X,AC,ACP1,A,C,N,NM1)
REAL FV(50),V(50),R(50),COSTA(50),Y(50),X(50),AC,ACP1,
1A,C
INTEGER N,NM1

```

C THIS SUBROUTINE EVALUATES THE PARAMETERS A AND C AND THEN  
 C COMPUTES R AND COS(THETA). IT THEN REPLACES THE VALUES OF  
 C LOG(R/A-K) BY Y AND LOG COS(THETA) BY X.

```

ACP1=V(N)-V(1)
AC=ABS(FV(1))
A=ACP1-AC
C=AC/A

```

C R IS THE POSITION VECTOR OF EVERY POINT AND COSTA IS THE  
 C COSINE OF THE ANGLE OF THE POSITION VECTOR WITH THE AXIS.

```

DO 10 I=3,N,2
R(I)=SQRT((ABS(FV(I)))**2+(V(I)**2))
COSTA(I)=V(I)/R(I)
Y(I)=ALOG((R(I)/A)-(C))
X(I)=ALOG(COSTA(I))
10 CONTINUE
11 RETURN
END

```



## SUBROUTINE LSQFIT

```

SUBROUTINE LSQFIT (X,Y,Q,QT,C,D,A,N,M,M1)
REAL X(50,25),Y(50),Q(25,50),QT(50,25),C(25),D(25,25),
1A(25)
INTEGER N,M,M1,I,K,J,IM1,IP1,M2,KP1
200 DO 201 J=1,N
    Q(1,J)=1.0
201 CONTINUE
    M1=M+1
    DO 202 I=2,M1
        IM1=I-1
        DO 203 J=1,N
            Q(I,J)=X(J,IM1)
203 CONTINUE
202 CONTINUE

C THE MATRIX Q(I,J) MAY BE TERMED AS A COEFFICIENT
C MATRIX IN WHICH THE FIRST ROW IS 1 AND THE SUBSEQUENT ROWS
C HAVE X11,X21,X31,ETC THIS MATRIX HAS BEEN TRANSPOSED FROM
C THE ORIGINAL SET OF EQUATIONS.SEE DIGITAL COMPUTATION FOR
C CHEMICAL ENGINEERS BY LAPIDUS.
C NOW WE SHALL TRANSPOSE Q(I,J) AGAIN SO THAT WE MAY EXPRESS
C THE LEAST SQUARE FORMULATION.

204 DO 205 I=1,N
    DO 206 J=1,M1
        QT(I,J)=Q(J,I)
206 CONTINUE
205 CONTINUE

C A COLUMN VECTOR C(I) IS DETERMINED WHICH CORRESPONDS
C TO SIGMA(1 TO N) OF EACH COLUMN OF Q(I,J)*Y(J),THIS GIVES
C N COLUMN VECTORS WHICH ON ADDITION OF CORRESPONDING
C ELEMENTS YIELDS C(I).

    DO 207 I=1,M1
        C(I)=0.0
        DO 208 J=1,N
            C(I)=C(I)+Q(I,J)*Y(J)
208 CONTINUE
207 CONTINUE

C A MATRIX OF Q(I,J)*QT(I,J) IS NOW DETERMINED.

    DO 209 K=1,M1
        DO 210 J=1,M1
            D(K,J)=0.0
            DO 211 I=1,N
                D(K,J)=D(K,J)+Q(K,I)*QT(I,J)
211 CONTINUE
210 CONTINUE

```



SUBROUTINE LSQFIT

209 CONTINUE  
212 RETURN  
END





## SUBROUTINE GAUSS

```

SUBROUTINE GAUSS(X,Y,Q,QT,C,D,A,DAUG,N,M,M1)
REAL X(50,25),Y(50),Q(25,50),QT(50,25),C(25),D(25,25),
1A(25),DAUG(25,25)
INTEGER N,M,M1,I,K,J,IV1,IP1,I2,KP1

```

C GAUSSIAN ELIMINATION METHOD IS USED TO EVALUATE THE  
 C ELEMENTS OF THE RESULTANT COLUMN MATRIX.THE METHOD HOLDS  
 C PRETTY WELL FOR SMALL SIZED,DENSE COEFFICIENT MATRICES.

```

M2=M+2

```

C AN AUGMENTED MATRIX WITH C(I) FORMING THE M+2TH COLUMN OF  
 C D(I,J) IS DERIVED.

```

      DO 310 I=1,M1
      DO 311 J=1,M1
      DAUG(I,J)=D(I,J)
311  CONTINUE
      312 DAUG(I,M2)=C(I)
      310 CONTINUE
      313 DO 300 I=1,M1
      DMAX=0.0
      DO 301 K=1,M1
      IF(ABS(D(K,I)).LT.DMAX)GO TO 301
      DMAX=ABS(D(K,I))
      ISTORE=K
      301 CONTINUE

```

C THE ABOVE STATEMENTS SEEK THE MAXIMUM ELEMENT IN A COLUMN  
 C AND THE AIM IS TO BRING THE MAXIMUM ELEMENT ON THE  
 C DIAGONAL.THIS MINIMISES ROUND OFF ERROR.

```

      IF(I.EQ.ISTORE) GO TO 302
      DO 303 L=1,M2
      TEMP=DAUG(I,L)
      DAUG(I,L)=DAUG(ISTORE,L)
      DAUG(ISTORE,L)=TEMP
303  CONTINUE
      302 IP1=I+1
      DO 304 K=IP1,M1
      RATIO=DAUG(K,I)/DAUG(I,I)
      DO 305 L=1,M2
      IF(L.EQ.I) GO TO 308
      DAUG(K,L)=DAUG(K,L)-RATIO*DAUG(I,L)
      GO TO 305
308  DAUG(K,L)=0.0
305  CONTINUE
      304 CONTINUE
      300 CONTINUE

```



## SUBROUTINE GAUSS

C THE AUGMENTED MATRIX NOW CONSISTS OF AN UPPER DIAGONAL  
 C MATRIX WITH A COLUMN VECTOR ATTACHED AT ITS M+2TH COLUMN  
 C THE SOLUTION FOR THE RESULTANT VECTOR (A) STARTS FROM THE  
 C BOTTOM TOP.

```

      A(M1)=DAUG(M1,M2)/DAUG(M1,M1)
      DO 306 I=1,M
      SUM=0.0
      K=M1-I
      KP1=K+1
      DO 307 J=KP1,M1
      SUM=SUM+A(J)*DAUG(K,J)
307  CONTINUE
      A(K)=(DAUG(K,M2)-SUM)/DAUG(K,K)
306  CONTINUE
      RETURN
      END

```



## SUBROUTINE STD

```
SUBROUTINE STD(A,Y,QT,DEV,SD,N,M1)
REAL A(25),Y(50),QT(50,25),DEV(50),SD
INTEGER N,M1
DO 400 I=1,N
  SUM=-Y(I)
  DO 401 J=1,M1
    DEV(I)=SUM+QT(I,J)*A(J)
401  CONTINUE
400  CONTINUE
  SUMDSQ=0.0
  DO 402 I=1,N
    SUMDSQ=SUMDSQ+DEV(I)**2
402  CONTINUE
  SD1=SUMDSQ/FLOAT(N-1)
  SD=SQRT(SD1)
RETURN
END
```





## SUBROUTINE GAQ10

```
SUBROUTINE GAQ10(XL,XU,FCT,Y,A,C,P)
REAL XL,XU,Y,A,C,P(25)
EXTERNAL FCT
A1=0.5*(XU+XL)
B=XU-XL
C1=0.4869533*B
Y=0.03333567*(FCT((A1+C1),A,C,P)+FCT((A1-C1),A,C,P))
C1=0.4325317*B
Y=Y+0.07472567*(FCT((A1+C1),A,C,P)+FCT((A1-C1),A,C,P))
C1=0.3397048*B
Y=Y+0.1095432*(FCT((A1+C1),A,C,P)+FCT((A1-C1),A,C,P))
C1=0.2166977*B
Y=Y+0.1346334*(FCT((A1+C1),A,C,P)+FCT((A1-C1),A,C,P))
C1=0.07443717*B
Y=B*(Y+0.1477621*(FCT((A1+C1),A,C,P)+FCT((A1-C1),A,C
1,P)))
RETURN
END
```



## FUNCTION FCT1

```
FUNCTION FCT1(Z,A,C,P)
REAL Z,A,C,P(25)
B1=-(A**2)*SIN(Z)
B2=C+(COS(Z)**P(2))
B3=(SIN(Z)**2)*((C+(P(2)+1)*(COS(Z)**P(2))))**2)
B4=(P(2)*(SIN(Z)**2)*(COS(Z)**(P(2)-1))-C*COS(Z)
1-COS(Z)**(P(2)+1)
1**2
FCT1=B1*B2*SQRT(B3+B4)
RETURN
END
```



## FUNCTION FCT2

```
FUNCTION FCT2(Z,A,C,P)
REAL Z,A,C,P(25)
B1=-(A**3)*(SIN(Z)**3)
P2=(C+(COS(Z)**P(2)))**2
B3=C+((P(2)+1)*(COS(Z)**P(2)))
FCT2=B1*B2*B3
RETURN
END
```





- FORMING -

- FORMING -

```

      REAL FV(50),V(50),OR(4),PHI(50),C(10),ERR(50),T(100),
      1S(100),VOL(100),DERI(50),FXV(50),FXV1(50),Y(50),G,SP,
      2TIMER,U,D,D1,INT1,INT2,H,APEX,PHI1(50),ERROR
      INTEGER N1,N,M,M1,L1,L,FV1(50),V1(50),OR1(4),K,NAPEX,
      1L2(50),K1(20)

```

C THE PROGRAM EVALUATES THE SURFACE AND VOLUME OF DESCRETE  
 C BUBBLES DURING FORMATION AT A GIVEN ORIFICE UNDER  
 C SPECIFIED CONDITIONS OF GAS AND LIQUID FLOW. THE TECHNIQUE  
 C INVOLVES NUMERICAL ANALYSIS. USE IS MADE OF THE LAGRANGIAN  
 C POLYNOMIAL FOR DERIVATIVES, FORSYTHE ORTHOGONAL POLYNOMIALS  
 C AND NEWTON COTES INTEGRATION FORMULAE.

```

      READ(5,92)ERROR
92   FORMAT(E10.2)
      READ(5,95)NUMRUN
95   FORMAT(I4)
      NRUN=1
94   READ(5,99)G,U,SP,D,TIMER, (C(I),I=1,4)
99   FORMAT(2F9.5,F12.2,F9.5,I7, 4F7.2)
      L=1
      READ(5,100)L1
100  FORMAT(I4)
101  READ(5,102)M1
102  FORMAT(I4)
      M=1
98   READ(5,103)N,N1
103  FORMAT(2I3)
      K=N1/4
      K1(M)=K

```

C SO FAR THE TOTAL NUMBER OF BUBBLES L1, THE TOTAL NUMBER OF  
 C FRAMES PER BUBBLES M1, THE NUMBER OF INTERVALS N1, THE TOTAL  
 C DATA POPULATION N THE NUMBER OF PANELS IN THE NEWTON COTES  
 C FORMULA K AND THE NEWTON COTES COEFFICIENTS HAVE BEEN  
 C READ. THE DATA FROM EACH BUBBLE FRAME WILL NOW BE READ.

```

      READ(5,93)L2(M)
93   FORMAT(I5)
      READ(5,104)(OR1(I),I=1,4)
104  FORMAT(4I5)

```

C FOR REASONS WHICH WILL BE CLEAR LATER, A THIN ALMOST  
 C SPHERICAL SECTOR FROM THE BUBBLE APEX WILL BE CUT OFF AND  
 C TREATED SEPARATELY FOR SURFACE AND VOLUME.

```

      READ(5,97)(V1(I),FV1(I),I=1,N)
97   FORMAT(16I5)

```



## - FORMING -

C THE APEX VALUE WILL BE READ SEPARATELY. NOTE THAT THE VALUE  
 C OF FV AT APEX IS BEING ASSUMED TO BE EQUIVALENT TO ZERO,  
 C THE POINT BEING ON THE AXIS.

```
      READ(5,96)NAPEX
96   FORMAT(15)
```

C THE DATA WILL NOW BE TRANSFORMED THROUGH AN AXIS SHIFT AND  
 C CORRECTED FOR MAGNIFICATION AND DISTORSION.  
 C FLOATING DIGITAL DATA.

```
      DO 105 I=1,N
      FV(I)=FLOAT(FV1(I))
      V(I)=FLOAT(V1(I))
105   CONTINUE
      DO 111 I=1,4
      OR(I)=FLOAT(OR1(I))
111   CONTINUE
      APEX = FLOAT(NAPEX)
      D1=OR(4)-OR(2)
      DO 106 I=1,N
      FV(I)=FV(I)*D/D1
      V(I)=V(I)*(D/D1)*(3.48/3.42)
106   CONTINUE
      APEX=APEX*(D/D1)*(3.48/3.42)
```

C EVALUATING MEAN Y COORDINATE FOR TWO DATA POINTS IN THE  
 C SAME HORIZONTAL LEVEL. CONSIDERING TOTAL NUMBER OF POINTS  
 C TO BE ALWAYS EVEN.

```
      DO 107 I=2,N,2
      IM1=I-1
      V(I)=(V(I)+V(IM1))/2.0
      V(IM1)=V(I)
107   CONTINUE
```

C TRANSFORMING COORDINATES BY AXIS SHIFT.

```
      SHIFT=V(1)
      SHIFT1=(FV(2)+FV(1))/2.0
      DO 108 I=1,N
      FV(I)=FV(I)-SHIFT1
      V(I)=V(I)-SHIFT
108   CONTINUE
      APEX=APEX-SHIFT
```

C THE ABOVE TRANSFORMATION GIVES A POSITIVE AND A NEGATIVE  
 C VALUE OF FV FOR EACH VALUE OF V, THE TWO VALUES MUST BE OF  
 C THE SAME ABSOLUTE MAGNITUDE.



- FORMING -

```
DO 109 I=2,N,2
  IM1=I-1
  SUM=(ABS(FV(I))+ABS(FV(IM1)))/2.0
  FV(I)=SUM
  FV(IM1)=-SUM
109 CONTINUE
```

C THE DATA WILL NOW BE SMOOTHED BY THE USE OF THE FORSYTHE  
C ORTHOGONAL POLYNOMIAL.

```
N2=N/2
CALL FORSYT(FV,V,PHI,ERR,Y,ERROR,N2,N,N1)
```

C THE SMOOTHED DATA HAS PHI(V) INSTEAD OF F(V) AND FURTHER  
C WORK IS DONE WITH THE SMOOTHED DATA. THE DERIVATIVE OF THE  
C SMOOTHED FUNCTION AT DESCRETE POINTS WILL NOW BE DERIVED  
C USING LAGRANGIAN INTERPOLATION. THE SPHERICAL SEGMENT  
C CONTAINING THE BUBBLE APEX POINT WAS TREATED SEPARATELY  
C BECAUSE THE DERIVATIVE AT THE APEX IS INFINITE AND HENCE  
C NOT ACCEPTABLE. AN APPROXIMATION FOR THE SEGMENT WILL BE  
C USED.

```
CALL LADERI(PHI,ERR,Y,DERI,N2,N)
```

C HAVING EVALUATED THE DERIVATIVE WE SHALL EVALUATE THE  
C FUNCTION FXV.  
C WHERE FXV=F(V)\*SQRT(1+DERI\*\*2)

```
DO 110 I=2,N,2
  FXV(I)=ABS(PHI(I))*SQRT(1.0+DERI(I)**2)
110 CONTINUE
```

C THE FUNCTION FXV IS A COMPOSITE FUNCTION FOR EVALUATION OF  
C BUBBLE SURFACE. INTEGRATION IS BEING DONE BY THE USE OF A K  
C PANEL NEWTON COTES FORMULA OF FOURTH ORDER I.E. A FIVE  
C POINTS FORMULA APPLIED TO 4K+1 EQUIDISTANT POINTS.

```
DIST=APEX-V(1)
```

C AN ANGLE OF FIVE DEGREES ON EITHER SIDE OF THE MEDIAN OR  
C CENTRAL AXIS OF THE BUBBLE IS TAKEN AND A CHORD JOINING  
C THE TWO POINTS OBTAINED CORRESPONDS TO THE PORTION OF THE  
C BUBBLE SLICED OFF FROM THE APEX FOR SEPARATE TREATMENT.  
C THIS VERTICAL HEIGHT CORRESPONDS TO ABOUT 0.2 PERCENT OF  
C THE TOTAL BUBBLE HEIGHT.

```
SLICE=DIST*0.2/100.0
REMAIN=DIST-SLICE
HEIGHT=REMAIN/FLOAT(N1)
```





## - FORMING -

C 'HEIGHT' IS THE INTERVAL LENGTH OBTAINED BY DIVIDING THE  
C REMAINING VERTICAL DISTANCE INTO N1 PARTS. THE EQUISPACED  
C DATA CAN THUS BE GENERATED.

```
CALL LAGINT(FXV,Y,APEX,HEIGHT,N2,N,N1)
CALL NCOTES(HEIGHT ,FXV,C,INT1,K,N,N1)
S(M)=2.0*3.1415926*INT1
```

C THE ABOVE IS THE SURFACE OF THE BUBBLE EXCLUDING THE SMALL  
C SEGMENT AT THE APEX. IN THIS REGION THE DERIVATIVE IS VERY  
C LARGE AS COMPARED TO 1 AND THE EQUATION FOR THE SURFACE  
C MAY BE APPROXIMATED TO THE AREA OF A DISC WITH RADIUS  
C FV(N).

```
CALL LAGINT(PHI,Y,APEX,HEIGHT,N2,N,N1)
S1=3.1415926*(PHI(N)**2)
S(M)=S(M)+S1
```

C IF THE FRAME CORRESPONDING TO THE FINAL DETACHED BUBBLE IS  
C UNDER CONSIDERATION WE HAVE TO ADD THE AREA OF THE BOTTOM  
C DISC ALSO.

```
IF(M.LT.M1) GO TO 112
S2=3.1415926*(PHI(2)**2)
S(M)=S(M)+S2
```

C HAVING EVALUATED THE SURFACE WE SHALL NOW EVALUATE THE  
C VOLUME OF THE BUBBLE AT THAT TIME.

```
112 DO 114 I=2,N,2
    FXV1(I)=PHI(I)**2
114 CONTINUE
    CALL NCOTES(HEIGHT ,FXV1,C,INT2,K,N,N1)
    VOL(M)=3.1415926*INT2
```

C THIS ONCE AGAIN EXCLUDES THE VOLUME OF THE SEGMENT. THAT  
C VOLUME IS BEING APPROXIMATED TO THAT OF A SPHERICAL  
C SEGMENT.

```
H1=SLICE
V2=(3.1415926*H1/6.0)*((3.0*PHI(N)**2)+(H1**2))
VOL(M)=VOL(M)+V2
```

C THE VOLUME IS THUS EVALUATED. WE SHALL EVALUATE THE TIME AT  
C WHICH THE ABOVE SURFACE AND VOLUME EXISTS.  
C NOTE THAT THE EXACT SPEED MUST BE READ IN.

```
T(M)=FLOAT(L2(M))/SP
IF(M.GE.M1) GO TO 115
M=M+1
```



## - FORMING -

```

      GO TO 98
115  IF(L.GT.1) GO TO 128
      WRITE(6,129)NRUN
129  FORMAT('1',20X,'RESULTS FOR RUN NO. M=',I4)
128  WRITE(6,116)L
116  FORMAT('0',10X,'TIME VS SURFACE AND VOLUME FOR BUBBLE
1  NO.=',I4)
      WRITE(6,117)G,U,SP,D
117  FORMAT('0',10X,'G CC/SEC=',F10.5,5X,'U CM/SEC=',F10.5/
110X,'SP FPS=',F10.2,5X,'D CM=',F10.5)
      WRITE(6,123)
123  FORMAT('0',10X,'FRAME NO.',4X,'T SEC',4X,'S SQ.CM',
14X,'V CC',4X,'PANELS K')
      DO 124 I=1,M1
      WRITE(6,125)L2(I),T(I),S(I),VOL(I),K1(I)
124  CONTINUE
125  FORMAT(' ',11X,I4,5X,F10.6,2X,F11.6,1X,F9.6,4X,I2)
      IF(L.GE.L1) GO TO 126
      L=L+1
      GO TO 101
126  IF(NRUN.GE.NUMRUN) GO TO 131
      NRUN=NRUN+1
      GO TO 94
131  STOP
      END

```



## SUBROUTINE FORSYT

```

SUBROUTINE FORSYT(FV,V,PHI,ERR,Y,ERROR,N2,N,N1)
REAL FV(50),V(50),PHI(50),ERR(50),Y(50),ALPHA(20),
1BETA(20),B(20),PHI1(20,50),X(50),P(20,50),ER(20,50),
2VAR,ERROR
INTEGER N2,N,N1,ISTORE

```

```

C WE SHALL FIRST EVALUATE THE ORTHOGONAL POLYNOMIALS AND
C THEN THE COEFFICIENTS OF THE NORMAL EQUATIONS.FOR DETAILS
C SEE LAPIDUS(DIGITAL COMPUTATION FOR CHEM.ENGRS.)PP333-336
C REDEFINING INDEX OF DATA

```

```

DO 9 I=1,N2
X(I)=ABS(FV(2*I))
Y(I)=V(2*I)
9 CONTINUE
DO 10 I=1,N2
P(1,I)=0.0
P(2,I)=1.0
PHI1(1,I)=0.0
10 CONTINUE

```

```

C THE FIRST TWO POLYNOMIALS HAVE BEEN DEFINED.THE MAXIMUM
C DEGREE OF POLYNOMIAL TO BE USED IS 12.

```

```

DO 11 J=2,14
S1=0.0
S2=0.0
S3=0.0
S4=0.0
S5=0.0
DO 12 I=1,N2
S1=S1+Y(I)*P(J,I)**2
S2=S2+P(J,I)**2
S3=S3+Y(I)*P(J-1,I)*P(J,I)
S4=S4+P(J-1,I)**2
S5=S5+X(I)*P(J,I)
12 CONTINUE

```

```

C DEFINING ALPHAS AND BETAS

```

```

ALPHA(J+1)=S1/S2
IF(J.EQ.2) GO TO 5
BETA(J)=S3/S4
GO TO 6
5 BETA(2)=0.0
6 B(J)=S5/S2

```

```

C DEFINING P(J+1)

```

```

DO 13 I=1,N2

```





## SUBROUTINE FORSYT

```

      P(J+1,I)=(Y(I)-ALPHA(J+1))*P(J,I)-BETA(J)*P(J-1,I)
13  CONTINUE
      DO 14 I=1,N2
      PHI1(J,I)=PHI1(J-1,I)+B(J)*P(J,I)
      ER(J,I)=ABS(X(I)-PHI1(J,I))
      ERR(I)=ER(J,I)**2
14  CONTINUE
      S=0.0
      DO 15 I=1,N2
      S=S+ERR(I)
15  CONTINUE
      M=J-2
      ISTORE=J
      N22=N2-M
      IF(N22.EQ.1) GO TO 105
      VAR=S/FLOAT(N2-(M+1))
105  IF(N22.EQ.1) GO TO 16
      IF(VAR.LE.ERROR) GO TO 16
11  CONTINUE

```

C WE SHALL NOW REDEFINE THE VALUES THAT HAVE TO RETURN OUT  
C OF THE SUBROUTINE.

```

16  DO 17 I=1,N2
      PHI(I)=PHI1(ISTORE,I)
17  CONTINUE

```

C SINCE THIS DATA GOES DIRECTLY INTO THE NEXT SUBROUTINE WE  
C DO NOT NEED TO REINDEX AT THIS STAGE,BUT SHALL DO SO AT  
C THE END OF THE SUBROUTINE LADERI.

```

18  RETURN
      END

```



## SUBROUTINE LADERI

```

SUBROUTINE LADERI(PHI,ERR,Y,DERI,N2,N)
REAL PHI(50),ERR(50),Y(50),DERI(50),D(50,50),POLY(50)
INTEGER N2,N

```

```

C THIS SUBROUTINE IS USED TO EVALUATE THE DERIVATIVE AT
C INDIVIDUAL POINTS OF A TABULATED DATA SET. THE METHOD USED
C IS THE LAGRANGIAN INTERPOLATION.
C EVALUATING LAGRANGIAN POLYNOMIALS AND THE D(I,K)'S

```

```

      DO 201 I=1,N2
      POLY(I)=1.0
      DO 202 J=1,N2
      IF(I.EQ.J) GO TO 202
      POLY(I)=POLY(I)*(Y(I)-Y(J))
202  CONTINUE
201  CONTINUE
      DO 203 K=1,N2
      DO 204 I=1,N2
      IF(I.EQ.K) GO TO 204
      D(I,K)=(Y(K)-Y(I))*POLY(I)
204  CONTINUE
203  CONTINUE

```

```

C EVALUATING DERIVATIVES ONE BY ONE.

```

```

      DO 205 K=1,N2
      PROD=1.0
      SUM1=0.0
      DO 206 J=1,N2
      IF(K.EQ.J) GO TO 206
      PROD=PROD*(Y(K)-Y(J))
      SUM1=SUM1+(1.0/(Y(K)-Y(J)))
206  CONTINUE
      SUM2=0.0
      DO 207 I=1,N2
      IF(K.EQ.I) GO TO 207
      SUM2=SUM2+(PHI(I)/D(I,K))*PROD
207  CONTINUE
      DERI(K)=SUM2+PHI(K)*SUM1
205  CONTINUE

```

```

C THE VALUES OF PHI(I) AND DERI(I) AND ERR(I) WILL NOW BE
C REINDEXED TO SUIT THE MAIN LINE PROGRAM.

```

```

      DERI(N)=DERI(N/2)
      PHI(N)=PHI(N/2)
      ERR(N)=ERR(N/2)
      NM2=N-2
      DO 209 K=2,NM2,2
      I=N-K

```



## SUBROUTINE LADERI

```
    PHI(I)=PHI(I/2)
    DERI(I)=DERI(I/2)
    ERR(I)=ERR(I/2)
209  CONTINUE
210  RETURN
    END
```





## SUBROUTINE LAGINT

```

SUBROUTINE LAGINT(FN,Y,APEX,HEIGHT,N2,N,N1)
REAL FN(50),Y(50),APEX,HEIGHT,FCT(50),FXV2(50),Y1(50),
1L(30)
INTEGER N2,N,N1

```

```

C THIS SUBROUTINE GENERATES EQUISPACED DATA FROM THE
C UNEQUISPACED DATA AFTER THE COMPOSITE FUNCTION FXV HAS
C BEEN EVALUATED. A THIRD ORDER LAGRANGIAN INTERPOLATION
C POLYNOMIAL WILL BE MADE TO FIT 4 POINTS AND SOME
C EQUISPACED DATA DETERMINED. THE FIRST IS THEN DROPPED AND
C THE 5TH POINT IS ACCEPTED AND A NEW POLYNOMIAL TAKEN TO
C GIVE DATA FOR NEXT SET OF INTERVALS AND SO ON.
C REINDEX FN

```

```

      DO 10 I=1,N2
      FXV2(I)=FN(2*I)
10  CONTINUE
      N2P1=N2 + 1
      Y(N2P1)=APEX
      FXV2(N2P1)=0.0

```

```

C THIS POINT OF FXV2 IS DEFINED SO THAT IN EVALUATION OF
C THOSE VALUES OF FCT WHERE THE FINAL APEX POINT IS REQUIRED
C WE MAY NOT DRAW ON FICTITIOUS VALUES FROM COMPUTER MEMORY.
C GENERATING NEW VALUES OF Y WHICH ARE EQUISPACED.

```

```

      Y1(1)=Y(1)
      DO 11 I=2,N2
      IM1=I-1
      Y1(I)=Y1(IM1)+HEIGHT
11  CONTINUE
      KK=1
      II=1
13  KK1=KK+1
      KK2=KK+2
      KK3=KK+3
      DO 12 I=II,N2
      IP1=I+1
      IF(Y(KK3).LT.Y1(I)) GO TO 16

```

```

C THE ABOVE IS A SAFETY DEVICE TO CHECK IF THE NEW POINT
C FALLS WITHIN RANGE OF THE POLYNOMIAL BEING USED.

```

```

      FCT(I)=0.0
      DO 14 K=KK,KK3
      PROD=1.0
      PROD1=1.0

```

```

C EVALUATING LAGRANGIAN COEFFICIENTS.

```



## SUBROUTINE LAGINT

```
DO 15 J=KK, KK3
  IF(K.EQ.J) GO TO 15
```

C K MAY NOT BE EQUAL TO J BECAUSE THE LAGRANGIAN COEFF. IS  
C NOT DEFINED AT J.EQ.K

```
    PROD=PROD*(Y1(I)-Y(J))
    PROD1=PROD1*(Y(K)-Y(J))
15  CONTINUE
    L(K)=PROD/PROD1
    FCT(I)=FCT(I)+L(K)*FXV2(K)
14  CONTINUE
    IF(I.EQ.N2) GO TO 12
    IF(Y(KK3).GT.Y1(IP1)) GO TO 12
```

C THE ABOVE STATEMENTS IMPLY THAT IF THE NEXT NEW POINT IS  
C WITHIN THE RANGE OF THE EXISTING POLYNOMIAL THEN USE THE  
C SAME POLYNOMIAL INSTEAD OF A NEW ONE.

```
    II=I+1
```

C INCREMENTING KK TO ACCEPT THE NEXT POINT AND REJECTING THE  
C FIRST ONE.

```
16  KK=KK+1
    GO TO 13
12  CONTINUE
    DO 17 I=2, N, 2
      FN(I)=FCT(I/2)
17  CONTINUE
18  RETURN
    END
```



## SUBROUTINE NCOTES

```

SUBROUTINE NCOTES(HEIGHT ,FXV,C,INT,K,N,N1)
REAL HEIGHT,FXV(50),C(10),INT,H,A1,B1,C1,D2,D3
INTEGER K,N,N1,K1,K2,K3
H=HEIGHT
A1=2.0*H/45.0
B1=(FXV(2)+FXV(N))
C1=0.0
K1=8*K
DO 111 I=4,K1,4
C1=C1+FXV(I)
111 CONTINUE
D2=0.0
K2=(8*K)-2
DO 112 I=6,K2,8
D2=D2+FXV(I)
112 CONTINUE
D3=0.0
K3=(8*K)-6
DO 113 I=10,K3,8
D3=D3+FXV(I)
113 CONTINUE
INT=A1*(C(1)*B1+C(2)*C1+C(3)*D2+C(4)*D3)
114 RETURN
END

```





- SAMPLE -

- SAMPLE -

C THE VALUE OF A REPRESENTATIVE SAMPLE SIZE FROM A DATA  
C POPULATION OF SIZE N IS TO BE EVALUATED USING STATISTICS.

```
REAL X(250),N1,STDEV,MEAN,UP,X1(250)
INTEGER N,L,L1,M,M1,I,K1
```

C READ THE CODE WHICH IDENTIFIES THE DATA SET.

```
      READ(5,7)M1,K1
7     FORMAT(2I3)
21    L=1
19    READ(5,9)N,UP
9     FORMAT(I4,F10.4)
```

C N IS THE POPULATION SIZE AND UP THE SIGMA LIMIT.  
C THE INDIVIDUAL DATA POINTS WILL BE READ.

```
      READ(5,10)(X(I),I=1,N)
10    FORMAT(4E20.8)
      IF(L.GT.1) GO TO 8
      READ(5,6)L1
6     FORMAT(1X,I3)
8     SUM=0.0
      DO 11 I=1,N
11    SUM=SUM+X(I)
      MEAN=SUM/FLOAT(N)
      SUM1=0.0
      DO 12 I=1,N
      X1(I)=X(I)-MEAN
12    SUM1=SUM1+(X1(I))**2
      STDEV=SQRT(SUM1/FLOAT(N-1))
      N1=((UP*STDEV)/(0.01*MEAN))**2
```

C N1 IS THE REQUIRED SAMPLE SIZE.

```
      WRITE(6,13)M1,K1,L
13    FORMAT('1',10X,'ORIFICE NO.=' ,I2, 5X,'LIQ.FLOW NO.=' ,
112,5X,'RUN NO.=' ,I2)
      WRITE(6,14)
14    FORMAT('0',15X,'INDIVIDUAL DATA POINTS USED,X(I)')
      WRITE(6,15)(X(I),I=1,N)
15    FORMAT(' ',10X,F10.6,3X,F10.6,3X,F10.6,3X,F10.6)
      WRITE(6,16)MEAN
16    FORMAT('0',15X,'THE MEAN OF TOTAL POPULATION IS=' ,F12.
18)
      WRITE(6,17)STDEV
17    FORMAT('0',15X,'THE STANDARD DEVIATION IS=' ,F12.8)
      WRITE(6,18)N1
```



## - SAMPLE -

```
18  FORMAT('0',15X,'SAMPLE SIZE PEQUIRED=',F10.3)
    IF(L.GE.L1) GO TO 22
    L=L+1
    GO TO 19
22  STOP
    END
```



### Appendix C

The appendix is subdivided into the following sections:

- (1) Rotameter Calibration.
- (2) Titration Analysis to standardize  $\text{Ba}(\text{OH})_2$  and  $\text{HCl}$  solutions and to evaluate  $C_A^b$  the concentration of carbon dioxide in the bulk liquid phase.
- (3) Details of the velocity profile measurements, and calibration of the probes used to measure point liquid velocities in the column.

#### Calibration of Liquid Flow Rotameters

Two rotameters R13M-25-3 and R-10M-25-3 were calibrated to measure liquid velocities ranging from 0 to 4.06 cm/sec in a column of 20.2 cms internal diameter.

The calibration data is given in Table 7 and the calibration curves are shown in Figure 37.





Column I.D. = 20.2 cms: Sectional Area = 320 cm<sup>2</sup>.

R13M-25-3

<u>Rotameter Reading</u>	<u>Flow Rate (l/sec)</u>	<u>Average Liquid Velocity in Column (cm/sec)</u>
10	0.135	0.422
20	0.352	1.10
30	0.545	1.70
40	0.731	2.28
50	0.910	2.84
60	1.10	3.44
70	1.30	4.06

R10M-25-3

10	0.0496	0.155
20	0.0878	0.274
30	0.1230	0.384
40	0.1610	0.503
50	0.2010	0.628
60	0.2430	0.759
70	0.2860	0.894
80	0.3250	1.02
90	0.3730	1.17
100	0.4190	1.31

Table-7 ROTAMETER CALIBRATION DATA



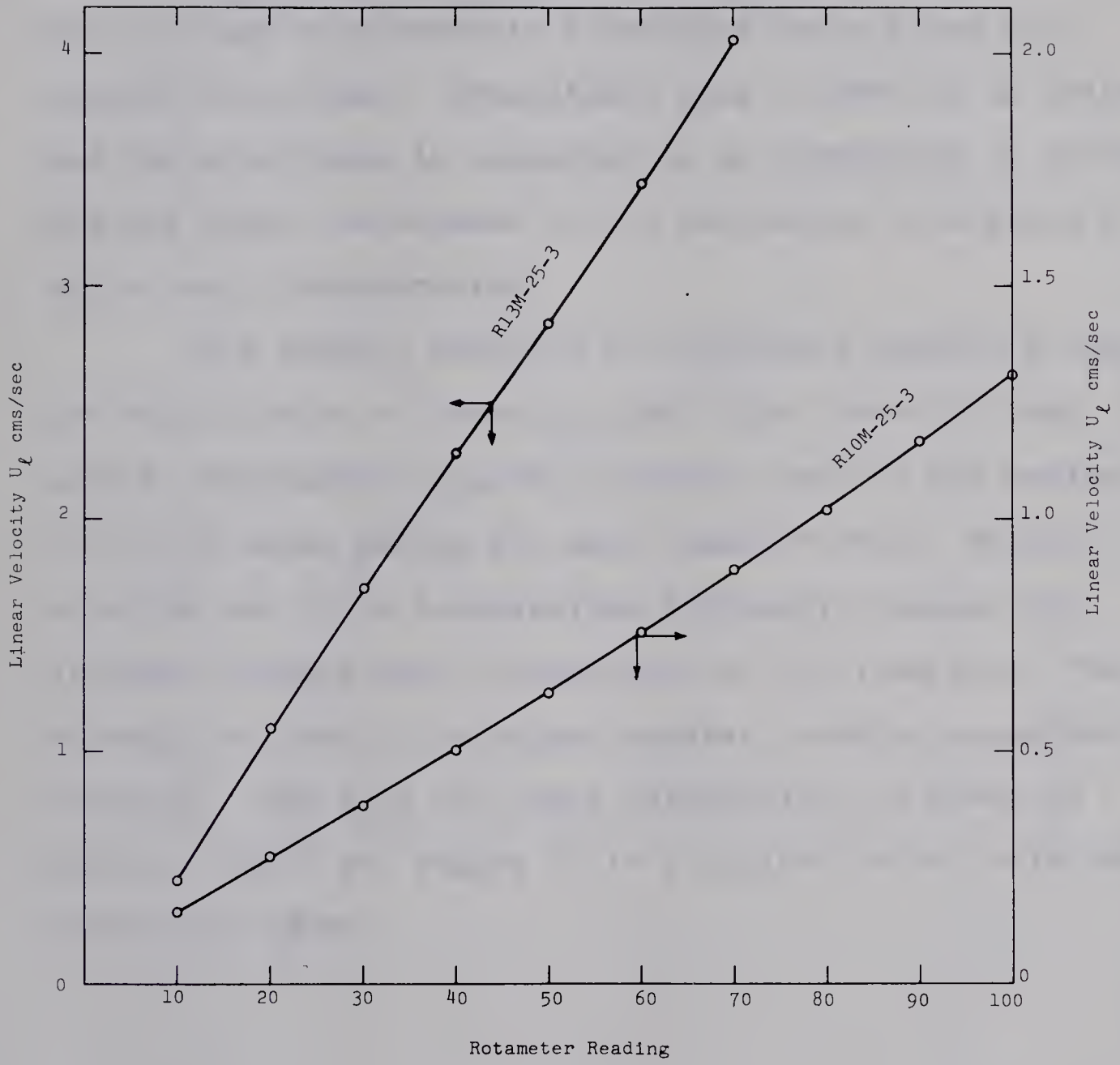


Figure 37: Calibration Curves for Rotameters



Titration Analysis(a) Standardization of  $\text{Ba}(\text{OH})_2$  and  $\text{HCl}$  solutions.

The standardization of  $\text{Ba}(\text{OH})_2$  and  $\text{HCl}$  solutions is done through electrometric titrations using glass and calomel electrodes. Bromothymol blue is used as an indicator and the experiment is conducted in an atmosphere of nitrogen. The end point corresponds to the inflexion in a curve of pH vs. acid concentration.

The  $\text{Ba}(\text{OH})_2$  solution is calibrated against a standard  $\text{HCl}$  solution of strength 0.2N. The former is then used to standardize the  $\text{HCl}$  solution used for the analysis of  $\text{CO}_2$  in water during the mass transfer runs.  $\text{Ba}(\text{OH})_2$  solution has to be standardized frequently because its strength changes due to absorption of  $\text{CO}_2$  from air. The strength of the  $\text{HCl}$  solution, however, remains essentially constant. The data for these calibrations is given in tables 8 and 9 and Figure 38 is a typical pH vs. acid concentration curve.





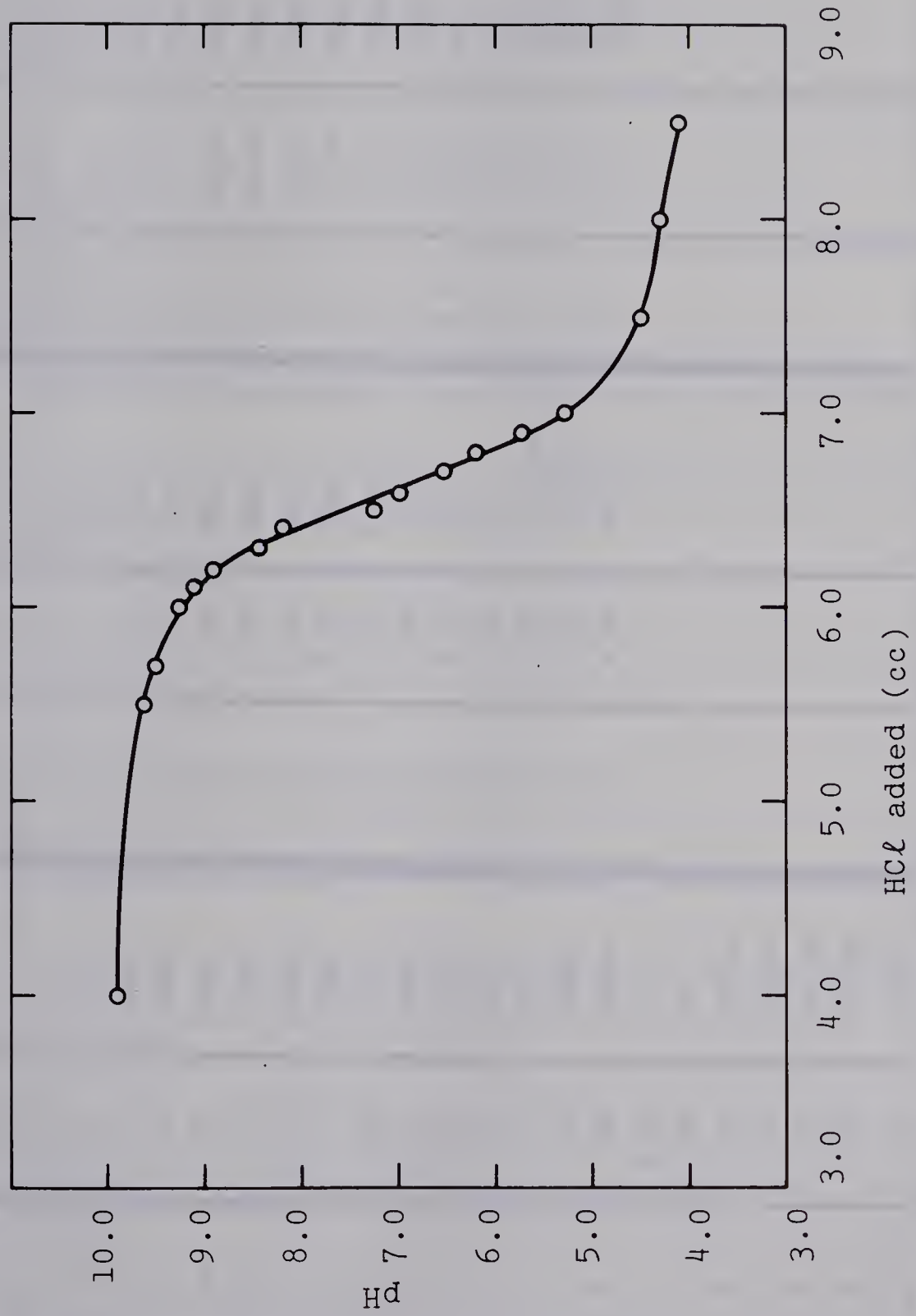


Figure 38: A Typical pH Titration Curve



V = Volume of HCl added (cc), Sample Volume = 20 ml (Ba(OH)<sub>2</sub>),  
Indicator = Bromothymol Blue, G-Y = Greenish-yellow, Y-G = Yellowish-green.

Run No. 1			Run No. 2			Run No. 3		
V(cc)	pH	Colour	V(cc)	pH	Colour	V(cc)	pH	Colour
0.0	>10	Blue	0.0	>10	Blue	0.0	>10	Blue
1.0	>10	Blue	3.0	>10	Blue	3.0	>10	Blue
2.0	>10	Blue	4.0	10.01	Blue	4.0	9.99	Blue
3.0	>10	Blue	5.0	9.85	Blue	5.0	9.72	Blue
4.0	9.9	Blue	6.0	9.45	Blue	6.0	9.35	Blue
5.0	9.51	Blue	6.2	9.05	Blue	6.2	9.28	Blue
5.5	9.62	Blue	6.4	8.80	Blue	6.4	8.90	Blue
5.7	9.51	Blue	6.5	8.30	Blue	6.5	8.52	Blue
6.0	9.25	Blue	6.6	7.25	Green	6.6	7.52	Green
6.1	9.10	Blue	6.7	6.80	Green	6.7	6.95	Green
6.2	8.92	Blue	6.8	6.30	G-Y	6.8	6.40	G-Y
6.3	8.42	Blue	6.9	5.80	Y-G	6.9	5.82	Y-G
6.4	8.19	Blue	7.0	5.30	Yellow	7.0	5.33	Yellow
6.5	7.25	Green	7.5	4.58	Yellow	7.5	4.40	Yellow
6.6	6.98	Green	8.5	4.18	Yellow	8.5	4.10	Yellow
6.7	6.52	G-Y						
6.8	6.19	Y-G						
6.9	5.75	Yellow						
7.0	5.28	Yellow						
7.5	4.51	Yellow						
8.0	4.28	Yellow						
8.5	4.12	Yellow						

Table 8 - Standardization of Ba(OH)<sub>2</sub> against standard 0.02N HCl



V = Volume of acid added (cc).

Volume of Sample = 20 mL Ba(OH)<sub>2</sub>

Indicator = Bromothymol Blue

Run No. 1			Run No. 2			Run No. 3		
V(cc)	pH	Colour	V(cc)	pH	Colour	V(cc)	pH	Colour
0.0	>10	Blue	0.0	>10	Blue	0.0	>10	Blue
5.0	>10	Blue	10.0	>10	Blue	10.0	>10	Blue
10.0	>10	Blue	15.0	9.70	Blue	15.0	9.92	Blue
12.0	9.92	Blue	17.0	9.42	Blue	17.0	9.62	Blue
13.0	9.82	Blue	19.0	8.95	Blue	19.0	9.00	Blue
14.0	9.70	Blue	19.1	8.82	Blue	19.2	8.88	Blue
15.0	9.82	Blue	19.2	8.42	Blue	19.4	8.62	Blue
17.0	9.53	Blue	19.3	8.48	Blue	19.5	8.18	Blue
19.0	8.63	Blue	19.4	8.10	Blue	19.6	7.85	Blue
19.5	7.20	Green	19.5	7.60	Green	19.7	7.20	Green
19.7	6.80	Green	19.6	7.30	Green	19.8	6.90	Green
19.9	6.50	Yellow	19.8	6.88	Green	20.0	6.48	Yellow
20.1	6.20	Yellow	20.0	6.45	Yellow	20.5	5.30	Yellow
20.3	5.51	Yellow	20.2	6.05	Yellow	21.0	4.80	Yellow
20.5	5.10	Yellow	20.4	5.65	Yellow	22.0	4.52	Yellow
20.7	4.85	Yellow	20.6	5.30	Yellow	23.0	4.30	Yellow
20.9	4.82	Yellow	21.0	4.90	Yellow			
22.0	4.45	Yellow	22.0	4.50	Yellow			
23.0	4.25	Yellow	23.0	4.28	Yellow			

Table 9 - Standardization of HCl Solution





Calculations:-

Ba(OH)<sub>2</sub>: Volume = 20 ml.

Run 1	HCl 0.02N	PH 6.95	HCl Volume at End Point	6.60 cc
Run 2	" "	" 7.00	"	6.65 "
Run 3	" "	" 7.10	"	6.65 "
Average				6.63 cc

Ba(OH)<sub>2</sub>: Volume = 20 ml.

Run 1	HCl Unknown	PH 6.70	HCL Volume at End Point	19.80 cc
Run 2	" "	" 7.00	"	19.80 "
Run 3	" "	" 7.00	"	19.75 "
Average				19.78 cc

$$\text{Normality of Ba(OH)}_2 = \frac{6.63 \times 0.02N}{20}$$

$$\begin{aligned} \text{Normality of HCl} &= \frac{6.63 \times 0.02N}{20} \times \frac{20}{19.78} = \frac{6.63}{19.78} \times 0.02N \\ &= 0.0067 \text{ N.} \end{aligned}$$

(b) Titration Analysis to Evaluate  $C_A^b$

The prestandardized Ba(OH)<sub>2</sub> and HCl solutions are used to determine the concentration of CO<sub>2</sub> in the bulk



water phase. A known volume of water containing dissolved  $\text{CO}_2$  is added to a known volume of the barium hydroxide solution. The  $\text{Ba}(\text{OH})_2$  reacts with  $\text{CO}_2$  in water to give  $\text{BaCO}_3$ . Addition of  $\text{HCl}$  during titration serves the following purposes:

- (i) To neutralize excess  $\text{Ba}(\text{OH})_2$  to  $\text{BaCl}_2$
- (ii) To convert the  $\text{BaCO}_3$  to  $\text{BaCl}_2$  with evolution of  $\text{CO}_2$ .

The conversion of  $\text{BaCO}_3$  to  $\text{BaCl}_2$  takes place in two stages namely:

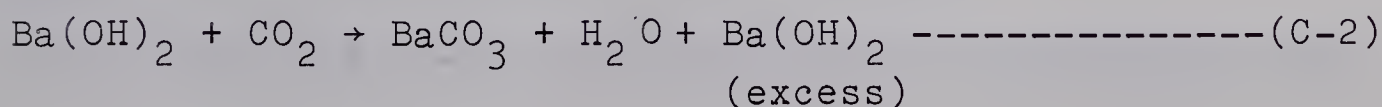
(i) conversion of  $\text{BaCO}_3$  to  $\text{Ba}(\text{HCO}_3)_2$  and  $\text{BaCl}_2$ . This corresponds to a change in color of the bromothymol blue indicator from blue to green.

(ii) conversion of  $\text{Ba}(\text{HCO}_3)_2$  to  $\text{BaCl}_2$  and  $\text{CO}_2$ . The indicator changes color from green to yellow.

The chemical reactions involved in the complete titration are given as follows:

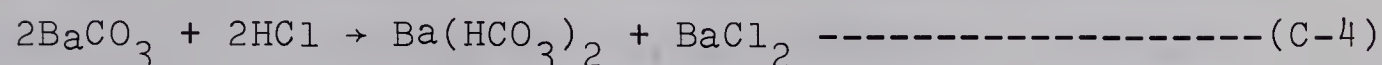
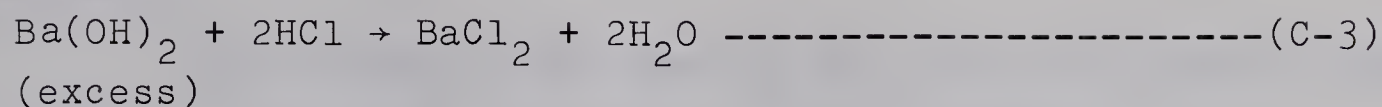


The above given reaction corresponds to the blank run wherein no  $\text{CO}_2$  is involved. The bromothymol end point is from blue to yellow.

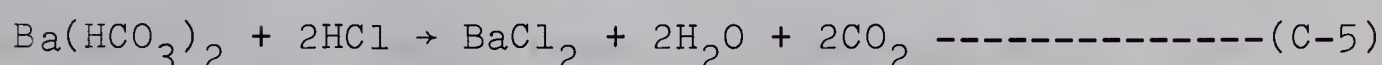




This corresponds to  $\text{CO}_2$  neutralization.



These reactions correspond to the end of the first stage of the back titration. The bromothymol blue end point is from blue to green.



This corresponds to the end of the second and final stage. The bromothymol blue end point is from green to yellow.

If the volume of HCl used to neutralize a given volume of  $\text{Ba(OH)}_2$  in a blank titration is  $V_1\text{ml}$  and the volume used at the end of the first stage of the back titration is  $V_2\text{ml}$ , then  $(V_1 - V_2)\text{ml}$  is a measure of the  $\text{CO}_2$  concentration in the water sample. This can be shown as follows:

Say that the initial volume of  $\text{Ba(OH)}_2$  used is = 20 ml.

Say volume of HCl required to neutralize 20 ml of  $\text{Ba(OH)}_2$   
=  $V_1\text{ml}$

then

$$20 \times N = V_1 \times N_1 \text{ ----- (C-6)}$$





Where  $N$  and  $N_1$  are the normalities of  $\text{Ba(OH)}_2$  and  $\text{HCl}$  respectively.

Say volume of  $\text{HCl}$  used at the end of the first stage is  $V_2 \text{ ml}$ .  $V_2$  includes the volume for neutralizing excess  $\text{Ba(OH)}_2$  and converting the barium carbonate to barium bicarbonate. The total volume of  $\text{HCl}$  used at the end of both stages must equal  $V_1 \text{ ml}$  because at the end of second stage effectively all the  $\text{Ba(OH)}_2$  has been consumed. In a blank titration the conversion of  $\text{Ba(OH)}_2$  to  $\text{BaCl}_2$  takes place directly and in the titration involving  $\text{CO}_2$ , the conversion to  $\text{BaCl}_2$  takes place through  $\text{BaCO}_3$ . The volume of  $\text{HCl}$  used in both cases for the same initial volume of  $\text{Ba(OH)}_2$  must be the same.

Thus the volume of  $\text{HCl}$  required to convert barium bicarbonate to barium chloride =  $(V_1 - V_2) \text{ ml}$ .

$\therefore$  Volume of  $\text{HCl}$  required to neutralize total  $\text{BaCO}_3 = 2(V_1 - V_2) \text{ ml}$ . This is so because equal volumes of  $\text{HCl}$  are used at each step of the barium carbonate conversion to  $\text{BaCl}_2$ .

If the absorbed  $\text{CO}_2$  is taken from a 20 ml Sample of water then

$$20 \times N_{\text{CO}_2} = 2(V_1 - V_2) \times N_1 \text{ ----- (C-7)}$$

Where  $N_{\text{CO}_2}$  is the normality of  $\text{CO}_2$  in water.

If  $C_A^b$  is the concentration of  $\text{CO}_2$  in water in  $\frac{\text{gm moles}}{\text{litre}}$



then

$$N_{\text{CO}_2} = 2 \times C_A^b$$

$$\therefore 20 \times 2 \times C_A^b = 2(V_1 - V_2) \times N_1$$

$$\text{or } C_A^b = \frac{(V_1 - V_2) \times N_1}{20} \text{ ----- (C-8)}$$

$$\text{or } C_A^b = f[(V_1 - V_2)]$$

A sample pH curve for a blank and  $\text{CO}_2$  titrations is shown in Figure 39.

#### Measurement of Liquid Velocity Profile.

The measurement of liquid velocity profile in the column involves the following experiments.

- (i) Determination of the limiting current voltage range.
- (ii) Calibration of the platinum probes.
- (iii) Measurement of point velocities in the column cross section.

#### Determination of the Limiting Current Voltage Range.

The effect of liquid velocity on the limiting current and the voltage range for which the latter persists is given by a curve of polarographic current vs. applied voltage at different liquid velocities.

A typical set of data for such curves is given in



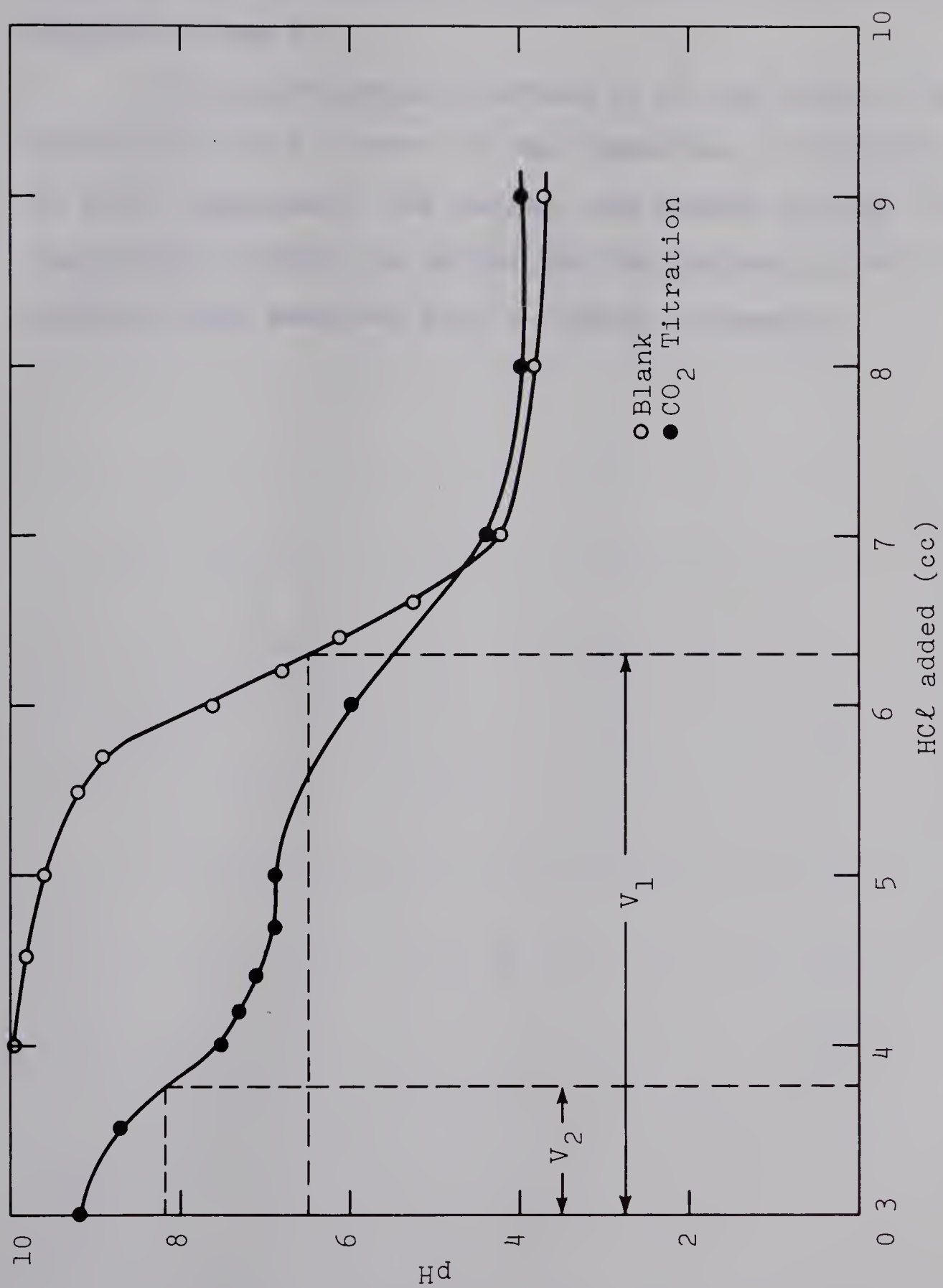
Figure 39: Blank and CO<sub>2</sub> titration curves





Table 10 and the curves for probes 1 and 2 are shown in Figures 40 and 41.

The polarographic current is of the order of  $\mu\text{A}$  and measurement of a current of this magnitude is difficult. To avoid inaccuracy, the current was passed through a high resistance ( $10.8\text{k}\Omega$ ) in series and the voltage (order of  $\text{mV}$ ) across it was measured with a digital voltmeter.



Constant Resistance in Calibration Circuit = 10.8k $\Omega$

Applied Voltage (Volts)	$U_L = 0.484$		$U_L = 1.50$		$U_L = 2.38$		$U_L = 3.80$		$U_L = 4.75$	
	mV	$\mu A$	mV	$\mu A$	mV	$\mu A$	mV	$\mu A$	mV	$\mu A$
1.2	4.0	0.370	3.0	0.278	5.0	0.462	4.0	0.370	-	-
1.3	21.0	1.94	26.0	2.40	30.0	2.78	28.0	2.59	-	-
1.4	44.0	4.07	56.0	4.72	60.0	5.55	39.0	3.69	12.0	1.11
1.5	56.0	4.72	85.0	7.86	94.0	8.70	101.0	9.34	84.0	7.77
1.6	60.0	5.55	115.0	10.62	125.0	11.60	150.0	13.90	165.0	15.30
1.7	65.0	6.01	124.0	11.50	154.0	14.20	191.0	17.7	210.0	19.4
1.8	70.0	6.48	139.0	12.90	175.0	16.20	221.0	20.4	245.0	22.6
1.9	65.0	6.01	144.0	13.30	191.0	17.7	237.0	21.9	270.0	25.0
2.0	69.0	6.40	149.0	13.80	195.0	18.0	247.0	22.8	283.0	26.1
2.1	66.0	6.11	147.0	13.60	198.0	18.3	249.0	23.0	283.0	26.1
2.2	84.0	7.77	155.0	14.30	203.0	18.8	255.0	23.6	300.0	27.8
2.3	105.0	9.72	182.0	16.80	220.0	20.4	275.0	25.4	352.0	32.6
2.4	-	-	234.0	21.60	280.0	25.9	325.0	30.1	-	-

$U_L$  = Liquid Velocity in cms/sec.

Table 10 - Polarographic Current vs. Applied voltage at

Different liquid velocities.



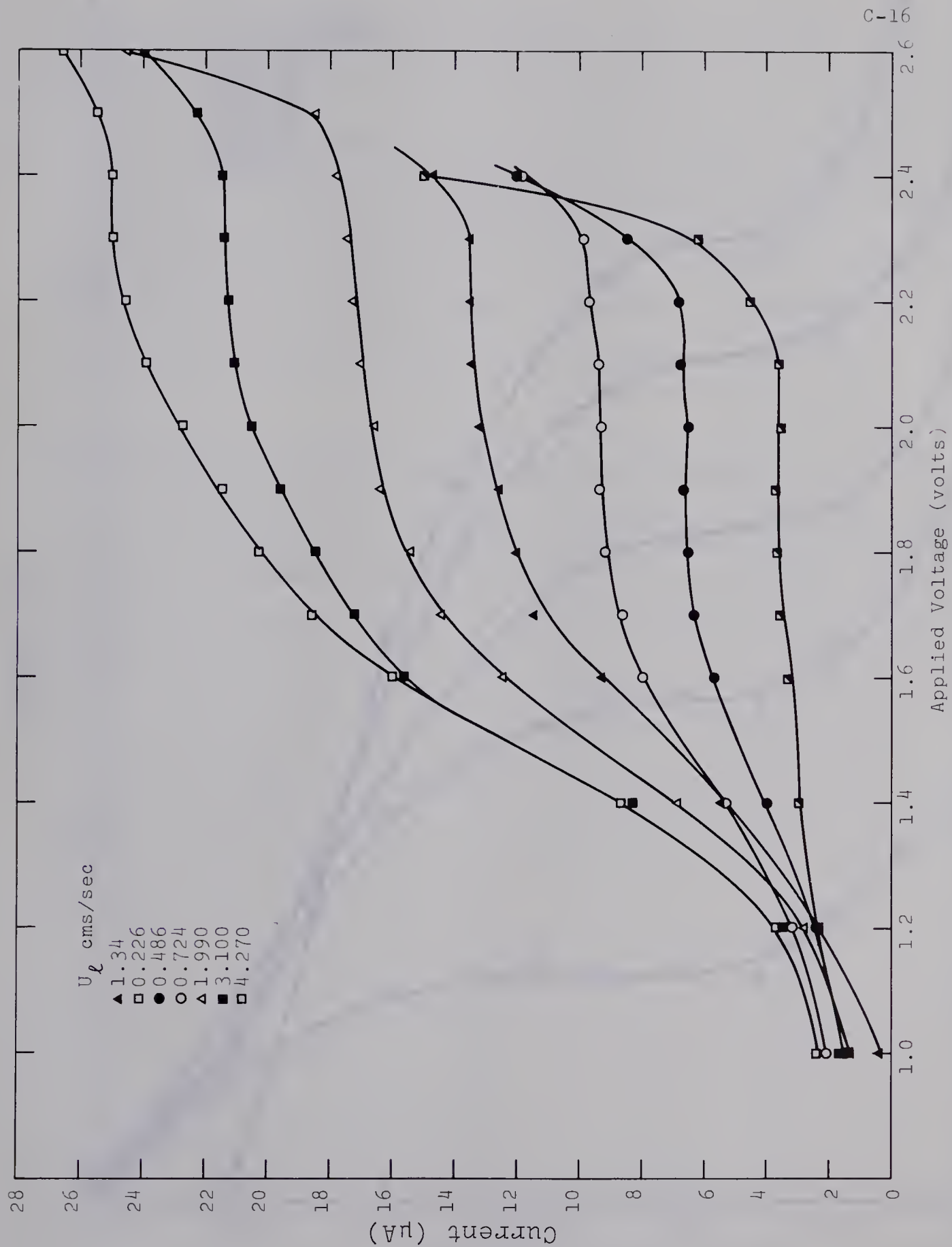


Figure 40: Curves of Polarographic Current vs. Applied Voltage for Probe 1





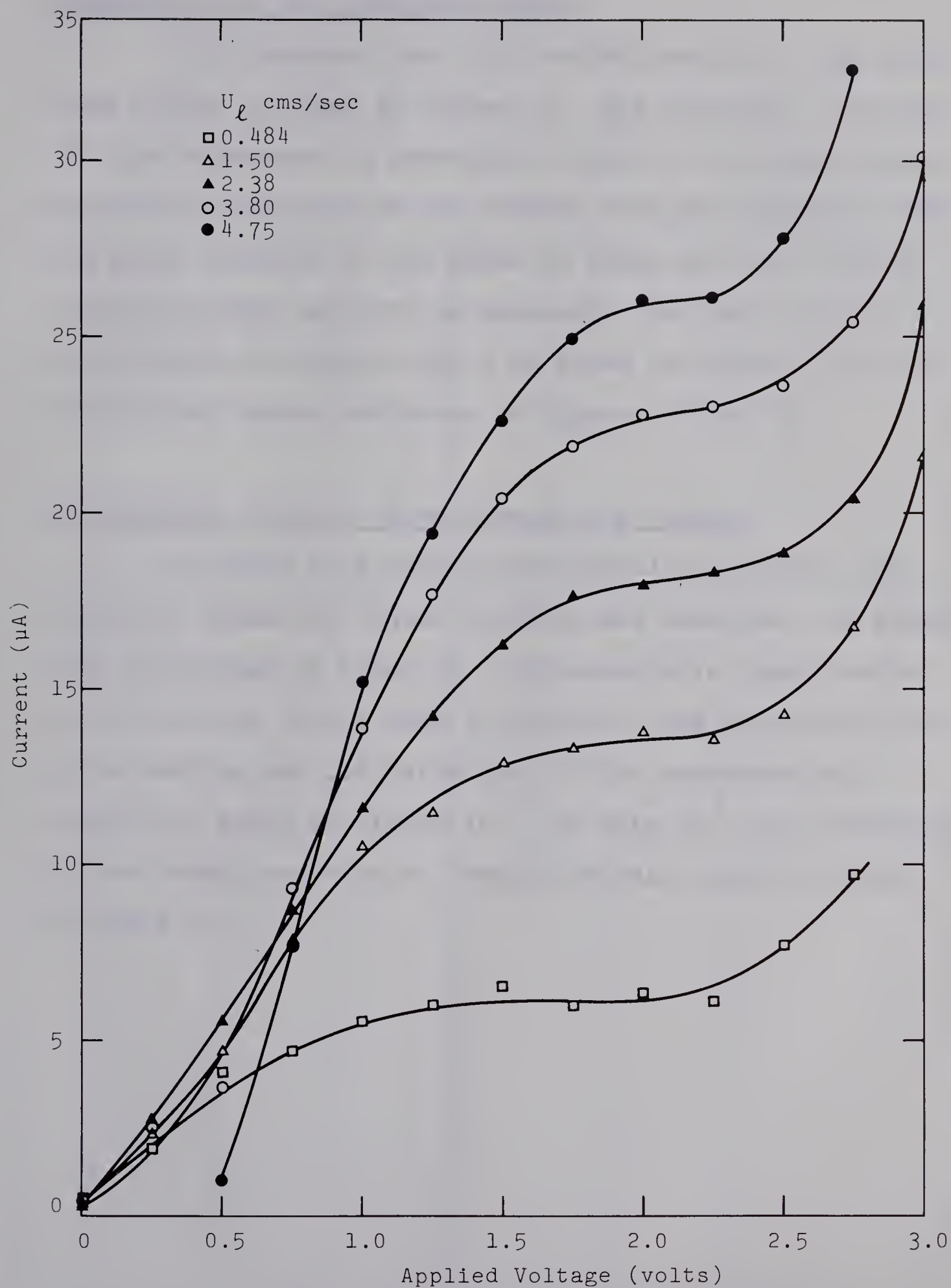


Figure 41: Curves of Polarographic Current vs. Applied Voltage for Probe 2



### Calibration of the Platinum Probes.

The apparatus used for the calibration of the platinum probes is shown in Figure 11. The technique involved in this experiment is identical to that of the measurement of velocity profiles in the column, with the exception that the point velocity at the probe is known and the limiting current at this velocity is measured. The data for the calibration of probes 1 and 2 is given in Table 11 and the calibration curves are shown in Figures 42 and 43.

### Measurement of Point Velocities in the Column.

In order to ascertain the radial position in the column at which the liquid velocity was measured, the probes were calibrated in terms of a characteristic length which was a function of the radial position. The details of the probe setting and the definition of the characteristic length are given in Figure 44. The data for the calibration of the radial position vs. characteristic length is given in Table 12.



Resistance in the calibration circuit =  $10.8k\Omega$ .

mV = Voltage on digital voltmeter (mV).

$\mu A$  = Current through probe ( $\mu A$ ).

$U_\ell$  = Liquid velocity at the probe (cms/sec).

r = Radius of moving arm (cms).

r	Probe 1			Probe 2		
	mV	$\mu A$	$U_\ell$	mV	$\mu A$	$U_\ell$
5.0	120.0	11.1	0.555	135.0	12.5	1.180
	100.0	9.25	0.395	101.0	9.35	0.549
	111.0	10.3	0.441	62.0	5.74	0.264
	101.0	9.35	0.368	73.0	6.75	0.290
	79.6	7.37	0.206	79.0	7.31	0.358
	97.0	8.98	0.281	87.0	8.06	0.460
	114.0	10.60	0.440	121.0	11.2	0.945
10.0	197.0	18.20	2.01	230	21.2	3.17
	172.0	15.90	1.46	355	32.8	6.35
	127.0	11.80	0.65	310	28.6	5.06
	122.0	11.30	0.63	265	24.5	3.92
	138.0	12.80	0.82	204	18.9	2.50
	166.0	15.40	1.22	180	16.6	1.79
	201.0	18.60	1.95	159	14.7	1.42
	220.0	20.40	2.50	146	13.5	1.30
	246.0	22.80	3.16			
	136.0	12.60	0.856			
	153.0	14.20	1.11			
	322.0	29.80	5.10			
	359.0	33.20	5.86			
	299.0	27.70	4.39			
	280.0	25.90	4.10			
	269.0	24.90	3.76			
	176.0	16.30	1.52			
	149.0	13.80	0.966			

Table 11 - Calibration Data for Probes 1 and 2.





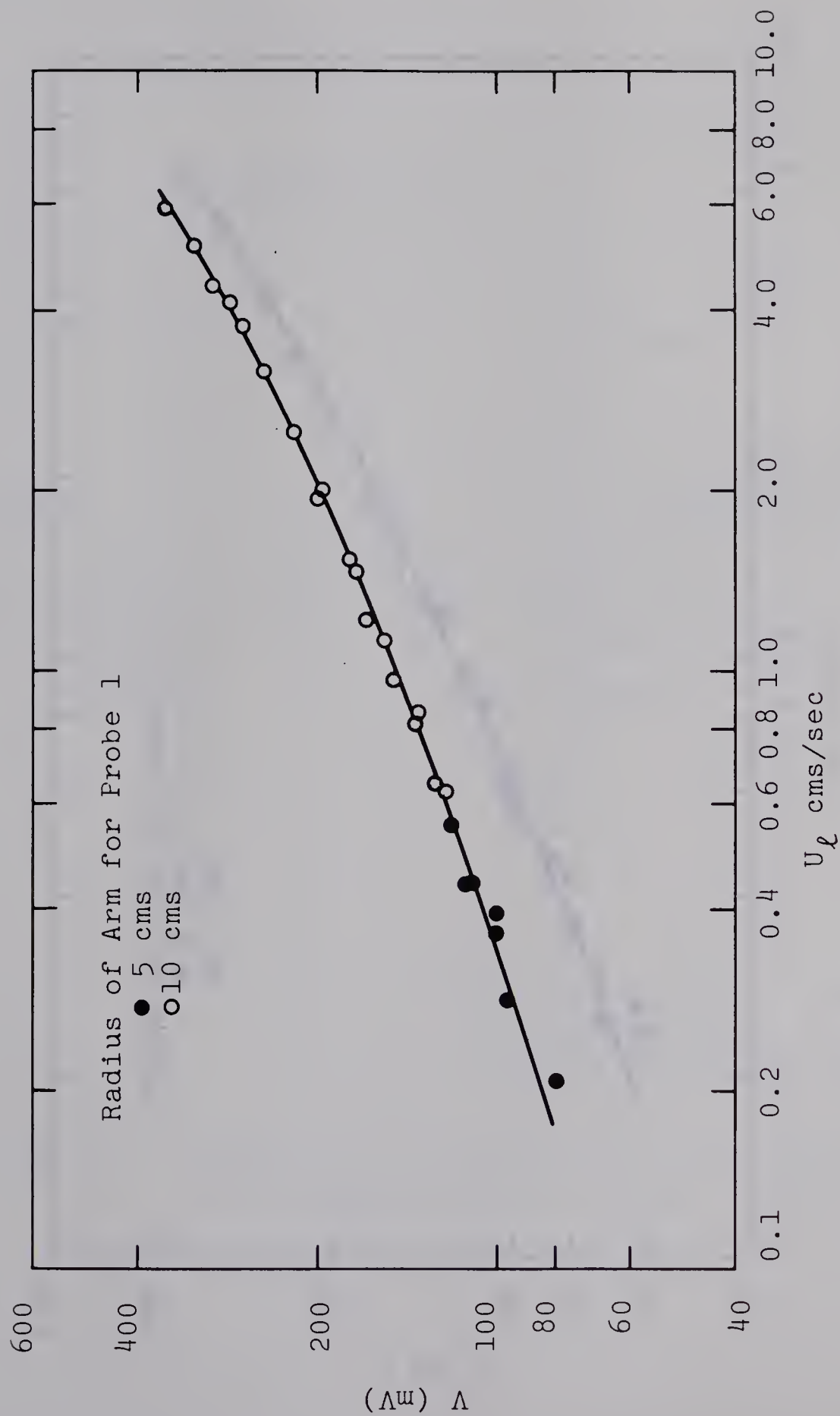


Figure 42: Calibration Curve for Probe 1



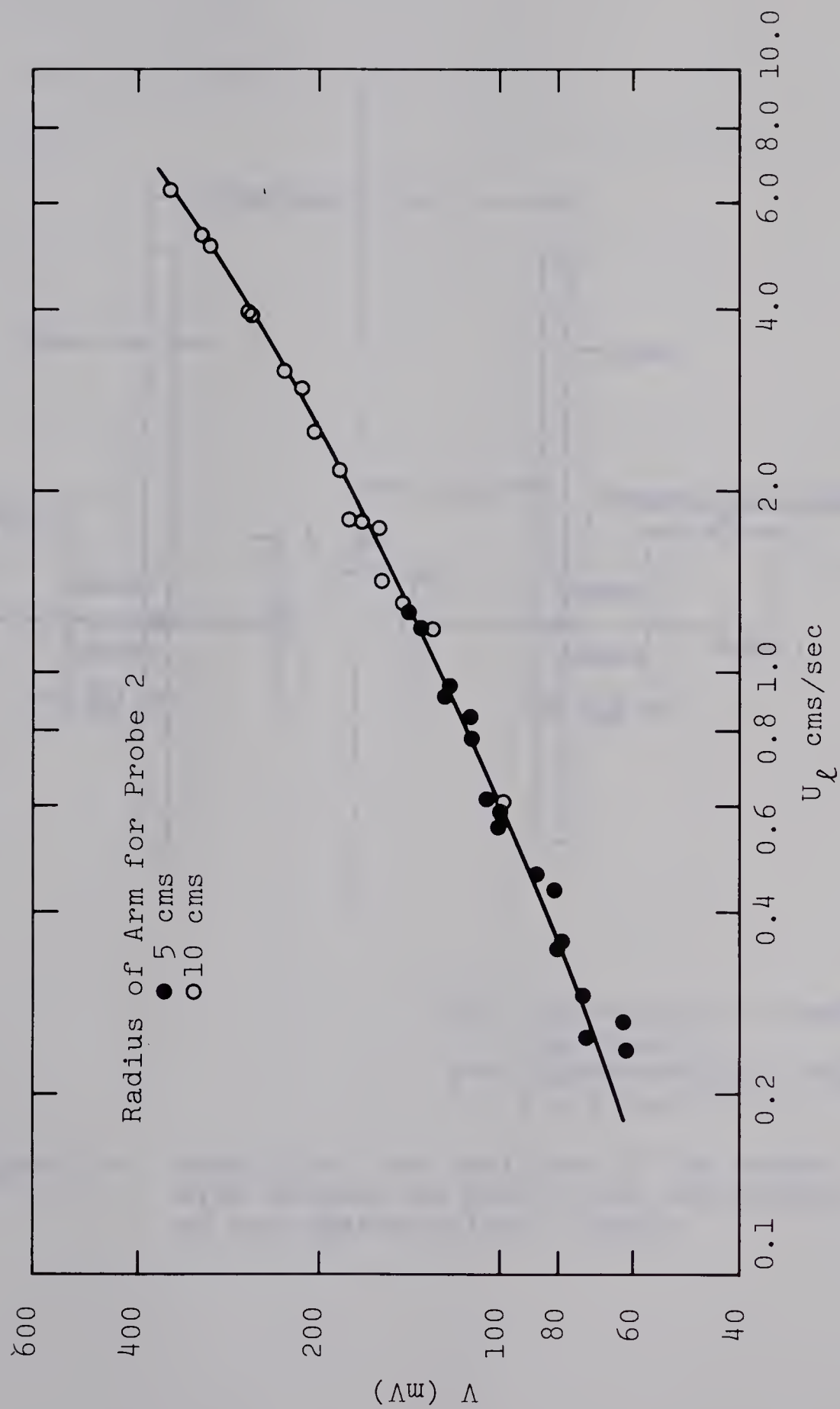
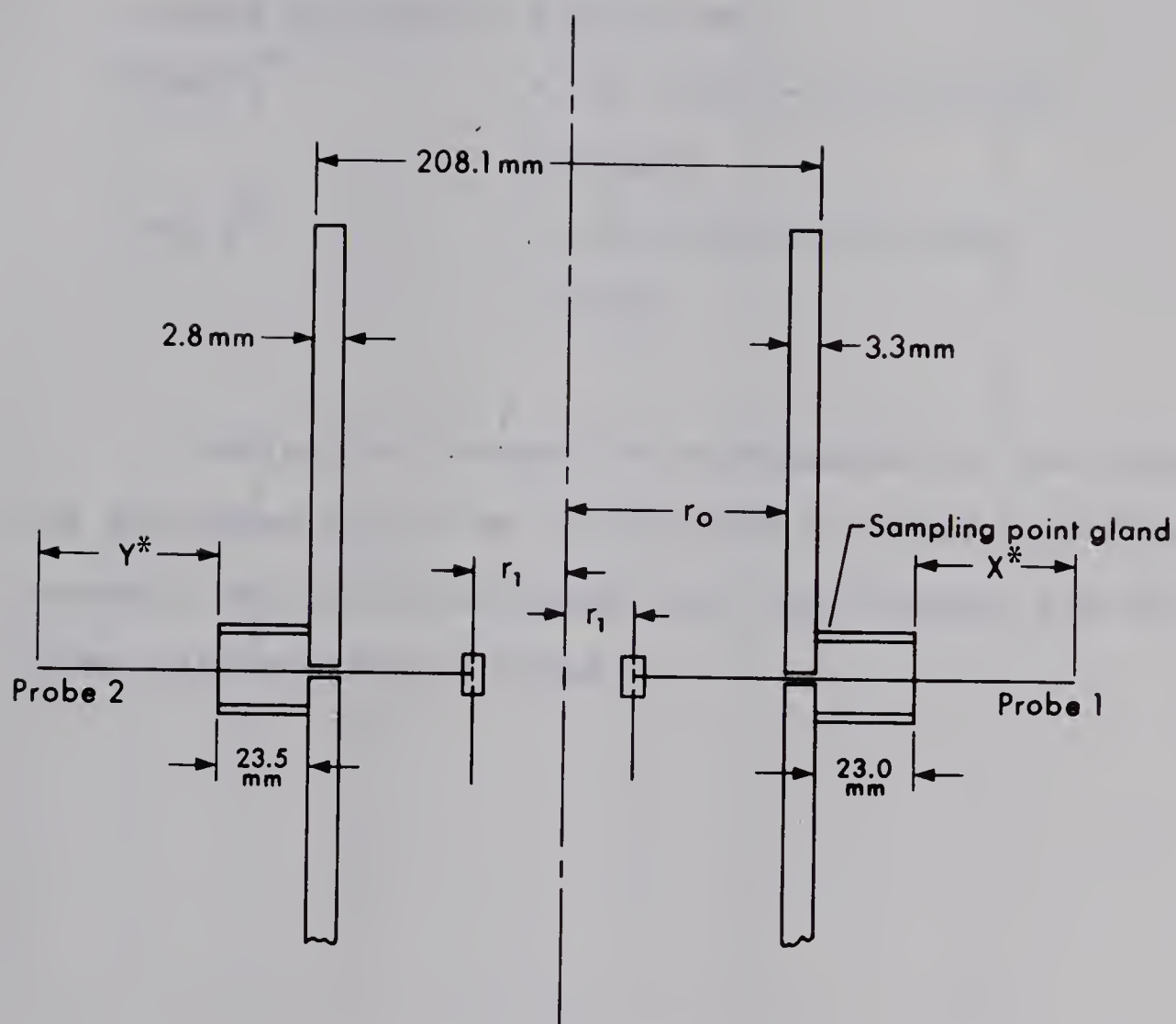


Figure 43: Calibration for Probe 2





$X^*$  = Characteristic Length  
for Probe 1

$Y^*$  = Characteristic Length  
for Probe 2

Figure 44: Details of the position of the probe with respect to the column and details of the characteristic length





With reference to Figure 44:

Length of Probe 1 = 196.3 mm.

Length of Probe 2 = 197.3 mm.

$$\begin{aligned}\text{Then } X^* &= 196.3 - 23.0 - 3.3 - 101.0 + r_1 \\ &= 69.0 + r_1.\end{aligned}$$

$$\begin{aligned}\text{and } Y^* &= 197.3 - 23.5 - 2.8 - 101 + r_1 \\ &= 70 + r_1\end{aligned}$$

During the process of experimentation the probe 1 was shortened by 3.3 mm. to restore a broken electrical contact; table 12 thus gives both the original and the later calibrations of probe 1.



$r_1/r_0$	X*(mm) Prior to Short- ening	X*(mm) After Short- ening	Y*(mm)
0.0	69.0	65.7	70.0
0.1	79.1	75.8	80.1
0.2	89.2	85.9	90.2
0.3	99.3	96.0	100.3
0.4	109.4	106.1	110.4
0.5	119.5	116.2	120.5
0.6	129.6	126.3	130.6
0.7	139.7	136.4	140.7
0.8	149.8	146.5	150.8
0.9	159.9	156.6	160.9
-0.1	58.9	55.6	59.9
-0.2	48.8	45.5	49.8
-0.3	38.7	35.4	39.7
-0.4	28.6	25.3	29.6
-0.5	18.5	15.2	19.5
-0.6	8.4	5.1	9.4

Table 12 - Radial position vs.  
Characteristic length  
for probes 1 & 2.



The negative values of  $r_1/r_0$  in table 12 indicate the position past the centre of the column.

At points very close to the orifice and the column walls the radial position is reported in terms of the characteristic length only.

The data for measurement of point velocities corresponding to Figure 16, 17 and 18 is given in Tables 13, 14 and 15 respectively.





D1, D2, D3, D4 : Four diametric positions at which data was taken.

Each diameter is at an angle of  $45^\circ$  from previous one.

$X^*, Y^*$  = Characteristic length (mm)

mV = Voltage on digital voltmeter (mV)

$U_\ell$  = Liquid velocity (cms/sec)

$r_o$  = Radius of column (cms)

$r_1/r_o$  = Radical position

Probe	$r_1/r_o$	D1			D2			D3			D4		
		$X^*, Y^*$	mV	$U_\ell$	$X^*, Y^*$	mV	$U_\ell$	$X^*, Y^*$	mV	$U_\ell$	$X^*, Y^*$	mV	$U_\ell$
+1		165.5	105	0.53	165.5	114	0.54	165.5	114	0.54	165.5	110	0.54
	0.9		156	1.25		149	1.14		156	1.25		150	1.11
	0.8		152	1.18		150	1.16		152	1.18		151	1.17
	0.7		144	1.07		146	1.09		148	1.13		147	1.11
	0.6		143	1.05		145	1.08		144	1.07		141	1.01
	0.5		143	1.05		146	1.09		143	1.05		140	1.00
	0.4		143	1.05		144	1.06		141	1.01		137	0.96
	0.3		142	1.03		146	1.09		140	1.00		137	0.96
	0.2		143	1.05		142	1.03		140	1.00		135	0.93
	0.1		140	1.00		136	0.94		137	0.96		134	0.92
		65.3	122	0.75	63.8	116	0.67	62.7	119	0.71	64.5	116	0.67

(Column Centre Line) →







# Operating Conditions and Nomenclature for Tables 14 and 15

Data at Position D3 (diametric position)

Average Liquid Velocity = 1.0 (cms/sec) [Table 14]

= 2.0 (cms/sec) [Table 15]

Applied voltage for limiting current = 1.85 volts

Orifice diameter = 2.1 mm

Pressure at the nozzle = 14.8 psia

System Temperature = 25.0°C

R1, R2, R3, R4, R5 = Identification numbers of the runs taken

	TABLE 14					TABLE 15				
	R1	R2	R3	R4	R5	R1	R2	R3	R4	R5
Probe	1	2	1	1	1	1	2	1	1	1
Gas Press. (psig)	-	-	20	20	30	-	-	20	20	30
Freq. (1/sec)	0	0	5.2	14.3	25.0	0	0	4.93	15.05	25.13
Gas Flow (cc/sec)	0	0	0.0108	0.389	0.746	0	0	0.106	0.393	0.746







$r_1/r_0$	R1			R2			R3			R4			R5		
	$X^*, Y^*$	mV	$U_\ell$	$X^*, Y^*$	mV	$U_\ell$	$X^*, Y^*$	mV	$U_\ell$	$X^*, Y^*$	mV	$U_\ell$	$X^*, Y^*$	mV	$U_\ell$
	165.5	127	0.82	165.5	119	0.88	165.5	109	0.58	165.5	115	0.65	165.5	96	0.44
0.9		155	1.24		146	1.33		152	1.18		154	1.22		150	1.16
0.8		151	1.17		142	1.25		150	1.16		149	1.13		149	1.13
0.7		145	1.08		136	1.15		146	1.09		143	1.05		143	1.05
0.6		145	1.08		135	1.14		146	1.09		142	1.03		143	1.05
0.5		143	1.05		133	1.10		143	1.05		141	1.01		142	1.03
0.4		141	1.01		132	1.09		142	1.03		142	1.03		143	1.05
0.3		142	1.03		132	1.09		143	1.05		142	1.03		144	1.07
0.2		142	1.03		133	1.10		145	1.08		146	1.09		149	1.13
0.1		141	1.01		131	1.07		145	1.08		150	1.16		161	1.34
<del>0.0</del>	65.3	113	0.63	73.3	113	0.788	73.4	144	1.07	75.2	167	1.45	75.0	193	1.99

mV = Voltage on digital voltmeter (mv)

 $U_\ell$  = Liquid velocity at probe (cms/sec) $X^*, Y^*$  = Characteristic length (mm)



	73.2	125	0.79	65.0	108	0.720	73.3	148	1.12	73.4	171	1.53	74.3	184	1.80
0.1		138	0.90		130	1.05		138	0.98		144	1.07		153	1.20
0.2		130	0.85		125	0.98		134	0.91		138	0.98		142	1.03
0.3		137	0.96		130	1.05		137	0.96		140	1.00		142	1.03
0.4		139	0.99		133	1.10		138	0.98		140	1.00		141	1.01
0.5		140	1.00		135	1.14		140	1.00		140	1.00		140	1.00
0.6		143	1.05		136	1.15		142	1.03		142	1.03		142	1.03
0.7		143	1.05					143	1.05		144	1.07		142	1.03
0.8		150	1.16					149	1.13		149	1.13		147	1.11
0.9		154	1.22					153	1.20		152	1.18		148	1.12
	163.3	125	0.79				163.3	126	0.80	163.3	122	0.75	163.3	105	0.52


Table 14: Point Velocity Measurement for an average liquid velocity = 1.0 (cms/sec)



mV = Voltage on digital voltmeter (mV)

$U_\ell$  = Liquid velocity at probe (cms/sec)

$X^*, Y^*$  = Characteristic length (mm)

$r_1/r_0$	R1			R2			R3			R4			R5		
	$X^*, Y^*$	mV	$U_\ell$	$X^*, Y^*$	mV	$U_\ell$	$X^*, Y^*$	mV	$U_\ell$	$X^*, Y^*$	mV	$U_\ell$	$X^*, Y^*$	mV	$U_\ell$
	165.5	201	2.17	165.5	190	2.27	165.5	198	2.10	165.5	195	2.03	165.5	197	2.08
0.9		228	2.79		216	2.87		223	2.67		227	2.76		225	2.72
0.8		205	2.25		203	2.57		211	2.38		212	2.41		211	2.38
0.7		198	2.10		196	2.40		205	2.25		204	2.23		203	2.20
0.6		206	2.28		197	2.43		203	2.20		203	2.20		199	2.13
0.5		206	2.28		193	2.34		200	2.13		200	2.13		199	2.13
0.4		201	2.17		190	2.27		198	2.10		200	2.13		196	2.06
0.3		199	2.12		187	2.20		193	1.99		192	1.97		194	2.01
0.2		201	2.17		190	2.27		199	2.13		199	2.13		200	2.13
0.1		198	2.10		186	2.18		197	2.08		203	2.20		203	2.21
	60.4	186	1.85	73.9	179	2.02	73.7	200	2.13	73.7	214	2.46	74.8	229	2.81







<del>0.0</del>	68.7	189	1.91	66.1	158	1.57	69.7	209	2.34	68.7	215	2.48	69.3	262	3.66
0.1		193	1.99		186	2.18		195	2.03		196	2.06		202	2.18
0.2		190	1.93		178	2.00		190	1.93		190	1.93		197	2.08
0.3		194	2.01		182	2.08		192	1.97		191	1.95		192	1.97
0.4		196	2.05		186	2.18		196	2.06		193	1.99		195	2.03
0.5		203	2.20		193	2.36		202	2.18		197	2.08		198	2.10
0.6		207	2.30		195	2.38		207	2.30		202	2.18		204	2.23
0.7		208	2.32					208	2.32		203	2.21		204	2.23
0.8		212	2.41					210	2.37		206	2.28		208	2.32
0.9		231	2.86					228	2.79		225	2.72		226	2.74
	160.7	224	2.70				160.7	220	2.60	160.7	215	2.48	160.7	219	2.58

Table 15: Point Velocity Measurement for an averageliquid velocity = 2.0 (cm/sec)



## Appendix D

### Evaluation of The Mass Transfer Coefficient from CO<sub>2</sub>-Water Data

The amount of mass transfer during bubble formation is obtained by the difference  $(V-V^*)$  where

$V$  = The equivalent volume of a gas bubble determined by the equation  $G = vV$ .

$V^*$  = The volume of the gas bubble at detachment as determined from photographs.

The general equation for total mass transfer upto a time  $T_f$  is given by

$$N_A = (C_A^S - C_A^b) k_{Lav} \int_0^{T_f} A(t) dt \text{ -----(D-1)}$$

In order to determine  $k_{Lav}$  the following data must be known:

$N_A$  - The amount of mass transfer during bubble formation.

This is given by  $(V-V^*)$ .

$C_A^b$  - The concentration of the solute CO<sub>2</sub> in the bulk liquid phase.

$C_A^S$  - The concentration of the solute CO<sub>2</sub> at the interface. If the resistance to mass transfer at the interface is assumed negligible then  $C_A^S$  is given by the solubility of the gas in the liquid phase at the system temperature and gas partial pressure.



$\int_0^{T_f} A(t) dt$  = The value of the area integral which represents the variation of the bubble surface area with time during bubble formation.

The value of  $C_A^b$  is essentially zero. This can be shown by the following sample calculation.

Size of water sample = 20 cc.

Titre value of a blank

titration = 21.2cc HCl

Titre value for a  $CO_2$

titration = 20.95 cc HCl

Normality of HCl = 0.0067N

$$\begin{aligned} \therefore C_A^b &= \frac{(21.2 - 20.95) \times 0.0067}{20} \frac{\text{moles}}{\text{litre}} \\ &= \frac{0.25 \times 0.0067}{20} = 8.38 \times 10^{-5} \frac{\text{moles}}{\text{litre}} \\ &= 8.38 \times 10^{-8} \frac{\text{moles}}{\text{cc.}} \end{aligned}$$

$$C_A^s = 3.59 \times 10^{-5} \frac{\text{gm moles}}{\text{cc soln}} \text{ at the system conditions}$$

$$\therefore (C_A^s - C_A^b) = (3.59 - 0.008) \times 10^{-5} = 3.582 \times 10^{-5} \frac{\text{moles}}{\text{cc.}}$$

The error involved in assuming  $C_A^b = 0$  is  $\approx 0.2\%$ .

This is well within the limitation of the experiment.





The value of  $C_A^S$  is evaluated from solubility data as follows:

Temperature of investigation =  $25^\circ\text{C}$

Assuming Henry's Law to hold for  $\text{CO}_2$ -water

The Henry's Constant =  $1.64 \times 10^3$  [73]

$$X_A = \frac{p_A}{H}$$

where

$$X_A = \frac{\text{moles CO}_2}{\text{moles Solution}}$$

$p_A$  = partial pressure of  $\text{CO}_2$

The gas  $\text{CO}_2$  enters the orifice saturated with water vapour.

The vapour pressure of water at  $25^\circ\text{C}$  is given by 23.76 mm Hg [74]  $\equiv$  0.46 psia.

Total system pressure = 14.8 psia

$\therefore p_A = 14.8 - 0.46 = 14.34$  psia

Atmospheric pressure = 13.5 psia

$\therefore p_A = \frac{14.34}{13.5} = 1.062$  atm.

$\therefore X_A = \frac{1.062}{1.64 \times 10^3} = 0.6477 \times 10^{-3} \frac{\text{gm moles}}{\text{mole soln.}}$   
 $= \frac{0.6477 \times 10^{-3}}{18.04} = 3.59 \times 10^{-5} \frac{\text{gm moles}}{\text{cc soln.}}$

The area integral is evaluated from Figures 23, 24 and 25.

$k_{\text{Lav}}$  is then determined using equation (D-1).









**B29922**